LEHRSTUHL FÜR VERFAHRENSTECHNIK DES INDUSTRIELLEN UMWELTSCHUTZES
Montanuniversität Leoben
Franz-Josef-Straße 18
vtiu.unileoben.ac.at
A-8700 Leoben

Dissertation

MONITORING OF GAS-LIQUID MASS TRANSFER WITH SINGLE DROPLET EXPERIMENT

Vorgelegt von
Drs. Anda Lucia M.T
M01335607

Betrauer
Univ.-Prof. Dipl.-Ing. Dr.-Ing Markus Lehner

Leoben, November 2017

LEHRSTUHL FÜR VERFAHRENSTECHNIK DES INDUSTRIELLEN UMWELTSCHUTZES
Montanuniversität Leoben
Franz-Josef-Straße 18
vtiu.unileoben.ac.at
A-8700 Leoben

EIDESSTATTLICHE ERKLÄRUNG

Ich erkläre an Eides statt, dass ich dieseArbeit selbständig verfasst, andere als die angegebenen Quellen und Hilfsmittel nicht benutzt und mich auch sonst keiner unerlaubten Hilfsmittel bedient habe.

AFFIDAVIT

I declare in lieu of oath, that I wrote this thesis and performed the associated research myself, using only literature cited in this volume.

08 November 2017
Datum

Anda Lucia
Unterschrift

He is Allah, (the) One. "Allah-us-Samad
(The Self-Sufficient Master, Whom all creatures need,
He neither eats nor drinks)."He begets not, nor was He begotten;
"And there is none co-equal or comparable unto Him."
QS. Al-Ikhlaas : 1-4

Then did you think that We (God) created you uselessly and
that to Us you would not be returned?"
Q.S. Al-Mu'minun 115

And I (Allah) created not the jinns and humans
except they should worship Me.
QS. Adh-Dhariyat : 56

Abstract

MONITORING OF GAS-LIQUID MASS TRANSFER WITH SINGLE DROPLET EXPERIMENT

Reduction and capture of carbon dioxide (CO_2) gas emissions has attracted global attention in order to avoid global warming. Physical absorption is one method to reduce the CO_2 gas from various sources.

The spray method is one common process for separation of CO_2. For the selection of an absorbent and a design optimization of the spray column, in-depth knowledge of mass transfer characteristics between CO_2 and individual droplets are necessary. The physical data properties such as droplet diameter, contact time between gas-liquid systems and mass transfer coefficient are needed to design and optimize the absorption or desorption column.

An experimental set-up comprising of a rectangular gas chamber, a shadowgraph system and an analytical method for the determination of CO_2 concentration in water has been elaborated in order to study the characteristics of mass transfer between CO_2 and liquid droplets. This system allows the observation of droplet size, droplet velocity and droplet behaviour during formation and falling accurately.

A series of water droplets are generated by pushing liquid through a needle by means of a peristaltic pump. The water droplets were detached from the needle and fell down through a gas chamber filled with nitrogen, and are collected in the bottom of the chamber covered with a kerosene layer. Droplet diameter, droplet formation time and falling droplets velocity are determined by means of a high-speed camera. CO_2 desorption analysis from water droplets is carried out before and after dripping droplets. The liquid phase mass transfers coefficients of CO_2 desorption from liquid droplets are determined at different droplet formation times, droplet falling heights and droplet diameters.

The coefficient of liquid mass transfer of CO_2 desorption from water droplets during formation and falling are evaluated at formation times 0.2328 s, 0.859 s and 1.08 s, falling heights 5 cm, 10 cm, 15 cm and 20 cm and droplet diameters 1.61 mm, 2.67 mm and 3.0 mm, respectively.

The droplet velocity for all droplet diameters in this study matched with the model equation and this trends are also same with experiment of Takagaki and Komori [94] especially at short height. The experimental data for the terminal velocity of the droplets were similar to a study performed by Beard [95].

The average desorption rate of CO_2 from water droplets during formation and falling at different distances and droplet diameters increases as droplet diameter decreases and decreases as the contact time increases.

The experimental results on the ratio between CO_2 concentrations at a certain time and initial CO_2 concentration for droplet diameters 2.67 mm and 3.0 mm are in good agreement with the model from Hsu et.al [77], whereas for droplet diameter 1.61 mm the results fit Angelo's model [75] because of pulsation during formation.

Kurzfassung

BESTIMMUNG DES GAS-FLÜSSIGPHASEN-STOFFAUSTAUSCHES MITTELS EINZELTROPFENEXPERIMENTEN

Die Reduktion und Abtrennung von CO_2-Emissionen hat durch die Einschränkung der globalen Klimaerwärmung weltweite Beachtung erlangt. Eine mögliche Methode zur Reduktion des CO_2-Anteils in verschiedenen Abgasen ist die physikalische Absorption.

Ein sehr gängiger Prozess zur CO_2-Abtrennung ist die Gaswäsche in Sprühwäschern. Für die Wahl eines geeigneten Waschmediums und zur Konzeptionierung des Sprühturms ist ein detailliertes Verständnis des Massentransfers zwischen CO_2 und den einzelnen Tropfen notwendig. So sind die physikalischen Eigenschaften wie Tropfendurchmesser, Kontaktzeit zwischen Gas-Flüssig-Systemen und Stoffaustauschkoeffizienten für Auslegung und Optimierung von Absorptions- oder Desorptionskolonnen unumgänglich.

Um die Eigenschaften und Charakteristika des Stoffaustausches zwischen CO_2 und flüssigen Tropfen zu untersuchen, wurde ein Versuchsaufbau bestehend aus rechteckiger Gaskammer, Shadowgraphiesystem und Analytik zur Bestimmung des gelösten CO_2 erarbeitet. Dieses System ermöglicht die genaue Beobachtung von Tropfengröße, Tropfengeschwindigkeit und dem Verhalten der Tropfen während der Bildung und Fallphase.

Der Tropfengenerator erzeugt eine definierte Tropfenserie, indem Flüssigkeit über eine peristaltische Pumpe durch eine Nadel gepresst wird. Nachdem sich die Tropfen von der Nadel gelöst haben, fallen sie durch eine mit Stickstoff gefüllte Gaskammer, werden am Boden der Kammer aufgefangen und mit einer Schicht aus Kerosin überdeckt. Durch Verwendung einer

Hochgeschwindigkeitskamera können die Tropfengröße, Tropfengenerationszeit und die Tropfenfallgeschwindigkeit in der Kammer ermittelt werden. Die zugehörige Analyse der CO_2-Desorption der Wassertropfen erfolgt jeweils vor und nach dem eine Reihe von Tropfen erzeugt wurde. Der Flüssigphasen-Stofftransportkoeffizient der CO_2-Desorption aus Tropfen wird bei verschiedenen Tropfengenerationszeiten (0.2328 s, 0.859 s und 1.08 s), Tropfenfallhöhen (5 cm, 10 cm und 20 cm) und Tropfengrößen (1.61 mm, 2.67 mm und 3.0 mm) bestimmt.

Die ermittelten Tropfenfallgeschwindigkeiten aller Tropfengrößen dieser Studie zeigten eine hohe Übereinstimmung mit der Modellberechnung. Zudem konnten speziell bei geringen Fallhöhen große Ähnlichkeiten der Trends mit Experimenten von Takagaki und Komori [94] gefunden werden. Selbiges gilt für die Endfallgeschwindigkeit der Tropfen, welche mit Daten von Beard [95] vergleichbar waren.

Während die durchschnittliche CO_2-Desorptionsrate bei Tropfenbildung und Tropfenfall mit abnehmendem Tropfendurchmesser zunahm, wurde durch Erhöhung der Kontaktzeit eine Verringerung der Desorptionsrate festgestellt.

Die Versuchsergebnisse des Verhältnisses von CO_2-Konzentration bei einer definierten Zeit und dem ursprünglichen CO_2-Anteil, stimmten für Tropfendurchmesser von 2.67 mm und 3.0 mm gut mit dem Model von Hsu et.al [77] überein. Bedingt durch die Pulsation während der Tropfenbildung sind für einen Tropfendurchmesser von 1.61 mm vergleichbare Ergebnisse im Modell von Angelo [75] zu finden.

Acknowledgements

First and foremost, I would like to express my deepest gratitude to Allah Subhanahu Wa Ta'ala, the Creator, the Almighty God for the blessing, kindness, and inspiration in giving me to accomplish my doctoral program.

Sincere thanks to my academic supervisors Professor Markus Lehner and Professor Christian Weiß for their guidance, deepest knowledge and constructive suggestions on my experimental work.

This work is dedicated to my parents, my wife, my children, siblings and parents-in-law who have been constantly supported and prayed me while studying in Leoben.

I am also indebted to all colleagues in VTiU laboratory especially Hannes for teaching me how to operate the high speed camera and giving suggestion if I had problems, Mark for supporting technical drawing of absorption unit and other colleagues such as Philipp, Jan, Ana, Iris, Verena, Nici, Fritz for their sharing and suggestion, Christa and Heidi for administration support. I express my deepest appreciation to Lisa, a staff of OeAD Bureau of Montanuniversität Leoben for her assistance.

Last but not least, to all Indonesian students and Indonesian people in Leoben who have been helping me in many official and personal matters.

Finally, I would like to thank toward Ministry of Energy and Mineral Recourses of Republic of Indonesia and LEMIGAS for giving me a chance to get a doctoral degree and special thanks to PERTAMINA which financially supported me during my four years at Montanuniversität Leoben.

Anda Lucia
Leoben, November 2017

Table of Contents

List of Figures

List of Tables

1.INTRODUCTION

1.1 Background

Nowadays, the environmental issues related to carbon dioxide (CO_2) emission have been paid more attention in industries, especially power plants and oil processes, which used fossil fuel as primary energy. A high amount of carbon dioxide emission released to the atmosphere by industries and human activities cause global warming. The quantity of the carbon dioxide released to the atmosphere from fossil fuel for four last decades raise over the years as illustrated in Figure 1-1 and percentage of greenhouse gas emission by gas species can be seen in Figure 1-2.

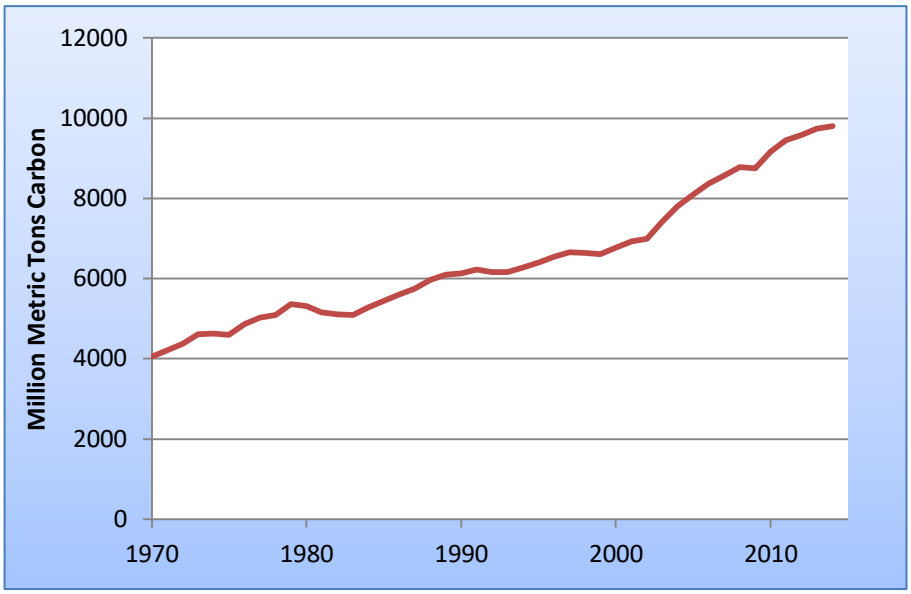

Figure 1-1 Global carbon emission from fossil fuel from period 1970-2014; redrawn from[1].

Carbon dioxide is the major greenhouse gas that contributes more than 60 percent of the greenhouse effect from combustion of fossil fuel and industrial processes [2]. For reducing global warming, more than 30 industrialized

nations and the European Union are pushed to diminish their greenhouse gas emissions to a level of 5.2 on average lower than those of 1990 during the period of 2008 to 2012 under Kyoto Protocol[3].

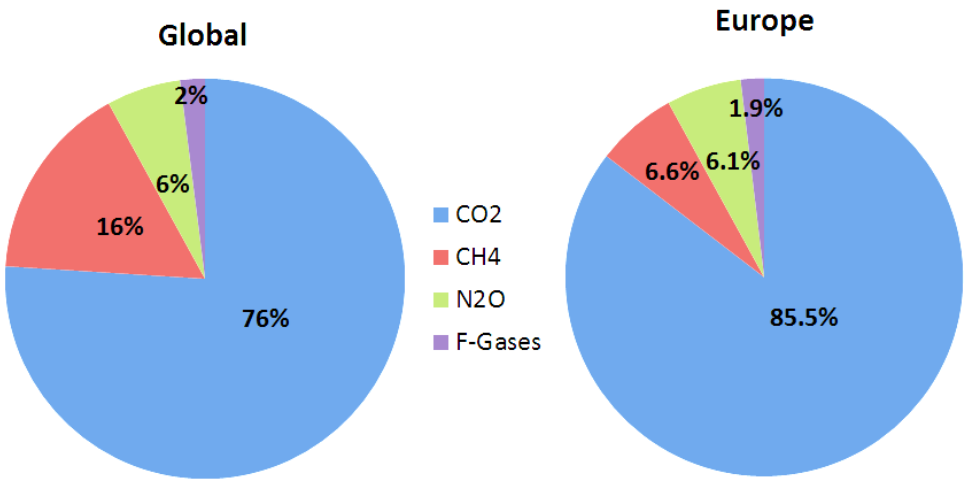

Figure 1-2 The Greenhouse Gas Emission by gas species in the World and in Europe [4, 5] (percent weight).

In order to capture only CO_2 from the combustion of fossil fuel or industrial processing, carbon dioxide must be separated from other gases. The main three technological options for CO_2 capture and separation are post-combustion, pre-combustion and oxy-fuel combustion[6]. Some technologies [7] have been applied for removal, capture, and separation of CO_2 from air or flue gas (see Figure 1-3) including physical absorption[8–10], chemical absorption[11–18], adsorption [8, 10], cryogenic techniques [19] and membrane separation [2].

Gas absorption is certainly the most significant industrial operation of gas separation mass transfer processes and is used in a wide amount. This process is often paired with a desorber for regeneration and recycling of the absorbent. Several publications of researchers point out that absorption remains attractive due to its high efficiency, and is a viable option for large-scale.

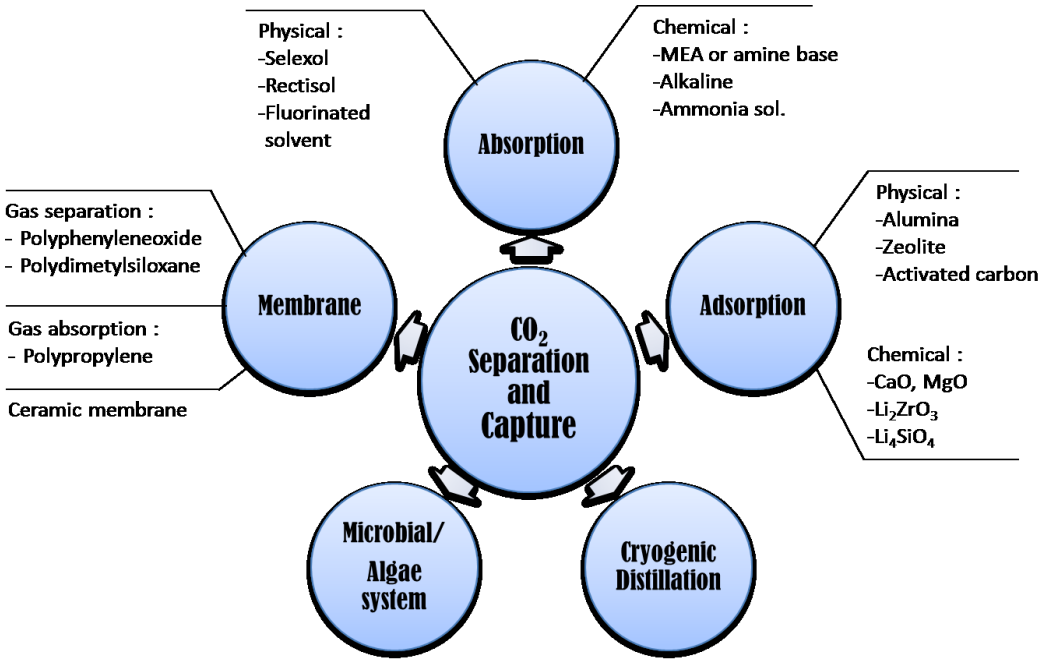

Figure 1-3 Technological alternatives for CO_2 capture and separation; drawn from various sources[20–22]

Chemical absorption is a process that utilizes a solvent which collects carbon dioxide such as amines. This solvent cause problems like equipment corrosion in the usage of amines for CO_2 absorption, and consumes a lot of energy during solvent regeneration. Cryogenic capture process involves drying, multiple compressions and cooling stages used directly to liquefy high purity carbon dioxide stream where gas forms a liquid. This method needs also huge energy amounts, and is only appropriate when the CO_2 concentration is very high. Membrane separation increases CO_2 purity as a multistage formation but lacks on the final recovery rate.

Gas absorption using an aqueous solution as solvent is applied in most of the industries for capturing CO_2 until 2030 [3] and is oftentimes took into account for large-scale CO_2 removal from flue gases [23]. Gas absorption, also known as scrubbing, is a unit operation in chemical engineering whereby a desired component in mixed gases are dissolved in a solvent as the bulk phase [24]. Gas absorption process for reducing CO_2 at most industries are commonly performed with a packed column or a spray tower.

Gas desorption or stripping is the opposite of gas absorption where the gas that dissolved in the solution is removed for other purposes, and for regeneration of the solvent. The principles for both systems are the same. The contact between the gas and the liquid phase is an important aspect in gas absorption or gas desorption.

Gas absorption in the form of a liquid spray in spray columns is a potential option for CO_2 capture from large point sources. A spray column has some advantages like a simple design, low gas phase pressure drop [11, 25], low maintenance cost [25], large surface contact area between gas-liquid phases[26], could be combined with other phase systems and the possibility of its application in liquid systems containing solids [27]. Spray column provides a high CO_2 absorption performance to a packed column because of the availability of a larger interface area [26, 28, 29]. In-depth knowledge of the mass transfer in the spray column is needed for the design of the column. Furthermore, predictions of liquid phase mass transfer have to consider the spray formation process.

From earlier studies[30–34], the form of liquid phase in the gas absorption can be divided into two main types: dripping droplets and streaming droplets. A few researchers investigated the absorption of CO_2 in pure water for improvements in process of remineralization of soft water and photo bioreactor design[35]. Research on CO_2 gas desorption from water droplets has not been widely performed, especially for a single droplet.

The aim of this study is to give a useful contribution to the knowledge and understanding of transport phenomena in gas-liquid systems, especially focusing on the desorption of CO_2 from water droplets into a nitrogen atmosphere.

1.2 Motivation of this study

Among the technologies which effectively separate CO_2, absorption in spray columns is an appropriate option. The scheme of solving the CO_2 gas emission in spray columns and the CO_2-water droplet system can be seen in the Figure 1-4.

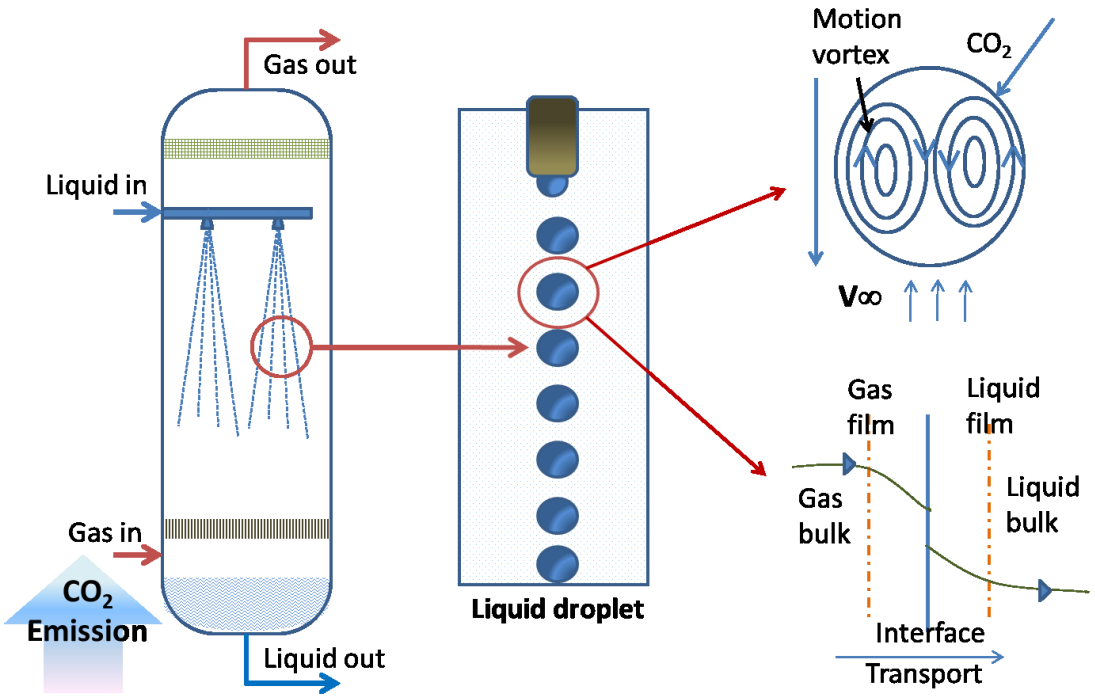

Figure 1-4 Scheme of problem-solving with mass transfer approach.

Spray columns are usually operated in counter-current flow, where the gas is introduced to the column in the bottom section and flows upwards, whereas the liquid is dispersed by spray nozzles and finally forms droplets falling down. The mass transfer between the gas phase and the liquid droplet may be influenced by induced internal flows in the droplet, as well as the transport resistance at the gas-liquid interface.

Absorption of CO_2 by is often considered to be the most cost effective and viable option for large scale CO_2 removal from flue gas, but these technologies are considered to be too expensive, because the flow rate of

the flue gas is large, the pressure close to atmospheric, and the CO_2 volume fraction is low.

Spray column can potentially be applied for absorbing CO_2 from large emission sources. Advantages are a large surface area for gas absorption, low gas phase pressure drop, potential application for gas phase containing dispersed solids, a simple design and low maintenance cost. However, the performance of spray columns cannot be well predicted because drop size, and distribution, collision and coalescence between drops, internal circulation and oscillation and distortion of droplets in column are influencing the mass transfer. The data on absorption of CO_2 in aqueous sprays is rare and partially contradictory in literature.

Mass transfer data for CO_2-liquid systems is required for vigorous design of spray columns. Further, the absorption efficiency of sprays is highly influenced by the surface area of droplets or droplets diameter. Measurement of droplet diameter and droplet velocity is very important in providing a basic concept into spray absorption. However, experimental investigations for a precise droplet diameter measurement in aqueous sprays have not been widely performed.

Some investigators [30][31] measured only the droplet diameter by weighing which are collected after falling, and droplet volume as well as droplet velocity is calculated manually, where for latter the falling droplet height is divided by the travel time. Recent research [36] was conducted using precision equipment like high speed camera, but the resulting data is still not detailed and conflict with the results of other researchers.

There are still some data conflicts over mass transfer in droplets, for example, whether droplet formation or droplets falling is dominating the mass transfer. Therefore, more research is needed to ensure the role of each of these stages for mass transfer. More precise observations are required by means of a high speed camera with shadowgraph method, especially on the

measurement of droplet diameter and droplet formation time as well as for the determination of the free falling droplet velocity. The present study is a step towards addressing this knowledge gap using a chemical analysis method for concentration of CO_2 in liquid, and comparing the obtained results with existing equation models. Until now, studies of CO_2 gas desorption from water droplets have not been investigated in detail, which is the primary motivation for the selection of this system.

1.3 Objectives

The objective of the work is to obtain the physical characteristic of the water droplet (droplet diameter and velocity) under variation of the droplet diameter and the free falling height, and to investigate mass transfer characteristics between CO_2 and water droplets. The main targets are:

a. Measure droplet diameter, droplet velocity and contact time (during formation and falling) by means of shadowgraph method (high-speed camera equipped with Davis software). Compare the measured data with a calculation, and analyze the uncertainties of the droplet diameter and droplet velocity.

b. Develop an analytical method to determine the concentration of CO_2 in water accurately in a certain range of concentration.

c. Create a new experimental set-up to study mass transfer characteristics between CO_2 and liquid droplets. Determine liquid phase mass transfer coefficients of CO_2 desorption from water droplets at different droplet diameters, droplet formation times, and droplet falling heights. Compare the liquid phase mass transfer coefficients of CO_2 desorption from liquid droplets with some model equations from literature.

d. Calculate and analyze the dimensionless number of experiments and compare with existing models.

1.4 Hypothesis

Accurate measurements of water droplet characteristics (droplet diameter and droplet velocity) will be the basis for obtaining better mass transfer data. Later this data can be used in optimization and design of spray columns. Furthermore, the investigations determine the role of the droplet formation in the mass transfer of the CO_2 water droplet system.

Using the precipitation-titration method for determination of the CO_2 concentration in water is expected to result in a more accurate analysis in low concentration range also with a small sample volume which is intended for the single droplet monitoring of CO_2 absorption/desorption.
The obtained experimental data shall match to the existing model equations for both the liquid mass transfer coefficient and the dimensionless Sherwood number from literature.

1.5 Dissertation layout

The dissertation consists of five chapters. Chapter 1 introduces the fundamentals of CO_2 capture technology, the background and objectives of this study. The gas liquid contactor, mechanism of droplet formation, droplet velocity, the technical process, experimental parameters and reaction mechanism of water with CO_2 were discussed. The theories of mass transfer between gas-liquid phases and literature review from some references are presented in Chapter 2, including three fundamental mass transfer theories, mass transfer models between liquid droplets and a continuous phase and literature review of some corresponding investigations.

Chapter 3 summarizes the experimental set-up and analytical method. This chapter describes the various apparatus which are used in this study such as a high-speed camera and long-range microscopes, saturation equipment, a design and manufacture of absorption/desorption chamber and measurement

of CO_2 concentration using automatic titration. The verification of the method is also discussed in this chapter.

Chapter 4 presents the physical properties measurement, analysis of CO_2 concentration, desorption rate during formation and falling, experimental data of the mass transfer study of CO_2 desorption from water droplets, comparison with model equations for physical properties measurement, comparison with models equation from literature for mass transfer coefficient calculation and also includes the discussion section.

The conclusions of this work are summarized in Chapter 5. Moreover, the suggestions for the future work, mainly on the droplet chamber experiments, the use of mechanical electrical traversing system is a breakthrough that can be applied in order to capture an object or picture without changing the gas chamber and the use of piezoelectric generator which serves as an alternative to produce small droplets with micro diameter range.

2. THEORY AND LITERATURE REVIEW

2.1 Gas-liquid contactor

There are many different types of contactors used in industry for ensuring a good contact between the gas and liquid streams like tray column, packed column, bubble column and spray column. There are several key parameters for designing columns for CO_2 absorption like physical properties of gas and liquid involved in the system and internal data of the absorber [37]. A good understanding of the behavior of gas-liquid contactors is essential for design purposes to obtain an efficient separation process that requires a minimal size for the absorber. Mass transfer can take place from the liquid phase to gas phase or vice versa. Chemical reactions may occur in the gas and/or in the liquid phase respectively [38]. The contactors usually apply one of the mechanisms[39]:

a. Spreading the liquid into a thin film that flows through a continuous gas phase (e.g. tray column; packed column).
b. Contacting between the continuous liquid phase and gas phase in form of gas bubble (e.g. bubble column)
c. Forming the liquid phase as small droplets in a continuous gas phase (e.g. spray column).

A spray tower is one of the gas-liquid contactors that is commonly used. It has some advantages: low-pressure drop, simple design and the possibility of its application in three-phase systems [40] especially solid dispersed in liquids. The liquid is sprayed from one or more levels and moves downward, while the gas stream usually enters the bottom of the tower and moves upward. This flow is called countercurrent flow. Typical absorber and desorber setups for CO_2 separation can be seen in Figure 2-1.

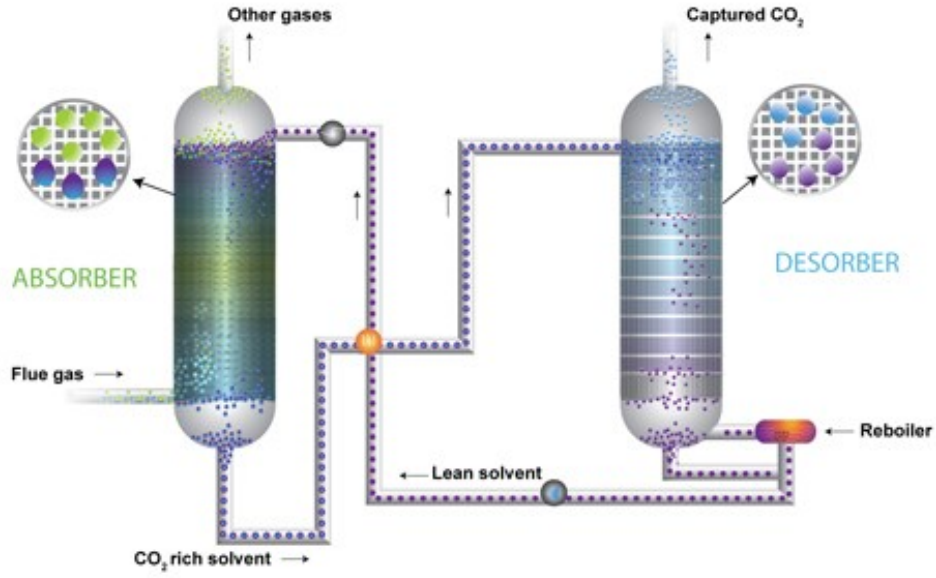

Figure 2-1 Typical CO_2 capture using absorber and desorber[41]

In Figure 2-1, an absorber column can be designed as a spray column, a packed column or a bubble column. In this study, the focus is on the spray column with some reasons that have been presented in the previous section. The flue gas (for example, containing CO_2) is fed into the absorption column (absorber) and gets in contact with the solvent (water/chemical) in countercurrent flow. The CO_2-rich solvent will be regenerated to recover the solvent and separate the CO_2 in the stripping column (desorber).

2.2 Droplet formation

The first scientist who investigated the droplet generation due to jet instabilities was Rayleigh in 1878[42]. A deep knowledge of basic phenomena, principles, and mechanisms in droplet processes is needed in order to increase the efficiency of droplet formation and to handle droplet properties.

There are four common types of droplet formation based on the characteristic of bulk liquids [43]:

a. Liquid dripping
b. Liquid jet breakup
c. Liquid ligament breakup
d. Liquid film breakup

The liquid dripping is type of droplet formation that is used in this work. The liquid dripping is the simplest mode among other modes of droplet formation. This mode is frequently observed in nature. In a laboratory, this mode can be seen by forcing liquid through a needle or syringe by means of a pump or mechanical force, and the liquid drops fall under its own weight. The water dripping out from a syringe and liquid jet breakup from a nozzle are shown in Figure 2-2.

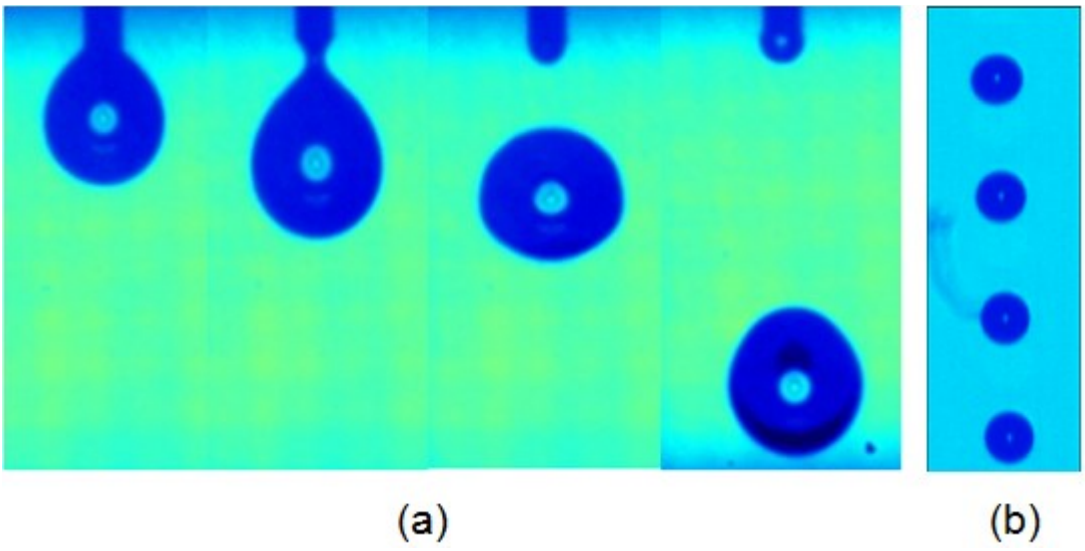

Figure 2-2 (a) Water dripping (droplet diameter 2.67 mm) and (b) stream droplet from nozzle diameter 100 μm (droplet diameter 187 μm)

The form of a droplet when falling freely in the air under the influence of gravity and friction resistance, generally grouped into either spherical or ellipsoidal (oblate or prolate spheroid) [44]. The small diameter droplets (< 1 mm) tend to form spheres when they fall free in the atmosphere.

When the gravity force on the liquid exceeds surface tension force, the liquid will be withdrawn away from its attachment and forms a droplet. The gravitational and surface tension forces on the droplet govern the formation

process of the droplet and determine the droplet's mass and diameter in case the flow velocity of the liquid in the dripping mechanism is low. The stream droplets are produced by pumping a liquid through a needle and by pressing the liquid with inert gas (N_2) through a piezoelectric nozzle.

The droplet diameter can be calculated from the following equation based on the force balance [43] (this equation is valid only for spherical droplet):

$$d_d = \left(\frac{6 \cdot d_n \cdot \sigma}{\rho_L \cdot g}\right)^{1/3} \quad 2\text{-}1$$

Here d_d is the droplet diameter, d_n is the diameter of nozzle, σ is the surface tension, ρ_L is the density of liquid and g is the gravity.

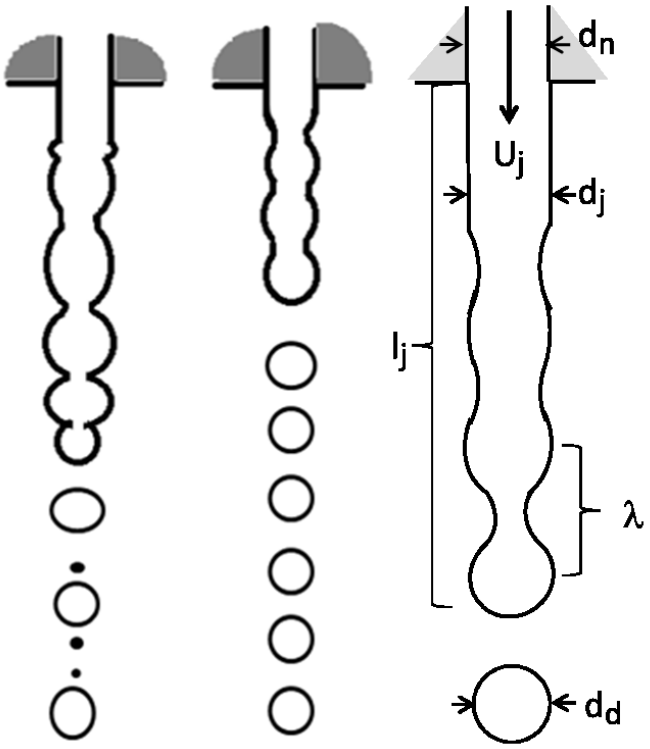

Figure 2-3 Breakup mechanism of Rayleigh theory, redrawn from[43, 45]

When a liquid jet comes out from a nozzle, due to capillary instability, the jet will break up into a stream of droplets[42] as illustrated in Figure 2-3. Rayleigh theoretically defined that an inviscid liquid jet in vacuum breaks up

into droplets if $l_j/d_j > 3$ (l_j is the length of the jet column and d_j is the jet diameter). Rayleigh also pointed out that the droplet diameter is about nine times the jet radius for the unstable wavelength.

Rayleigh developed a linear stability analysis of the inviscid laminar jet finding the dimensionless wavelength, λ/d_j, in this case, λ is the distance between two wave peaks that will form a droplet, corresponding to the maximum growth rate factor to be:

$$\frac{\lambda}{d_j} = 4.508 \qquad 2\text{-}2$$

The droplet diameter can be predicted using the correlation of jet diameter and droplet wavelength if a constant density and spherical shape are assumed, the droplet diameter, d_d, can be calculated by the following expression:

$$d_d = d_j \left(\frac{3\lambda}{2d_j}\right)^{1/3} \qquad 2\text{-}3$$

A relation between droplet diameter and the jet diameter can be found by substituting Equation 2-2 into Equation 2-3. The droplet diameter is approximately twice of the jet diameter:

$$d_d = 1.89 d_j \qquad 2\text{-}4$$

2.3 Droplet velocity

Droplets falling through the air have two forces working on the droplets. The first force is the force of gravity, expressed as the droplet weight (W), which pulls the droplet toward the earth and the second force is the viscous drag force of the droplet (F_D) which pushes a droplet rather against the velocity direction (see Figure 2-4). In this case buoyant force (F_b) is neglected.

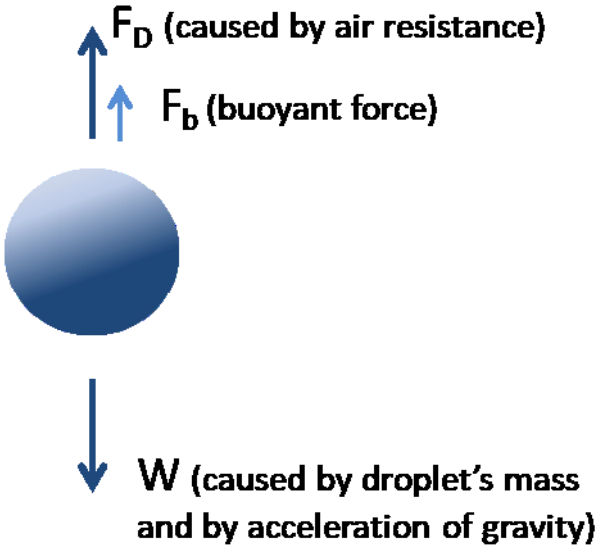

Figure 2-4 Forces acting on a falling droplet [46]

The weight equation W is defined as the mass droplet (m) times the gravitational acceleration (g):

$$W = mg \tag{2-5}$$

The viscous drag force, F_D is can be calculated by the coefficient of resistance C_D times one half of the air density ρ_G times the velocity of droplet U_d square times the reference area of droplet A as:

$$F_D = \frac{1}{2} C_D \rho_G A_d {U_d}^2 \tag{2-6}$$

Droplet terminal velocity is calculated by integrating the motion equation (Eq. 2-8) derived from the force balance between the drag force and the gravitational acceleration for the air-droplet system. The equations of motion can be expressed as:

$$F = ma = mg - F_D \tag{2-7}$$

$$m\frac{dU_d}{dt} = mg - \frac{1}{2}C_D\rho_G A_d {U_d}^2 \qquad 2\text{-}8$$

By integrating Eq. 2-8 with boundary condition $U_d = 0$; $U_d = U(t)$ at $t = 0$; $t = t$, respectively, we find the droplet velocity as:

$$U(t) = U_t\left[1 - exp\left(\frac{-2gt}{U_t}\right)\right]^{1/2} \qquad 2\text{-}9$$

Where, $U_{(t)}$ is droplet velocity, U_t is terminal velocity and t is time.

2.4 Mass transfer in gas-liquid systems

The transport of one substance from a side of higher concentration to that of a lower concentration is called *mass transfer* [47]. When it occurs over the phase boundary into another phase, it is then called *overall mass transfer* [48]. Gas-liquid absorption is a process in which one or more species transfer from the bulk of a gas phase to a gas-liquid interface, and then across the interface into the liquid phase, and finally diffuses from the interface into a bulk of a liquid phase [24, 39] and vice versa in gas desorption.The mechanism of this mass transfer is shown in Figure 2-5. In this study, the liquid was in the form of a droplet.

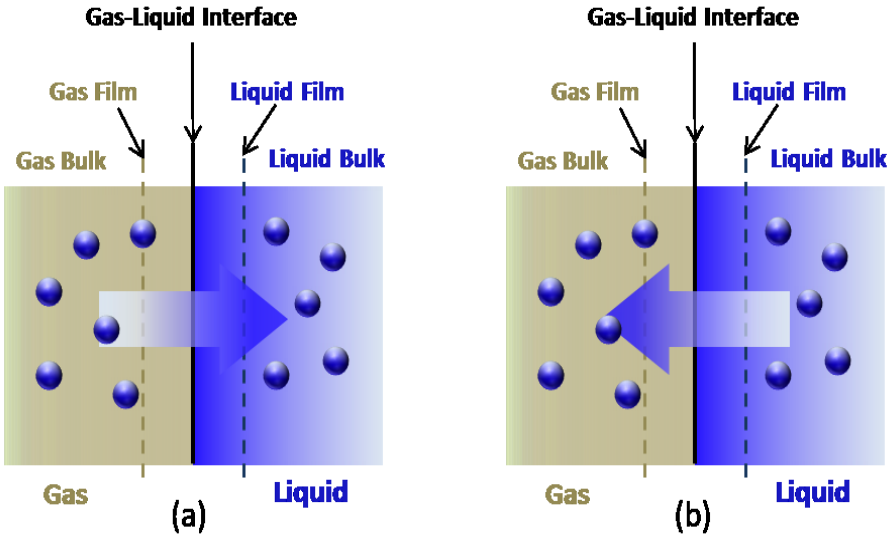

Figure 2-5 Mechanism of mass transfer for gas-liquid mass transfer (a) Absorption (b) Desorption, redrawn and modified from [49]

There are two common types of gas-liquid absorption: physical or chemical absorption. Physical absorption or non-reactive absorption takes place between two phases of matter: a liquid absorbs a gas, occurs when the component being absorbed is more soluble in the liquid absorbent than other components of the gas stream but does not react chemically with the absorbent. For example, water may absorb carbon dioxide from the air. The rate of mass transfer at the interface between the liquid and the gas depends on the solubility of gases, the pressure and the temperature of operation and also the surface area and contact time. At very short contact time, the absorption of CO_2 could be taken into account as physical absorption without any escalation due to the chemical reaction [50].

In the case of chemical absorption or reactive absorption, a chemical reaction takes place between the absorbed compound and a reactant in the solvent phase. Mass transfer depends upon the kinetic of the reaction and the concentration of its reactants. The removal of acid gases, such as CO_2 and H_2S from natural gas, by amine solutions, is one example for the application of gas absorption in industry.

The two common mechanisms of mass transfer are (1) molecular diffusion and (2) eddy (turbulent) diffusion. Molecular diffusion by random and spontaneous microscopic motion of molecules and eddy diffusion by random, macroscopic fluid motion [24]. Both of them may involve the movement of different species in different directions. Mass transfer in molecular diffusion is extremely slow but in eddy diffusion, the mass transfer is orders of magnitude more rapid. Molecular diffusion takes place in fluids that are stagnant, or in laminar or turbulent motion. Eddy diffusion takes place in fluids when turbulent motion exists. Examples are: absorption of gas components in a liquid phase in turbulent flow (high Reynolds number >4000) or in a stirred tank.

In gas absorption, the rates of mass transfer are controlled by the driving force that occurs and resistance to the mass transfer by the streams of liquid

and gas [51, 52]. The driving force is the concentration difference between the actual concentrations and the equilibrium concentrations. For the resistance, the two-film theory, as a simple model, assumes a gas film resistance and a liquid film resistance.

Mass transfer between the gas phase and the droplets of water depends on the physical properties of the gas diffusion, droplet diameter and hydrodynamic characteristics in and outside of the droplets.

2.5 Fick's law of diffusion

The rate of diffusion is dictated by Fick's Law and was proposed by Adolf Fick in 1855. Fick's first law can be used to derive his second law which in turn is identical to the diffusion equation. Fick's first law relates the diffusive flux from high concentration to low concentration or as a function of a concentration gradient. Fick's Law for steady state diffusion, in a mixture of two component gases A and B, may be written as (one-dimensional, for example y-axis):

$$N_{\mathrm{A}} = -D_{\mathrm{AB}} \frac{dc_{\mathrm{A}}}{dy} \qquad 2\text{-}10$$

N_A is the molar flux of component A, D_{AB} is the diffusion coefficient or diffusivity for components A in phase B, c_A is the concentration of component A in phase B and y is the distance in the direction of transfer. The equation (2-10) is valid when the concentration gradient dc_A/dy is linear, e.g. diffusion controlled mass transfer in boundary layer.

The diffusion coefficients in the gas are 3-4 orders of magnitude higher than those in the liquid; therefore, the resistance to mass transfer in spray columns is controlled by the liquid-phase resistance (dispersed-phase) [53]. This situation is valid if the absorption is physically and the gas is slightly soluble in the liquid. A highly soluble gas is controlled by the diffusion of gas

that passes through the gas film layer, while the slightly soluble gas is controlled by diffusion in the liquid film layer [54].

2.6 Theory of mass transfer models

There are four common gas-liquid mass transfer models which are described below.

2.6.1 The two-film theory

The two-film theory is the first and the simplest mass transfer model [55, 56]. The theory is proposed by Whitman in 1923. The assumptions for two film theory are as follows:

a. The mass transfer by molecular diffusion occurs through the two stagnant films, gas film, and liquid film, in steady state.
b. The mass transfer resistance occurs near the interface between two stagnant liquid and gas films with finite thickness, δ_L and δ_G. The resistance in the turbulent zone beyond the film can be neglected.
c. The total mass transfer resistance is the amount of the resistance in both films. The equilibrium of gas-liquid phases takes place at the interface.

The mass transfer coefficient, according to the two film theory can be expressed as:

$$k_L = \frac{D_L}{\delta_L} \qquad 2\text{-}11$$

Where k_L is the liquid-side mass transfer coefficient, D_L is the diffusion coefficient of liquid side and δ_L is the thickness of the film on the liquid side. k_L cannot be derived from the model itself because δ_L is unknown. This model is appropriate for the mass transfer without any clear interference at the interface.

The gradient concentration of the two-film theory is shown in Figure 2-6. The mass transfer k_L is linearly proportional to D_L and inversely proportional to δ_L but in an experimental result, the dependency of mass transfer coefficient on the diffusivity predicted by this theory is varied. In the gas phase, the partial pressure of A, $p_{Ab,}$ decrease after passing through a gas film to p_{Ai} adjacent to the interface between the two phases. Meanwhile, the concentration of component A, c_{Ai} from the interface decreases through a liquid film to c_{Ab} in the bulk liquid. There is a concentration gap at the interface due to ordinary equilibrium is assumed.

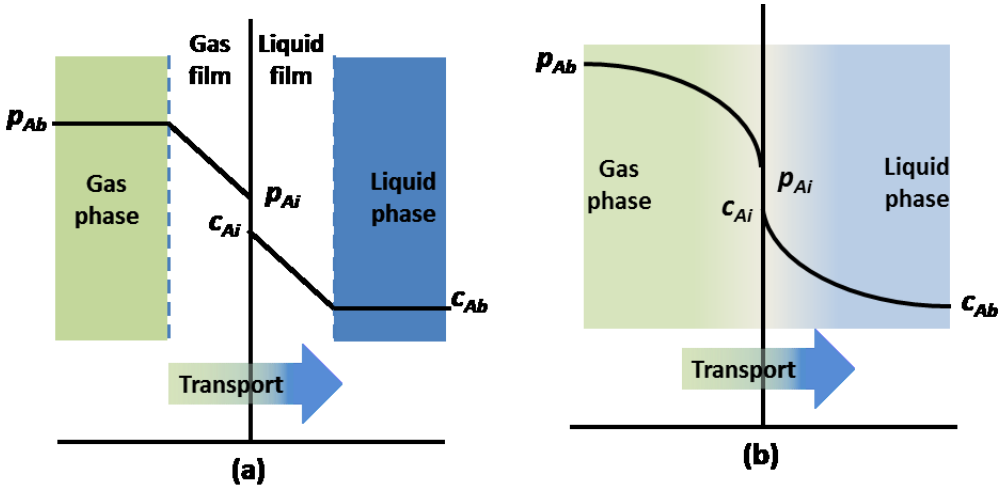

Figure 2-6 Concentration gradient for two film theory: (a) unrealistic gradient (b) realistic gradient, redrawn from [24].

2.6.2 The penetration theory

Higbie developed the penetration model in 1935. He observed whether or not a resistance to transfer occurred at the interface when a pure gas was absorbed in a liquid [57]. Higbie defined that the contact time between phases are too short for the steady state to be accomplished in many situations. The interface consists of a kind of micro liquid elements, which are continuously moved up to the surface from the bulk of the liquid by the movement of the liquid phase itself. The description of penetration theory can be seen in Figure 2-7. It is assumed that if t_e is the exposure time that a solute permeates from the interface to depth direction in liquid film gradually, and then the liquid mass transfer coefficient is given by:

$$k_L = 2\sqrt{\frac{D_L}{\pi t_e}} \qquad 2\text{-}12$$

Here t_e is the exposure time which is also not known a priori. It can be assumed as the ratio of the droplet diameter to the droplet velocity.

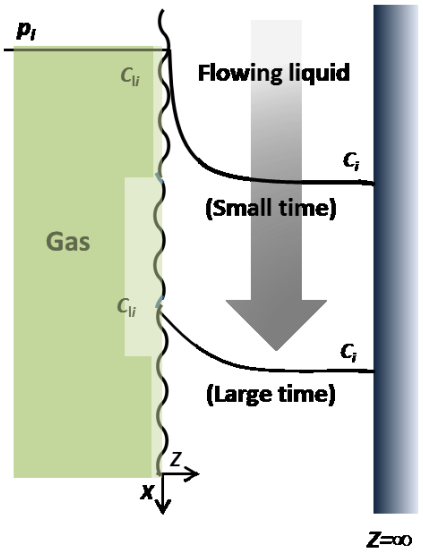

Figure 2-7 The graphic description of penetration theory, redrawn from [57]

2.6.3 The surface renewal theory

Danckwerts proposed the surface renewal theory in 1951. He improved the penetration theory of Higbie. He postulated that a part of the mass transfer surface is displaced with a fresh surface by the motion of eddies close the surface and suggested the following assumptions:

1) At the interface, the liquid element is exchanged randomly by fresh elements of the bulk
2) Each of the liquid elements at the surface has the same probability of being replaced by fresh element at any moment
3) Unsteady state mass transfer occurs to a constituent during its remain at the interface [58].

The illustration of the surface renewal theory is shown in Figure 2-8. The mass transfer coefficient in the surface renewal theory can be deduced as:

$$k = \sqrt{Ds} \qquad 2\text{-}13$$

Where *s* is the fractional rate of surface renewal [59, 60]

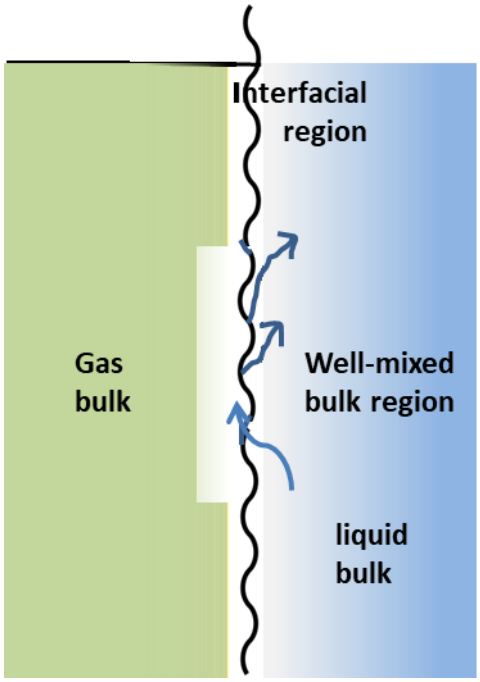

Figure 2-8 The graphic description of surface renewal theory

2.6.4 The Film-Penetration theory

Toor and Marcello proposed a film-penetration model in 1958 in which a stagnant film of definite thickness exists at the surface but is replaced piecewise from time to time by a liquid having the bulk composition [61]. If all the parameters are kept constant, then the model correlates with the equation as follows:

$$k = \alpha D^{\beta} \qquad 2\text{-}14$$

Here α is a constant and the value β gets the following value: β = 1 in the film model (long time), β = 0.5 represents the penetration model and the film-penetration model can get values $0.5<\beta<1$.

The liquid mass transfer coefficient (k_L) is proportionate to the diffusivity (D_L) in the Two-Film theory and the other models depend on square root of D_L. There is an unknown parameter for each model namely: δ_L for the Two-Film theory, t_e for the Penetration Theory, s for the Surface-Renewal Theory and α for the Film-Penetration theory, which constrains their application.

2.7 Mass transfer equation.

The general rate of mass transfer of a component through the gas boundary layer is[47]:

$$N = k_g (C_{gb} – C_{gi}) \quad 2\text{-}15$$

The rate of mass transfer of a component through the liquid boundary layer is:

$$N = k_l (C_{li} – C_{lb}) \quad 2\text{-}16$$

where:

N	= molar flux of a component [mol/m^{2}s]
k_g	= individual mass transfer coefficient in gas phase [m/s]
k_l	= individual mass transfer coefficient in liquid phase[m/s]
C_{gb}	= solute concentration in gas bulk phase [mol/m^3]
C_{gi}	= solute concentration at interface gas phase [mol/m^3]
C_{li}	= solute concentration at interface liquid phase [mol/m^3]
C_{lb}	= solute concentration in liquid bulk phase [mol/m^3]

And then Eq. 2-15 and Eq. 2-16 become;

$$N/k_g = C_{gb}–C_{gi} \quad 2\text{-}17$$

$$N/k_l = C_{li}– C_{lb} \quad 2\text{-}18$$

The interfacial solute concentration,C_{gi} , can be lower, equal or greater than C_{li}. The relation is dictated by the value of Henry's constant, Figure 2-9.

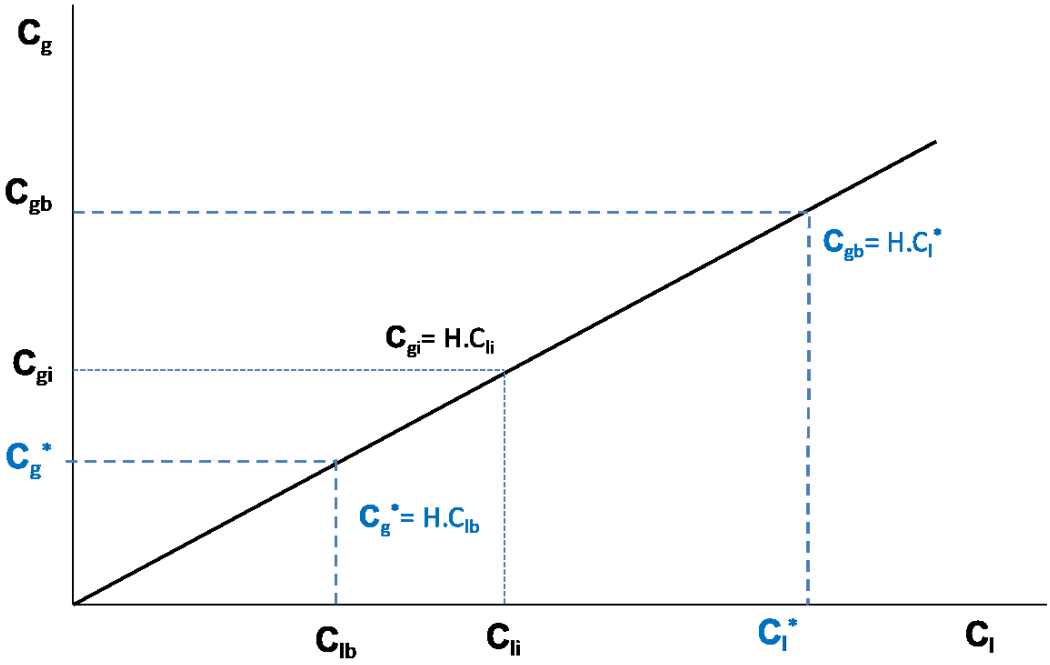

Figure 2-9 Gas-Liquid Equilibrium Curve

Phase equilibrium is assumed at the gas-liquid interface.
Applying Henry's law,

$$H = C_{gi} / C_{li} \qquad 2\text{-}19$$

In order to calculate the overall gas phase mass transfer coefficient, the equilibrium concentrations at the interface are needed. The overall coefficients are based on the difference between the bulk concentration in one phase and the concentration that would be in equilibrium with the bulk concentration in the other phase.

The concentration of gas in equilibrium with the solute concentration of liquid in bulk liquid is stated as C_g^*.

$$C_g^* = H\, C_{lb} \qquad 2\text{-}20$$

The concentration of liquid in equilibrium with the solute concentration of gas in the bulk gas is stated as C_l^*.

$$C_l^* = C_{gb} / H \quad \text{2-21}$$

The molar flux and an overall gas phase mass transfer coefficient (K_G) as

$$N = K_G (C_{gb} – C_A^*) \quad \text{2-22}$$

Rearrange Eq. 2-22 became

$$N = K_G [(C_{gb} – C_{gi}) + (C_{gi}–C_g^*)] \quad \text{2-23}$$

And then substitution with Eq. 2-16, 2-19 and 2-20 to 2-23 (and multiply each coefficient of mass transfer with total concentration of each phase, $C_{g,tot}$ and $C_{l,tot}$, respectively) became

$$\frac{1}{K_G C_{g,tot}} = \frac{1}{k_g C_{g,tot}} + \frac{H}{k_l C_{l,tot}} \quad \text{2-24}$$

The molar flux and an overall liquid phase mass transfer coefficient (K_L) as

$$N = K_L (C_l^* – C_{lb}) \quad \text{2-25}$$

Rearrange Eq. 2-25 became

$$N = K_L [(C_l^* - C_{li}) + (C_{li} – C_{lb})] \quad \text{2-26}$$

And then substitution with Eq. 2-18, 2-19 and 2-21 to 2-26 (and multiply each coefficient of mass transfer with total concentration of each phase, $C_{g,tot}$ and $C_{l,tot}$, respectively) became

$$\frac{1}{K_L C_{l,tot}} = \frac{1}{H k_g C_{g,tot}} + \frac{1}{k_l C_{l,tot}} \quad \text{2-27}$$

When solute of a component is very soluble in the liquid, for example, ammonia in water (H is very small), the liquid-phase resistance is small compared with that posed by the gas interfacial film, therefore,

$$\frac{1}{k_l C_{l,tot}} \ll \frac{1}{H k_g C_{g,tot}} \quad 2\text{-}28$$

$$\frac{1}{K_L C_{l,tot}} = \frac{1}{H k_g C_{g,tot}} \quad 2\text{-}29$$

$$K_L C_{l,tot} = H k_g C_{g,tot} \quad 2\text{-}30$$

Mass transfer is controlled by gas film resistance.

Conversely, if a component is poorly soluble in the liquid, e.g. carbon dioxide in water, the liquid-phase mass transfer resistance dominates and k_g is much larger than k_l, thus:

$$\frac{1}{k_l C_{l,tot}} \gg \frac{1}{H k_g C_{g,tot}} \quad 2\text{-}31$$

$$\frac{1}{K_L C_{l,tot}} = \frac{1}{k_l C_{l,tot}} \quad 2\text{-}32$$

$$K_L = k_l \quad 2\text{-}33$$

Mass transfer is controlled by liquid film resistance.

Combining equation 2-24 and 2-27 results in:

$$\frac{1}{K_G C_{g,tot}} = \frac{H}{K_L C_{l,tot}} = \frac{1}{k_g C_{g,tot}} + \frac{H}{k_l C_{l,tot}} \quad 2\text{-}34$$

2.8 Mass transfer equation for gas absorption by a falling droplet

Gas absorption into the liquid where the liquid is a droplet, is a common process used in industry, because of a large contact area and efficiency of mass transfer. The liquid droplets are called the disperse phase, and the gas is the continuous phase. Those gas-liquid systems are used for absorption or desorption processes, wherein a non-equilibrium system will tend to approach equilibrium.

The liquid phase resistance (in mass transfer) has an important role in controlling the absorption process because the molecular diffusion coefficient of a component is some orders of magnitude higher in gases than in liquids, the gas phase mass transfer coefficient is much greater than liquid phase mass transfer coefficient, in most of the gas-liquid experiments [33].The ratio of the gas phase mass transfer coefficient to the liquid phase mass transfer coefficient was about 10-15 on damped wall columns, a column of gas bubbles and droplets spray [62].

In general, there are three periods of gas absorption in liquid phase during droplet life-time: droplet formation, droplet falling and droplet coalescence [44, 63, 64]. The liquid phase mass transfer coefficient between liquid droplets and gas without chemical reaction is derived on the following assumption:

a. during formation and falling, the droplet is spherical;
b. during formation at a constant flow rate, the droplet grows;
c. the droplet diameter and droplet formation time is constant;
d. the experiment is in accordance with Henry's law and the equilibrium of absorption occurs at the gas-liquid interface.

The mass balance equation of gas absorption into liquid droplets without chemical reaction and constant droplet diameter (during falling) is given by:

$$V_d \frac{dc}{dt} = k_L A_d (c_l^* - c) \qquad 2\text{-}35$$

Integrating Eq. 2-35

$$\int \frac{dc}{(c_l^* - c)} = k_L \frac{A_d}{V_d} \int dt \qquad 2\text{-}36$$

$$\ln|c_l^* - c| = \frac{6k_L}{d} t \qquad 2\text{-}37$$

with boundary condition (at $t=t_1$, $c = c_1$; at $t = t_2$, the concentration is c_2):

$$\ln(c_l^* - c_2) - \ln(c_l^* - c_1) = \frac{6k_L}{d}(t_2 - t_1) \quad 2\text{-}38$$

$$k_L = \frac{d}{6(t_2 - t_1)} \ln\left(\frac{c_l^* - c_2}{c_l^* - c_1}\right) \quad 2\text{-}39$$

or from Eq. 2-39 rearranging:

$$\frac{c_l^* - c_2}{c_l^* - c_1} = exp\left[-\frac{6k_L}{d}(t_2 - t_1)\right] \quad 2\text{-}40$$

This equation was used to obtain the liquid phase concentration of CO_2 (c_2) in the models of for mass transfer coefficients (Table 2-1). More detailed explanation and results can be seen in section 4.8 (see Table 4-8 and Table 4-10).

2.9 Parameter used in experimental desorption

The concept of absorption or desorption of gas into/out of a liquid is based on the fact that a liquid-gas system, which is not in equilibrium, tends to approach equilibrium. So gas absorption occurs if the liquid is under saturated with certain gas and desorption occurs if the liquid is over saturated with certain gas. For example, water saturated with CO_2 at a given temperature will not desorb CO_2 or absorb further CO_2, if the CO_2 partial pressure in the atmosphere is in equilibrium with the liquid bulk.

There are several operating parameters associated with experiments that affect the physical desorption rate of a gas in the droplets, such as droplet diameter/surface area, the velocity of drops, temperature[65], partial pressure of gas[65], diffusivity of gas in liquid and solubility of gas in liquid[55].

2.9.1 Physical properties of droplet

Some physical properties are needed for calculation of the mass transfer coefficient. Droplet diameter and droplet velocity are the important physical parameters that influence the mass transfer besides the diffusion coefficient and solubility of gas in a liquid phase.

The diameter of a droplet defines the surface area which is the contact area between gas and liquid (in case of a spherical droplet). The larger the surface area or contact area, the higher the total transferred mass. The surface-volume ratio of small droplets is larger than that of large droplets.

The droplet velocity is correlated with contact time. The longer the contact time, the higher the total transferred mass. The temperature has a small impact on the initial absorption rate [62]

2.9.2 Gas solubility

The solubility of a component gas in liquid or solvent basically depends on the physical and chemical properties of the gas and the liquid such as on temperature, pressure and the pH of the solution. The extent of the solubility of gas in a liquid is measured as the saturation concentration, where adding more of a component gas does not increase the concentration of gas in bulk liquid.

The solubility of gases in a liquid solution at a certain temperature is important for calculating the overall mass transfer coefficient. Henry's law described physical solubility of the gas phase in the liquid phase. The solubility of a gas in a liquid is directly proportional to the partial pressure of that gas above the liquid. This relationship is shown as:

$$H' = \frac{p}{c_g^*} \qquad 2\text{-}41$$

Here H' is Henry's coefficient, p partial pressure of gas and c_g^* is a concentration of dissolved gas in the liquid at equilibrium.

Diffusivity or diffusion coefficient is a constant related to the ability of a component to move from one place to another because of differences in concentration. The diffusivity follows Fick's law, Eq. 2-10.

2.10 Carbon dioxide-water system

There are four different forms of carbon dioxide which may exist in aqueous solution: dissolved carbon dioxide CO_2 (aq.), carbonic acid H_2CO_3, bicarbonate ion HCO_3^-, and carbonate ion CO_3^{2-}. The relative concentrations of them are dependent on pH [62, 66, 67].

Carbon dioxide compared to sulfur dioxide is slightly soluble in pure water (in solubility g gas/kg water). The dissolved carbon dioxide in water forms carbonic acid, which is considered to be a weak acid. The equilibrium between CO_2 present in the gas phase CO_2 (g) with dissolved carbon dioxide CO_2 (aq.) is described by the reaction:

$$CO_2\ (g) \leftrightarrow CO_2\ (aq.) \qquad 2\text{-}42$$

A small portion of the CO_2 (aq.) reacts with water via hydration to form carbonic acid:

$$CO_2\ (aq) + H_2O \leftrightarrow H_2CO_3 \qquad 2\text{-}43$$

is the equilibrium constant for reaction The absorption of carbon dioxide in water is a physical absorption because of the small portion of the dissolved CO_2 (aq.) which reacts to give carbonic acid H_2CO_3, bicarbonate ion HCO_3^-, and carbonate ion CO_3^{2-}. The rate of CO_2 absorption into water under pure CO_2 concentrations is around $2.5x10^{-5}$- $3.0x10^{-5}$ mol/lm^2-second [62]. Figure 2-10 describes the correlation between pH and CO_2 species. CO_2 is more soluble in solution having high pH and in this condition carbonic acid may be formed [68]. Formation of carbonate ions significantly occurred at over pH 9.

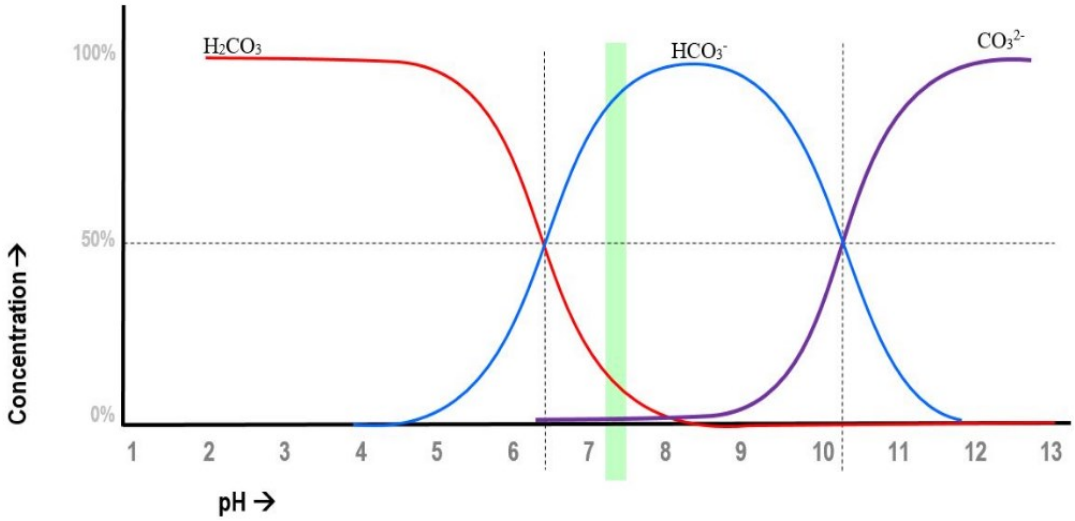

Figure 2-10. The percentage concentration of carbonic acid, bicarbonate and carbonate based on the pH of the solution. [69].

2.11 Dimensionless number on gas-liquid mass transfer

The characteristic of the common dimensionless groups frequently in mass transfer correlation[57]. Common dimensionless numbers as frequently used in mass transfer correlations are introduced below.

2.11.1 Sherwood number (Sh)

The Sherwood number represents the ratio of convective mass transfer (k_L) to diffusive mass transfer (D/d). Sherwood number is the dimensionless group for convective mass transfer in fluid flow and usually used in the mass transfer operation. This number is introduced by Thomas Kilgore Sherwood (1903-1976) and is defined as:

$$Sh = \frac{k_L d}{D} \qquad 2\text{-}44$$

where k_L is the convective mass transfer coefficient, D is the diffusivity constant, and d the representative dimension, in the present case, the diameter of a droplet. Sherwood number dependent upon two critical

dimensionless groups namely Reynolds number (*Re*), and Schmidt Numbers (*Sc*)

2.11.2 Reynold number (*Re*)

The Reynolds number can be represented as the ratio of the inertial force to the viscous force. This number is used to describe the flow pattern in different fluid flow situations, whether the flow is laminar, turbulent or in a transition between laminar and turbulent. When viscous forces are dominant, the flow is laminar (low Reynolds number) and when inertial forces are dominant, the flow is turbulent (high Reynolds number). The concept was proposed by George Gabriel Stokes in 1851, but Osborne Reynolds popularized its use in 1883 [48]. The number is defined as:

$$Re = \frac{\rho_L U d}{\mu_L} \qquad 2\text{-}45$$

where ρ_L is the density of a fluid, *U* is the velocity of a fluid, *d* the representative dimension, in this case, the droplet diameter, and μ_L is the dynamic viscosity of fluid.

2.11.3 Schmidt number (*Sc*)

The Schmidt number is defined as the ratio of viscosity and mass diffusivity and is used to characterize fluid flows in which simultaneous momentum and mass diffusion-convection processes occur. It is also a ratio of the fluid boundary layer to mass transfer boundary layer thickness. In order to determine the mass transfer coefficient by using the Sherwood number, the Schmidt number is needed. This number was proposed by Ernst Heinrich Wilhelm Schmidt and is defined as:

$$Sc = \frac{\mu_L}{\rho_L D} \qquad 2\text{-}46$$

where μ_L is the dynamic viscosity of a fluid, ρ_L is the density of a fluid, and *D* is the diffusivity.

2.11.4 Weber number (*We*)

The Weber number is introduced by Moritz Weber and is often useful in analyzing fluid flows with an interface between two different fluids, especially for multiphase flows with strongly curved interface. This number is a measure of the relative importance of the inertial force compared to the surface tension force [70]. The number is useful in analyzing the formation of droplets and is defined as:

$$We = \frac{U^2 \rho_G d}{\sigma} \qquad 2\text{-}47$$

where *U* is the velocity of a fluid, ρ_G is the density of a gas, *d* is the droplet diameter, and σ is the surface tension of the fluid. Increase of the *We* number results in different regimes of droplet deformation followed by disintegration steps namely the vibrational breakup, the bag breakup, the multimode breakup, the sheet stripping and the catastrophic breakup[71]. Weber's number less than 10 indicate stable droplets, in the sense that droplets keep their integrity. Higher Weber situations will lead to various breakup scenarios, e.g. for $10 \leq We \leq 50$ bag breakup will appear and $100 \leq We \leq 350$ sheet stripping can be expected. Futhermore, when a droplet of water impacts onto a liquid surface of liquid, we can observer one or more phenomena:

- The droplet bounces then floats on the surface of the liquid.
- The droplet coalesces into the liquid.
- The droplet splashes on the liquid, creating a crown around a crater.

2.11.5 Ohnesorge number (*Oh*)

The Ohnesorge number is a dimensionless number that correlates the viscous forces to inertial force and interfacial force. This number was introduced by Wolfgang von Ohnesorge in 1936. Higher Ohnesorge

numbers represent a greater influence of the viscosity. This number is of relation to jets and is used widely for dispersion, atomization and spray application [71]. If Ohnesorge number is too high, it indicates the formation of droplets not a jet stream. Meanwhile, lower Ohnesorge number indicates droplets formation with many satellite droplets. For low *Oh*-numbers (*Oh*<0.1), the droplet breakup is mainly controlled by the *We* number.

The general equation of this number is:

$$Oh = \frac{We^{1/2}}{Re} \qquad 2\text{-}48$$

where *We* is the Weber number and *Re* is the Reynolds number.

2.12 Model for absorptive mass transfer at droplets

Hydrodynamics in droplets affect the mass transfer, and have been studied by associating droplet diameters to Reynolds number. The form of a small droplet can be spherical or ellipsoidal and can indicate internal circulation meanwhile the shapes of a large droplet exhibit oscillation [62]. The mass transfer rate will increase if there is internal circulation within the droplets compared to diffusion only, and the mass transfer will increase if there is oscillation on droplets compared to a non-oscillating droplet. The flow patterns inside a droplet are depicted in Figure 2-11.

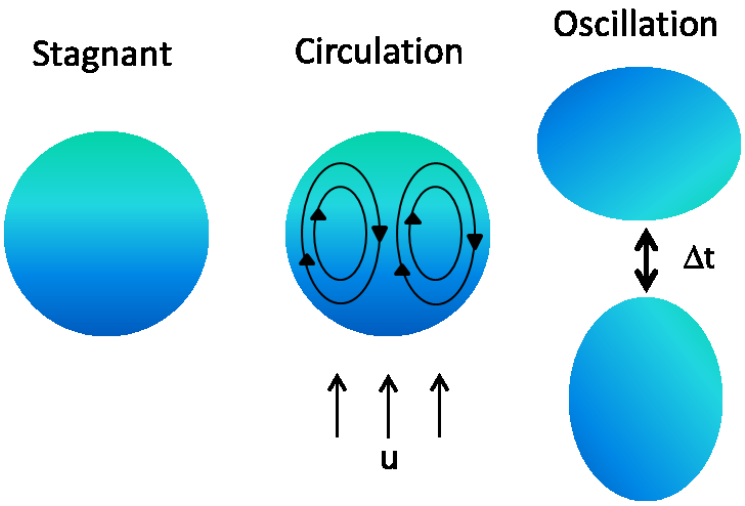

Figure 2-11 Flow pattern on a droplet, redrawn from [72]

2.12.1 Penetration model

The classical model for penetration theory is Higbie's model (Eq. 2-12) that has been discussed in section 2.6.2. This is a simple model which cannot inherently describe surface-renewal motion. This equation is valid only for short contact times. At longer time, eddies may be pictured as continually exposing fresh liquid surface to the gas, while at the same time sweeping into the bulk those parts of the surface which have been in contact with the gas [73].

2.12.2 Surface-renewal model

An original surface renewal model was proposed by Danckwerts and has been modified by a number of authors [74–80]. Handlos and Baron offered an equation model for internal mass transfer assuming turbulent flow inside a droplet for droplet diameter 4.14 mm to 6.16 mm and droplet velocity 10.6 cm/s to 15.1 cm/s. In term of k_L, the liquid mass transfer coefficient, the model can be expressed as [74]:

$$k_L = 0.00375\, U\, /(1 + \frac{\mu_L}{\mu_G}) \qquad \text{2-49}$$

where, U is the velocity of a droplet, μ_L and μ_G are the viscosity of droplet and gas, respectively.

Angelo et.al [75] postulated a model for oscillating droplets. The authors assume well mixing because during oscillation the fresh surface area was formed and returned to the bulk. The expression for k_L is found to be:

$$k_L = \frac{2}{\sqrt{\pi}}\left[fD\left(1 + \varepsilon + \frac{3\varepsilon^2}{8}\right)\right]^{1/2} \qquad \text{2-50}$$

where, f is the oscillation frequency of droplet, D is the diffusivity of the absorbed gas in the liquid and ε is the distortion parameter which represents

the maximum difference in surface area between the actual droplet and a perfect sphere having the same volume. The *f* can be predicted from the equation:

$$f = \left[\frac{8\sigma}{3\pi m}\right]^{1/2} \quad 2\text{-}51$$

where σ is the surface tension of droplet and *m* is the mass of the droplet.

Ruckenstein in 1967 proposed a model in which the entire resistance to mass transfer is limited to the liquid boundary layer, and the droplet itself is assumed to be completely mixed [76], with k_L given by:

$$k_L = \frac{2}{\sqrt{\pi}}[UD/d]^{1/2} \quad 2\text{-}52$$

Srinivasan and Aiken [33] used the model of mass transfer equations based on Levich's theory and modified by Davies and Ting [81]. Their experimental data show a good correlation with their derivative correlation, which is based on the Blasius equation for turbulent flow in smooth pipes (Blasius equation for fluid in pipe). The mass transfer equation, k_L as follows:

$$k_L = 0.045\left(\frac{\mu^3 D}{\rho^2 d_d^3 \sigma}\right)^{1/2} Re_d^{1.313} \quad 2\text{-}53$$

Development of Angelo's model was conducted by Hsu et al [77]. Based on experimental results of some investigators, the authors conclude that for prediction of the mass transfer coefficient for droplet diameter 0.6 to 6.0 mm and absorption of CO_2 or SO_2, a semi-empirical equation can be used, which is based on a surface stretch model:

$$k_L = 0.88[fD]^{0.5} \quad 2\text{-}54$$

As shown in Figure 2-12, the solid line obtained from the least-squares fit of experimental data from other investigators has a coefficient of correlation of

0.9 and a slope of – 0.70 ± 0.10. From least square fit of data using Eq.2-54, the dotted line is almost coincidental with the best fit of experimental data.

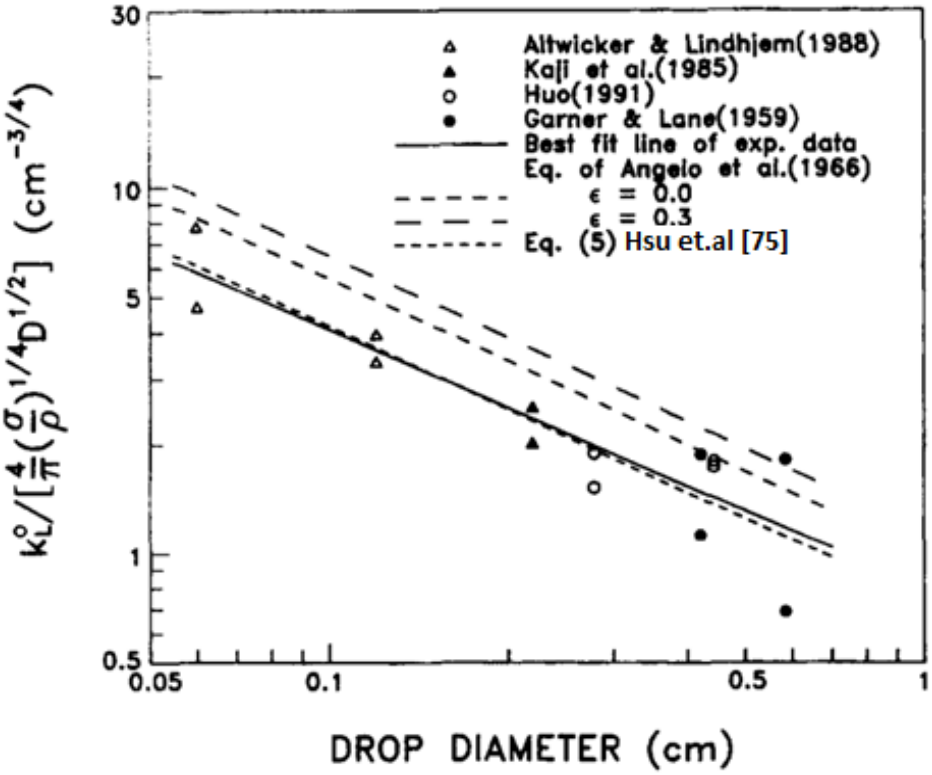

Figure 2-12. Variation of liquid phase mass transfer coefficient with drop diameters [77].

Amokrane et al. and their group [79, 80, 82, 83] proposed a model of mass transfer coefficient for SO_2 absorption and desorption for droplets larger than 1 mm. The model is an internal circulation model. A dimensionless number, Sherwood number, is used as a function of the Reynolds number and the Schmidt number (see Table 2-2). The model can be seen:

$$k_L = \omega \left(\frac{D_L u_*}{d} \right)^{1/2} \qquad 2\text{-}55$$

where,

$$u_* = U \left(\frac{1}{2} \frac{\rho_g}{\rho_l} C_D \right)^{1/2} \qquad 2\text{-}56$$

Summary of models of mass transfer equation, k_L from some references are tabulated in Table 2-1.

Table 2-1 Models of mass transfer equations k_L from some references

Model	Equation	Boundary condition/ summary
Higbie [57]	$k_L = 2\sqrt{\frac{D_L}{\pi t_e}}$	Penetration theory, short contact time
Handlos, et al. [74]	$k_L = 0.00375\ U\ /(1+\frac{\mu_L}{\mu_G})$	Turbulent condition, Liquid-liquid extraction
Angelo, et al. [75]	$k_L = \frac{2}{\sqrt{\pi}}\left[fD\left(1+\varepsilon+\frac{3\varepsilon^2}{8}\right)\right]^{1/2}$	Oscillation and penetration. Droplet dia. 2-10mm. Re number 200-2000. Velocity constant. Liquid-liquid extraction
Ruckenstein [76]	$k_L = \frac{2}{\sqrt{\pi}}[UD/d]^{1/2}$	Liquid boundary, well mixed, hill's vortex and single drop
Srinivasan and Aiken [33]	$k_L = 0.045\left(\frac{\mu^3 D}{\rho^2 d^3 \sigma}\right)^{1/2} Re^{1.313}$	droplet dia. is constant 84μm ; stream droplet velocity 4-9 m/s; Re : 377-790
Hsu, et al. [77]	$k_L = 0.88[fD]^{0.5}$	Extend Angelo model; droplet dia.: 0.6-6.0 mm
	$f = \left[\frac{8\sigma}{3\pi m}\right]^{1/2}$	For gas CO_2 and SO_2; based on surface stretch model
Amokrane et al. [78, 79]	$k_L = \omega\left(\frac{D_L u_*}{d}\right)^{1/2}$	Droplet dia:4.3 and 4.6 mm; exposure time : 0-1.3s; gas abs/desorption; SO_2;ω= 0.8; Sc Number = 550; temp.14-25°C
	$u_* = U\left(\frac{1}{2}\frac{\rho_g}{\rho_l}C_D\right)^{1/2}$	

All the model equation of mass transfer coefficient in Table 2-1 are used for obtaining some graphical depiction of experimental results as described in detail in section 4.8 (Figure 4-26 to Figure 4-28)

Some investigators model the mass transfer in form of dimensionless numbers, the expression in the gas phase for Sherwood number is shown in

Table 2-2. These models are used to calculate the mass transfer coefficient (see Eq. 2-44) and compared with the experimentally obtained mass transfer coefficient. The calculated mass transfer coefficients are also used to create some graphics as depicted in Figure 4-33.

Table 2-2 Summary of Sherwood number equations from some references

Reference	Equation	Boundary Condition/summary
Amokrane, et al. and Saboni & Alexandrova [78–80]	$Sh = 1.61 + 0.718\, Re^{0.5} Sc^{0.33}$	Sh number in the gas phase
Amokrane, et al. [78, 79]	$Sh = \omega\, Re_*^{0.5} Sc^{0.5}$	Droplet diameter: 4.3 and 4,6 mm Exposure time : 0 - 1.3 s Gas absorption/desorption : SO_2, ω = 0.8, Re and Sc in liquid phase
Kulmala, et al. [84]	$Sh = 2.009 + 0.514\, Re^{0.5} Sc^{0.33}$	Sh number in the gas phase
Srinivasan and Aiken [33]	$Sh = 0.045 Re^{5/16} Sc^{1/2} We^{1/2}$	From Levich theory diameter droplet is constant; stream droplet velocity 4-9 m/s; Re : 377-790 for turbulent flow and the Re number in liquid phase
Wedding et al[85]	$Sh = 1.755 + 0.535\, Re^{1/2} Sc^{1/3}$	droplet diameters of 100, 250 and 400μm.
Hoh, et al[86]	$Sh = 5.89\, Sc^{1/2} Oh\, Re^{0.75}$	Modified from Srinivasan

2.13 Literature reviews on experimental set-ups for mass transfer measurements

Many researchers have been conducting experimental studies on the absorption of CO_2 or SO_2 and its mixture in water droplets, such as, Whitman et al. in 1926 [30]. They have done studies on the absorption of CO_2 by using a fixed-length column with a height of 52 cm, by allowing water droplets falling freely at a constant rate. After falling, water droplets are collected with kerosene to avoid CO_2 coming in or out of solution. They focused on finding the rate of absorption of CO_2 during the falling water droplet on the humidification of air. They found that the mass transfer coefficient during formation is about 0.000011 to 0.000012 m/s at 23.9°C meanwhile during falling is about 0.000747 to 0.000939 m/s at the same temperature (the mass transfer coefficients for absorption during falling are obtained by linear extrapolation to zero time of formation). The diameter of a droplet that is measured by calibration of a capillary tip by letting ten or twenty drops of water fall. They determined the diameter of water droplets through weighing and assumed that the droplet is a sphere. They stated that the rates of absorption during formation and during falling are constant and the amount of absorption during falling droplet is higher than during formation.

Dixon and Russell [31] used equipment similar to that of Whitman, but they determined the rate of absorption of CO_2 at the time of the formation of water droplet and at the time of the formation and the falling of water droplets. They used a replaceable chamber for gas absorption. A short chamber was used to perform the absorption during formation, while a long chamber was used for determining the absorption during formation and falling. They directly measured the mass transfer during formation by experiments at the tip of the capillary tube. The mass transfer coefficients during formation have been determined to be in between 0.000057 to 0.000314 m/s at 21°C. They determined the diameter of water droplets through weighing and assumed that the droplet is a sphere. They stated that the rate of absorption at short time of formation is very high and is then gradually decreasing, the amount of CO_2 during falling decreases compared to formation time. Dixon and Russell

argued the term 'degree of turbulence' in which the mass transfer coefficient during the formation of the absorption is inversely proportional to the time function of the droplet formation. The high absorption rate of the droplet in the beginning of formation is caused by the presence of turbulences produced by a jet of water from the capillaries that can reduce diffusion resistance of the surface or diminish the effective thickness of the film.

Wang and Pruppacher [87] performed an experiment with rain shaft with height about 35 meters. They only focused on determining the velocity of the drop in various diameters at 20^{o}C. They determined the drop diameter based on volume of water that falls down into a dish. The water drops had diameters of 1.7, 2.7, 4.0, 5.0 and 7.0 mm. For all droplet diameters, the velocities increased sharply at the beginning of up to 6 meters and after that look stable. Altwicker and Lindhjem [32] performed experiments with a chamber that consists of two Lucite tubes. The gap between drop formation and the absorption chamber was 130 mm. They produced droplets by the well-known principle of disintegration where a liquid jet breaks with the help of vibration frequency. They focused on determining liquid-side mass transfer coefficients of droplets in a short time (< 0.1 s) after formation. They used two diameters of droplets, 0.6 mm and 1.2 mm. They found that the mass transfer coefficients of CO_2/Air in water at 23^{o}C were about 0.001013 to 0.000585 m/s.

Srinivasan and Aiken [33], studied absorption of CO_2 by distilled, deionized and de-aerated water in co-current flow using a chamber with length 10 mm. The droplets were generated by droplet generator (aerosol generator) that produced droplets with a diameter of 82.4 μm (ratio volumetric flow rate liquid and frequency of vibration is constant). They found that the mass transfer coefficient was about 0.0024 to 0.0064 m/s at temperature and pressure that had corrected to 25^{o}C and 760 mmHg. They used decyl alcohol as the shield liquid in the sampling device.

Some investigators [78–80, 83], studied SO_2 absorption by single water droplet in a 5-m rain shaft. The difference of their studies is only the diameter of the droplet, small droplets [78] and large droplets[78, 79]. They focused on

the determination of the concentration in the droplet after the absorption process. They stated that whatever the type of absorption/desorption experiments; their local models have fit perfectly with their experimental data. They determined the small drop diameter by weighing while for large droplet diameter by calibrating a hypodermic needle. They used hygrometers and thermocouples for measuring the temperature of the drop, the relative humidity and the temperature of air in the shaft. Marion et al.[83] investigated the effect of droplet vaporization onto the SO_2 absorption process in the column with 2.3 meters of height. They found that the absorption rate is high at short times (less than 0.1 s) and thereafter decrease gradually. They used a camera to determine the droplet diameter.

Yeh, et al.[88] have studied desorption of carbon dioxide in an air-water system using spray contactor. They have developed a satisfactory sampling method, which effectively reduces mass transfer during sample collection. The experiments were conducted with laboratory and pilot-scale. They stated that the amount of liquid-phase transfer due to the impact of sprays on the walls and liquid pools is often as much as the amount of mass transfer in the spray. More than half of the mass transfer occurred in liquid sheets before droplet formation. They used nozzle properties to determine the droplet diameter.

Recent research was conducted by Han et al. [34, 36]. They determined liquid phase mass transfer coefficient of carbon dioxide absorption by water droplet and used a new apparatus (with camera). They measure droplet diameter, droplet falling height and droplet formation time but the apparatus is not explained in detail. After falling, the water drop was collected with kerosene for avoiding any disturbance after treatment. For calculating the mass transfer coefficient, they used some assumptions;

a. there is no chemical reaction,
b. the droplets are kept in spherical form ,
c. the droplet grows at a uniform volumetric rate,
d. there is no change in the diameter of the droplet and the time of droplet formation and

e. the absorption is in equilibrium at the gas-liquid interface and in accordance with Henry's law.

The mass transfer coefficient during formation is about 0.000055 m/s to 0.000203 m/s at 303.65 K and 0.000177 m/s to 0.000355 m/s at 323.15 K.

In the past, mainly intrusive methods, also called sampling techniques, were used for the characterization of a droplet. With these techniques, droplets were collected and analyzed using mechanical sampling devices. However, these sampling devices may affect the behavior of spray and are used only to evaluate the droplet deposition and estimate the diameter of the droplets.
The limitations of the non-imaging techniques and the recent improvements in digital image acquisition and processing increased the interest in using high-speed imaging techniques in water droplets characterization.

Based on the literature review, there are differing results on the role of the formation of the droplet on absorption rate. Some authors state that formation is critically, other authors state that it could be neglected. At the time of droplet formation internal circulation or turbulence may occur. Also a significant difference of the mass transfer coefficient is reported, even though the same assumptions and the same method have been used. This is probably caused by the way how the droplet is characterized. This underlines the need for further research which is done in this work.

The studies on the physical mass transfer between gas and liquid are summarized in Table 2-3.

Table 2-3. Literature studies on mass transfer between liquid droplets and gases

Author	Gas-Liquid	Droplet Dia. [µm]	Droplet velocity [m/s]	Temperature [°C]	Reynolds Number
Whitman et al, 1926 [30]	CO_2-Water	5565	0.087-1.59	24.5	484-8848
Dixon and Russell, 1950[31]	CO_2-Water	3100-5640	0.104-1.04	21	322-5865
Scriven and Pigford,1958[89]	CO_2-Water	-	0.75-5.5	25	-
Davies and Ting, 1967[81]	CO_2-Water	-	> 16	-	7000-22000
Adewuyi and Carmichael,1982 [68]	CO_2-Water	100-3000	-	10 & 25	
Altwicker and Lindhjem, 1988 [32]	CO_2-Water	600; 1200	1.2 -1.4	23	720-1680
Srinivasan and Aiken, 1988[33]	CO_2-Water	82.4	4-9	25	350-800
Amokrane et al. 1994[78]	SO_2-Water	360; 2300	-	14 & 25	-
Schwarz and Smolik, 1994[90]	Air-Water	700-2300	0.5-1.7	41-176	30-180
Amokrane and Caussade, 1999[79]	SO_2-Water	2344	-	14-25	-
Han et al, 2013	CO_2-Water	2533	1.39-1.65	30-50	3536-4180

Note: - means no data available

3. EXPERIMENTAL AND ANALYTICAL METHOD

An experimental set-up for mass transfer studies was built as depicted in Figure 3-1. The experimental equipment consists of a gas bottle (N_2 and CO_2), a saturation apparatus for making CO_2-saturated solution, a droplet generation device, a desorption chamber, a high speed camera, a long distance microscope and an imaging system.

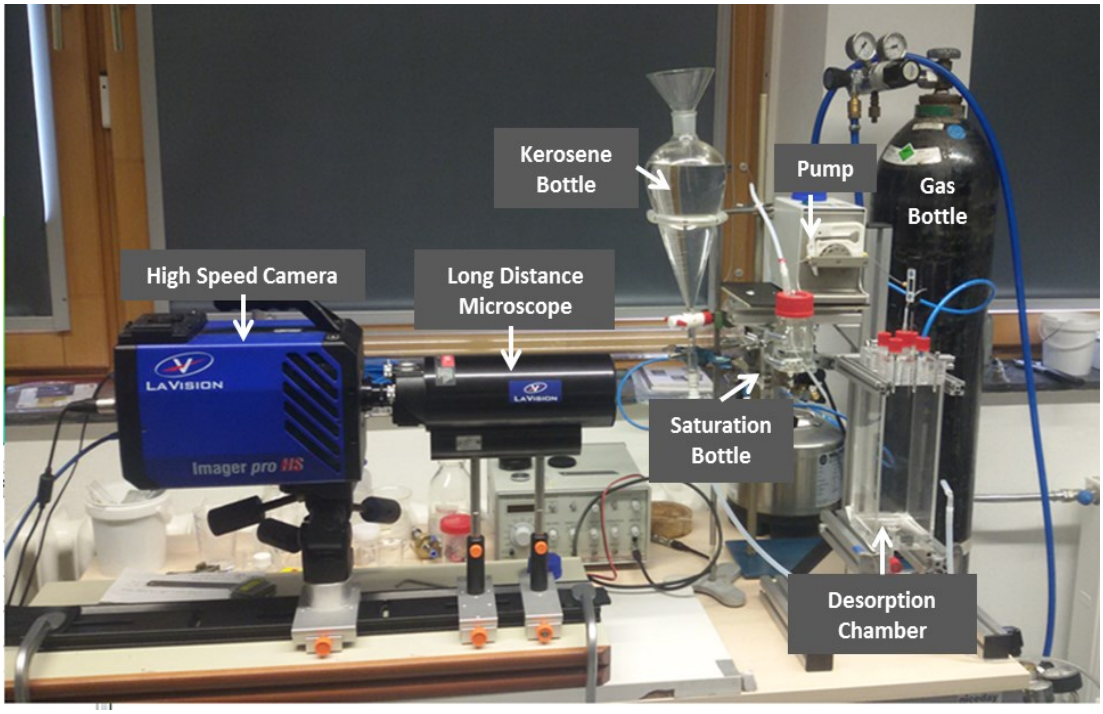

Figure 3-1. The picture of the experimental set-up for CO_2 gas desorption from water droplets.

CO_2-saturated water was mechanically driven with a peristaltic pump through a needle so that water drops fall freely in a desorption chamber. The water droplets that were captured by the camera were processed into diameter droplets data using the shadowgraph method. The collected droplets in the desorption chamber were analysed using the precipitation-titration method. A diagram sketch of the experimental set-up is shown in Figure 3-2.

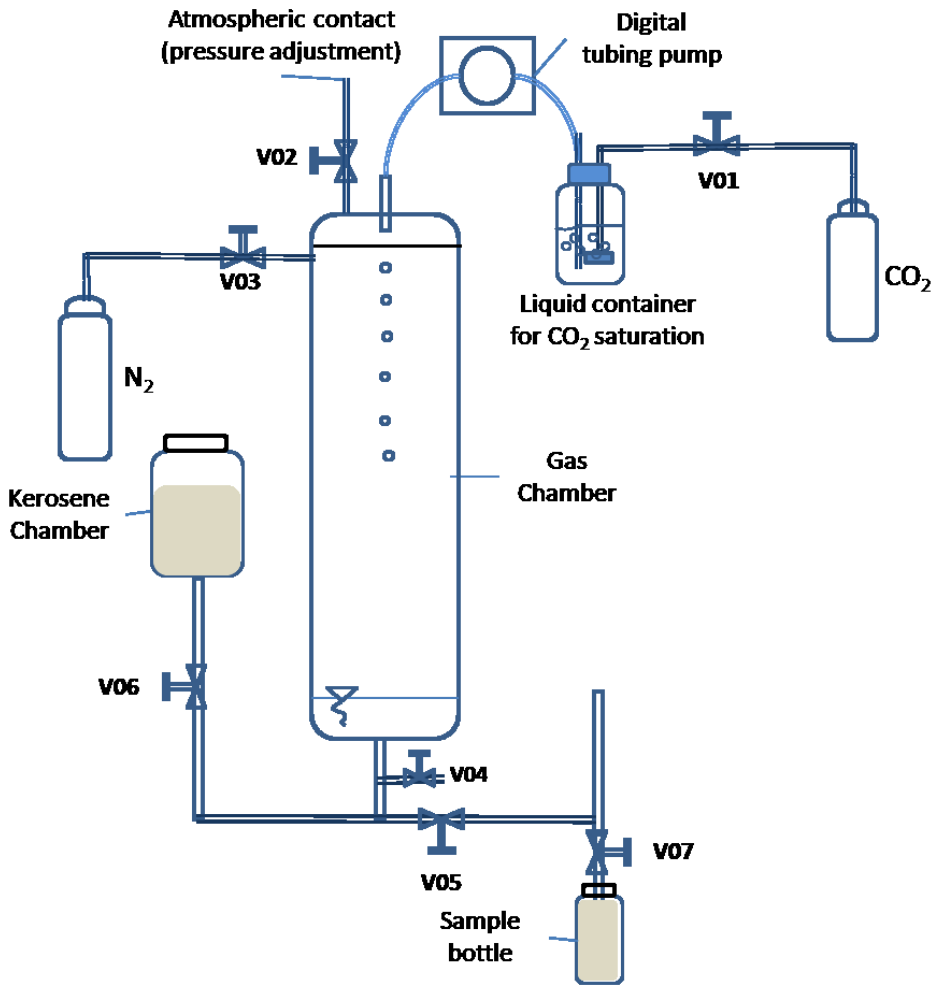

Figure 3-2 The sketch of experimental equipment for this study.

The nitrogen gas flowed into the chamber for purging the chamber from unwanted gases such as CO_2 that disturb the experimental results (N_2 feed from V03 and out through V04). This purging has been done before droplet formation. The flow rate passing through the needle must be stable in order to keep the droplet diameters and the distances between the droplets uniform. Droplets that fall into the kerosene layer were rapidly being deposited due to the difference of density. The use of kerosene is also useful to prevent the sample from being exposed to the surrounding gas because CO_2 is insoluble in kerosene.

3.1. Digital tubing pump

A digital tubing pump was used as driving force to produce a droplet dripping. The amount of droplet dripping out at a certain time from the needle through a Tygon hose depend on an adjustment of flow rate on the top of the pump. The general information and the picture of the digital tubing pump and a micro pump hose are shown in Figure 3-3 and Table 3-1.

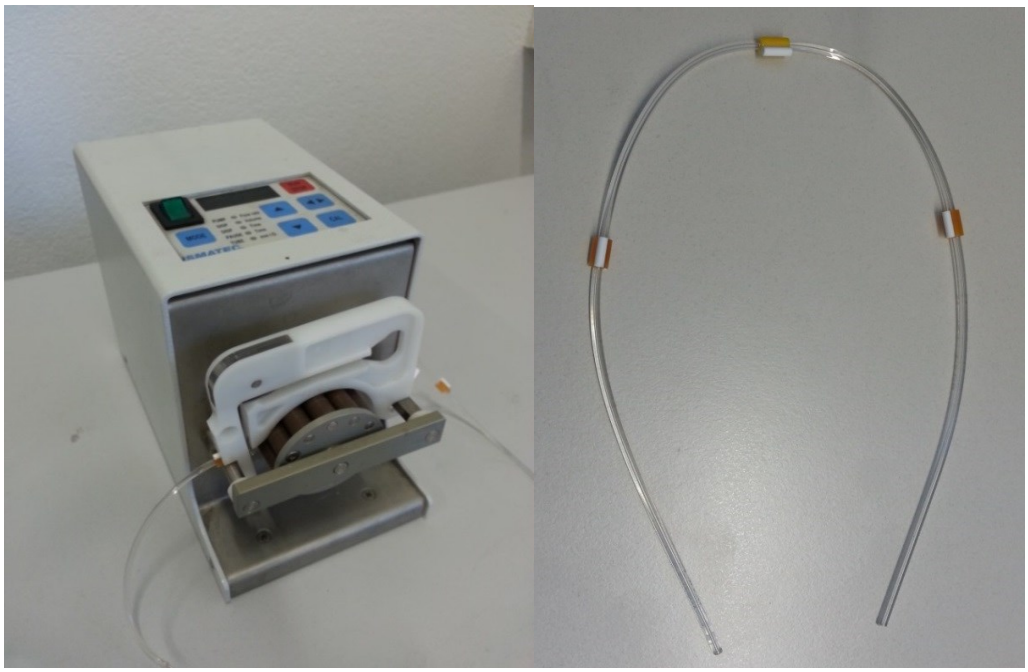

(a) (b)

Figure 3-3 The digital tubing pump Ismatec (a), micro pump hose Tygon (b).

Table 3-1 The general specification of the digital tubing pump

Unit or Part	Type	Specification	Remark
Digital tubing pump Model Reglo Digital MS-2/12	ISM 596B	Flowrate : 0.025 ml/min (min) 2.5 ml/min (max) Channel : 2 Pump roller : 12	Color-coded tubing id. 0.51 mm With three spacers for tube fixing
Micro pump hose Tygon R-3607	SC0053	0.51 mm	Color code: orange/yellow

There are three different types of needles that were used in the experiment with different outer diameters; 0.5 mm, 0.6 mm and 0.8 mm, as shown in Figure 3-4.

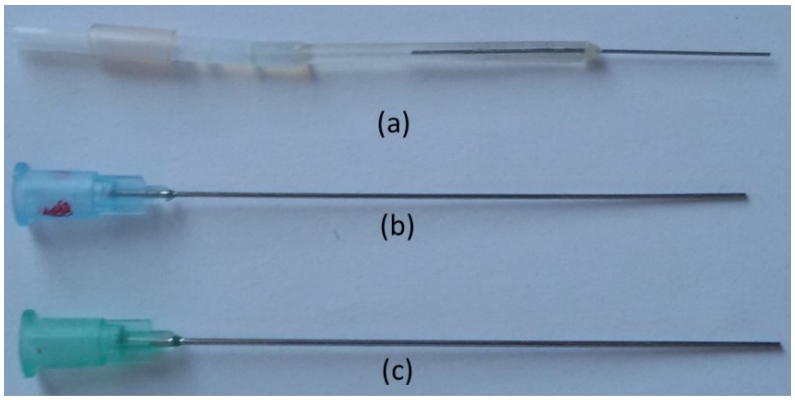

Figure 3-4 Three types of needles used in this study with different outer diameters; (a) 0.5 mm (b) 0.6 mm (blue) and (c) 0.8 mm (green)

3.2. Saturation apparatus

A gas wash bottle made of Duran (capacity of 250 ml) including a porous filter plate 100-160 μm is used as saturation bottle. Distilled water as a solvent was saturated with CO_2 before performing the experiment in a saturation apparatus as shown in Figure 3-5.

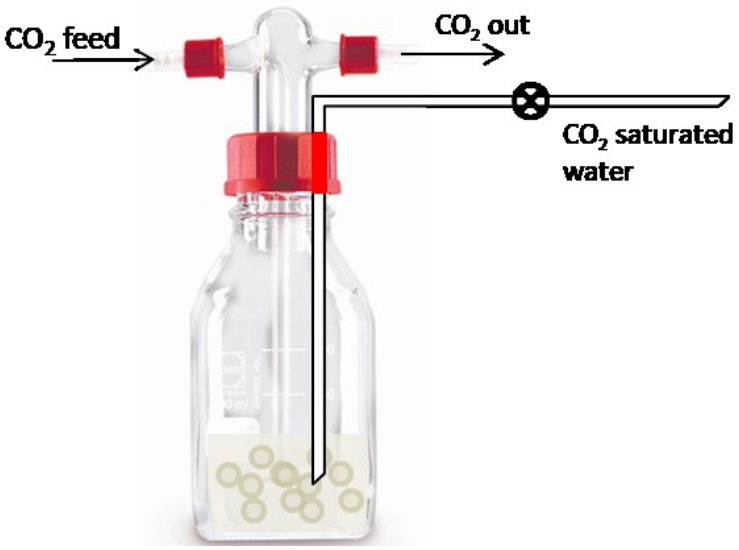

Figure 3-5 Gas wash bottle as saturation apparatus

3.3. High-speed camera and long distance microscope.

The high-speed camera Imager Pro HS4M from LaVision GmbH with long distance microscope was used for recording and observing of droplets during formation and falling period. A shadowgraphic method was used for measuring of the droplet diameter and the droplet velocity. The high-speed camera with long distance microscope is shown in Figure 3-6. Image processing was performed with Davis software (La Vision).

Figure 3-6 The Long distance microscope (right) with a high-speed camera imager Pro HS 4M (left)

3.3.1. Camera models

The Imager proHS4M is equipped with a, with monochrome CMOS image sensor containing 2016 x 2016 pixels, and camera memory of 18GB. Settings for the frame rate and the recording time depend on the desired pixel resolution as shown in Table 3-2.

3.3.2. Long distance microscope model

With the help of a long distance microscope QM1 (La Vision) it was possible to observe particle diameters between 5 μm to 500 μm at working distances of more than 50 cm.This microscope is used for measuring the diameter of

droplets during formation, droplets diameter and droplets velocity after being released from the needle in a short range.

Table 3-2 Possible settings of frame rate and maximum recording time at different resolution area

Resolution horizontal [pixel]	Resolution vertical [pixel]	Frame rate [fps]	Recording time [s]
2016	2016	1279	4.9
1920	1080	2470	5.0
1296	720	5087	5.4
1008	1000	4502	5.7

3.3.3. Lens model and type

In this study, droplet velocity measurements using high speed camera and a Nikon lens AFS micro Nikkor 105 mm 1:2 are more accurate because the image capture with this lens is clearer and has an observation range of up to 12 cm. Meanwhile, when using a long distance microscope (as Figure 3-6), the observation range is a maximum of 12 mm.

3.3.4. LED light.

A Constellation 120 LED from Imaging Solution GmbH was used as light source. The LED light has dimensions of 155 x 75 x 75 mm, a light output of 8500 lm (pulsed) and 15000 lm (continuous operation), an input of 120 W and a 28^{o} beam angle reflector.

3.4. Absorption/Desoprtion chamber

A gas desorption investigation is conducted by using a rectangular column with an inner cross section of 8 x 8 cm, height 23 cm and a volume of approximately 1500 ml. The sketch of the chamber is illustrated in Figure 3-7

The sketch of rectangular column (a) isometric view, (b) front view and (c) side view.

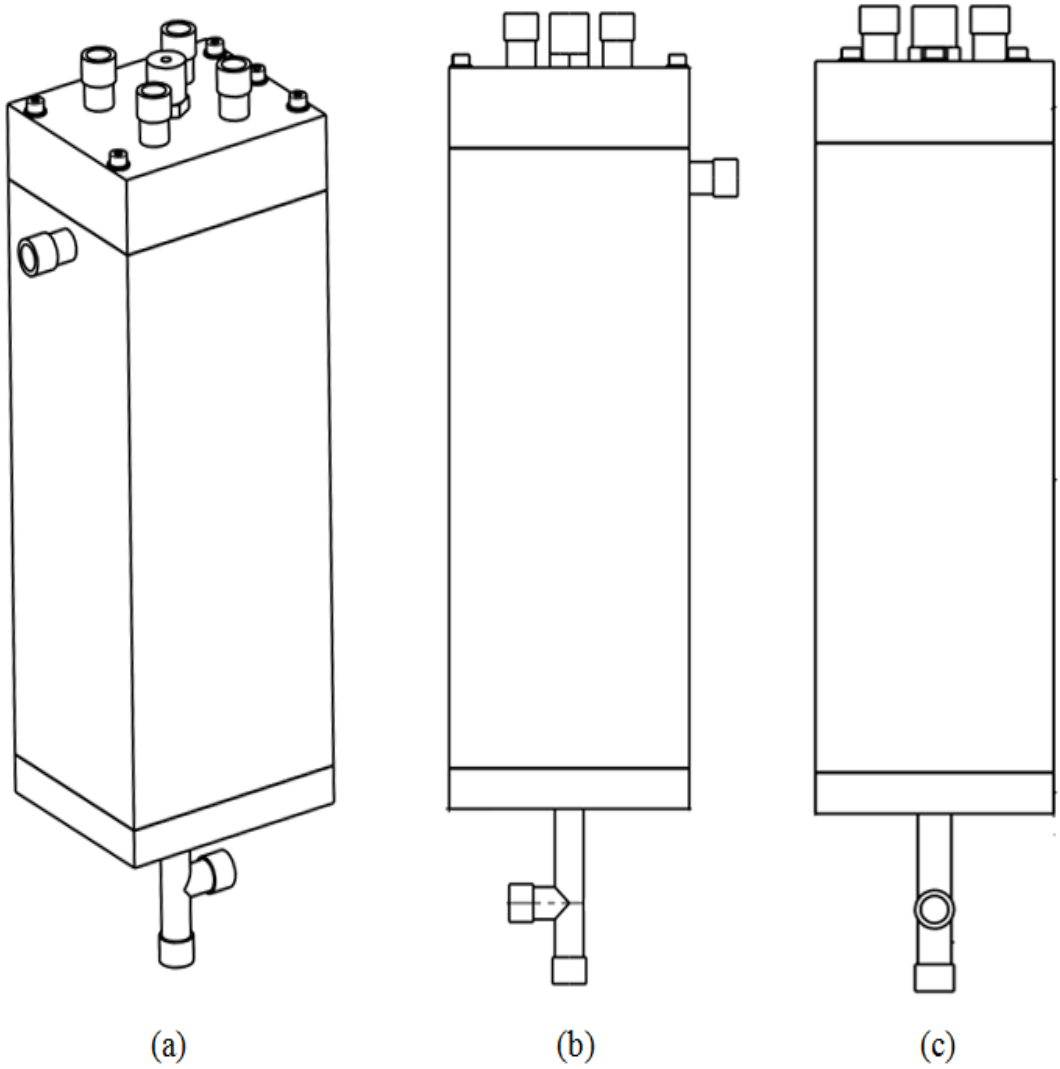

Figure 3-7 The sketch of rectangular column (a) isometric view, (b) front view and (c) side view.

The top part of the column consists of five openings to place the droplet generator in the center of the top and the other openings for a thermometer, outlet liquids or gases, pressure gauge. The additional openings allowed for introduction of the gases (CO_2 or N_2) to be absorbed or as medium gases for desorption investigations. The bottom part of column is cone-shaped, in order to facilitate the collecting of droplets as soon as they impacted a layer of kerosene. The function of the T-junction at the lower end was to fill kerosene and discharge the kerosene and the sample. The side connection of the T-junction was used to take the sample for analysing.

The chamber was manufactured by a private company based on a VTiU design. The gas chamber was made of polymethyl methacrylate (PMMA) in order to enable taking picture of the droplet. The top part of the column was fixed with M4 screws and seal. The internal structure of the cover-plate is designed for fixing the droplet generator and the needle. The procedure of the gas desorption from liquid is presented in Appendix 3-1. The procedure of image processing was expressed in Appendix 3-2.

3.5. Filtration apparatus

Thermo Scientific™ Nalgene™ filtration equipment was used in this study. This apparatus consists of a polysulfone bottle, a top filters, filter membrane and a vacuum pumps. The picture and the general information of the filtration apparatus are shown in Figure 3-8 and Table 3-3.

(a) (b) (c)

Figure 3-8 The filtration equipment consists of a) Nalgene filtration chamber, b) Peristaltic pump c) Nylon membrane filter.

Table 3-3 The general specification of filtration apparatus.

Unit and General Data	Specification
Filter Apparatus Brand, Type, Size, Volume	Nalgene, Polysulfone Reusable Bottle Filters screw securely onto glass bottles with 33 or 45mm neck sizes. Chamber 500 ml
Peristaltic Pump Brand, Type, flowrate, speed	Heidolph PD5206, Flowrate 1.3 to 3.9 ml/min, Speed 24 to 600 rpm
Membrane Brand, Material, diameter size, pore size	ALBET LabScience, Nylon membrane filters, white, plain, diameter 47 mm, pore 0.45 um

3.6. Automatic titration

The automatic titration instrument, Titrino GP 736 (Metrohm AG CH 9101 Herisau) was used to perform an analytical measurement such as:

a. Measurement of pH/temperature of samples (MEAS Method)
b. Measure and record the volume of acid or base required to achieve a certain end point in acid-base titration (Set Endpoint Titration – SET Method)

The Titrino GP 736 consists of the main part, the exchange unit system (reagent bottle, stopcock and burette tips), a pH glass electrode, a magnetic stirrer and the keypad as shown in Figure 3-9.The type of PH glass electrode is “Long Life”. The reference system consists of an Ag/AgCl cartridge with a silver ion barrier as described in Table 3-4.The main part displays the running mode of operation which is selected through the keypad. In the exchange unit the reagent bottle is safely positioned by retaining clips. To protect the reagent bottle a stopper is mounted on the reagent bottle. The liquid flows from the bottle to the analytical solution by means of a motorized micro syringe.

Figure 3-9 The complete set up of automatic titration unit (Titrino GP 736) and the combined pH glass electrode.

Table 3-4. The general specification of pH glass electrode from Metrohm Company.

General Data	Specification
Shaft length, diameter, material Min. immersion depth Temperature range	125 mm, 12 mm, glass 20 mm 0°C – 80°C
Indicator electrode Type, shape pH measuring range	Glass electrode, hemispherical 0 - 14
Reference electrode Diaphragm Bridge electrolyte type	Ceramic pin [KCl] = 3 mol/l

3.7. Analytical methods

3.7.1. Analyzing of pH

The pH glass electrode connected with the main part of Titrino GP 736 is used to determine the change of pH in the solution and records the used

volume of acid or base during titration experiment (SET Method) or alternatively measures the pH of the solution (MEAS Method).

The glass electrode had to be immersed at least 20 mm deep in the solution. The pH glass electrode must be calibrated before use with standard buffer solution. The data calibration of pH probe can be seen in Appendix 3-3. The calibration curve and the slope in Nernst equation are automatically performed and calculated by Titrino GP 736. The pH of the unknown solution is automatically calculated and the result is immediately displayed.

3.7.2. Analyzing of CO_2 concentration in solution.

A CO_2 saturated distilled water is analyzed by a precipitation $BaCO_3$ and titration method using Titrino GP 736 (Figure 3-9). A 1 ml sample was added to the mixture of 25 ml $BaCl_2$ 0.1 M solution and 50 ml NaOH 0.1 M solution. This mixture was heated until boiling for 4-5 minutes and then cooled down with cool water in a bath. After cooling, the mixture was filtered through 0.45 μm filter paper. The filter cake was dried in an oven for 30 minutes and then added with 50 ml distilled water. The solution was titrated with 0.1 M HCl solution to pH 2 and then back titrated with NaOH 0.1 M to pH 7 to determine the amount of excess HCl. Detailed information on chemicals, apparatus and procedures is presented in Appendix 3-4.

Involved reactions in the liquid phase during the analysis [36]:

$$BaCl_2 + 2NaOH + CO_2 \rightarrow BaCO_3\downarrow + 2NaCl + H_2O \quad (3\text{-}1)$$

$$BaCO_3\downarrow + 2HCl \rightarrow BaCl_2 + CO_2 + H_2O \quad (3\text{-}2)$$

$$HCl_{(excess)} + NaOH \rightarrow NaCl + H_2O \quad (3\text{-}3)$$

The amount of CO_2 dissolved in water is calculated as follows:

$$n_{CO_2}[mol] = \left(\frac{C_{HCl} \cdot V_{HCl} - C_{NaOH} \cdot V_{NaOH}}{2}\right)_{sample} - \left(\frac{C_{HCl} \cdot V_{HCl} - C_{NaOH} \cdot V_{NaOH}}{2}\right)_{blank} \quad 3\text{-}4$$

The blank experiment is needed for correcting a certain amount of CO_2 in the atmosphere that eventually was absorbed by NaOH solution.

Notation in Eq.3-4 are:

c_{HCl} = the concentration of HCl solution
V_{HCl} = the volume of HCl solution which reacts with $BaCO_3$
c_{NaOH} = the concentration of NaOH solution
V_{NaOH} = the volume of NaOH solution used to neutralize the excess HCl

For calculation the concentration of CO_2 in the sample:

$$c_{CO_2}[mol/l] = \frac{n_{CO_2}}{V_{sample}} \quad 3\text{-}5$$

An exemplary spreadsheet of calculation to the titration method is enclosed in Appendix 3-5.

3.8. Verification of method

Before analyzing the samples by means of a titration method, verification was needed to examine the accuracy of results, using a concentration series of a $NaHCO_3$ solution from 0.005 mol/l up to 0.03 mol/l. The data verification results can be seen in Appendix 3-6.

The result of verification indicated that the method is accurate, as can be seen in Figure 3-10.

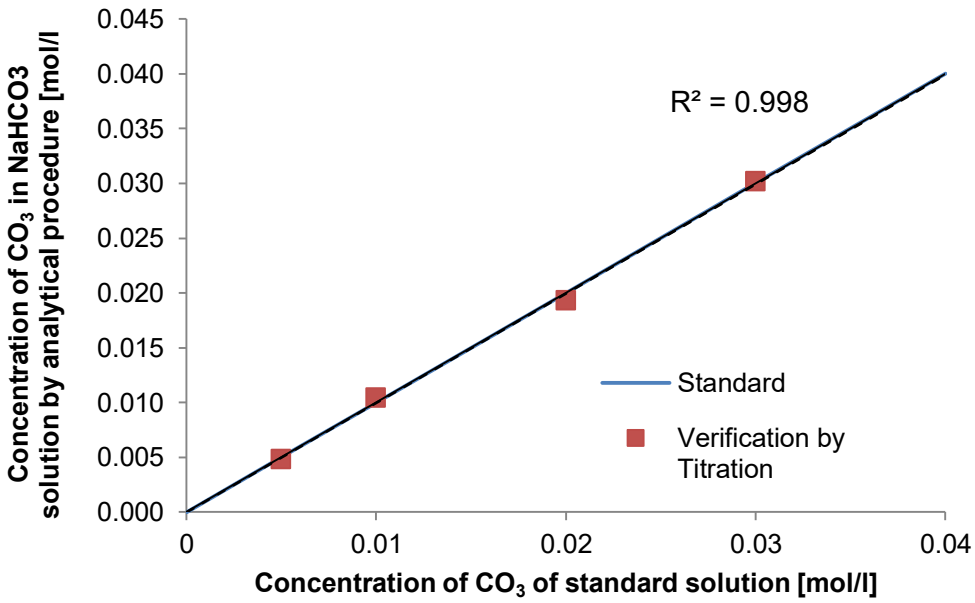

Figure 3-10 Verification curve of carbonate analyzing method in aqueous sample solution

4.RESULTS AND DISCUSSIONS

4.1. Physical properties measurement.

In this section, the physical properties measurement such as droplet diameters d_d, droplet diameters during formation d_{fr}, droplet diameters during falling d_{fl}, droplet formation time t_{fr}, droplet falling time t_{fl}, and contact time t_t, are presented. The subscript *fr* indicates the condition during droplet formation and *fl* during droplet falling.

4.1.1. The droplet diameter during formation d_{fr}

By using a high-speed camera with a long distance microscope, determination of a droplet diameter can be measured. The diameter of droplets formed at nozzle tips with outer diameters 0.5 mm, 0.6 mm and 0.8 mm, respectively at flow rate 1 ml/min is presented in Figure 4-1. The experimental data can be seen in Appendix 4-1.

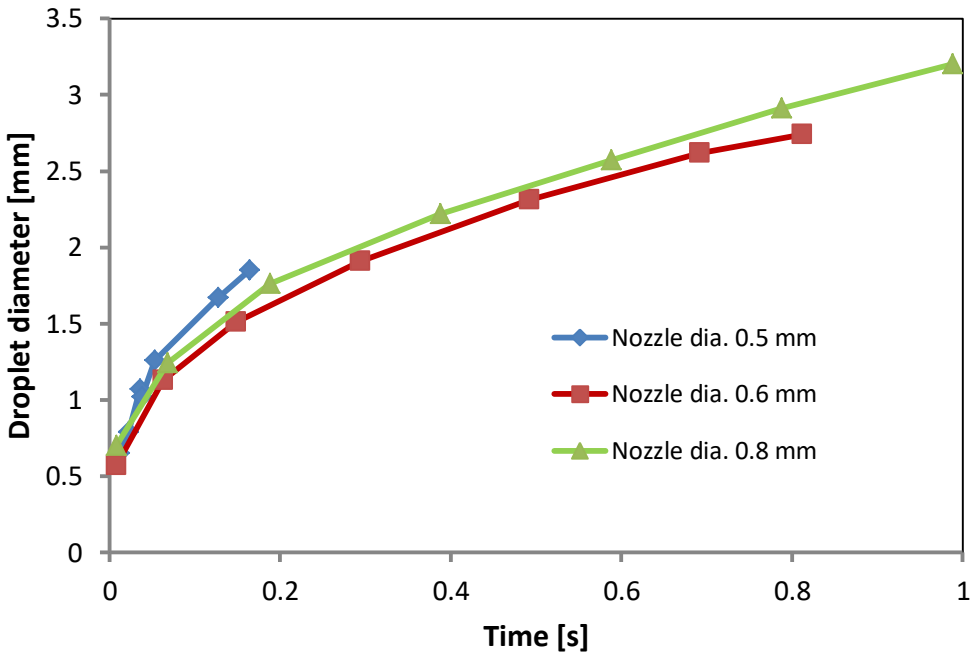

Figure 4-1 Temporal evolution of pending droplets diameters formed at different nozzle tips (formation period)

4.1.2. The droplet formation time t_{fr}

The droplet formation time t_{fr} can be calculated by analyzing a high-speed video as shown in Figure 4-2.

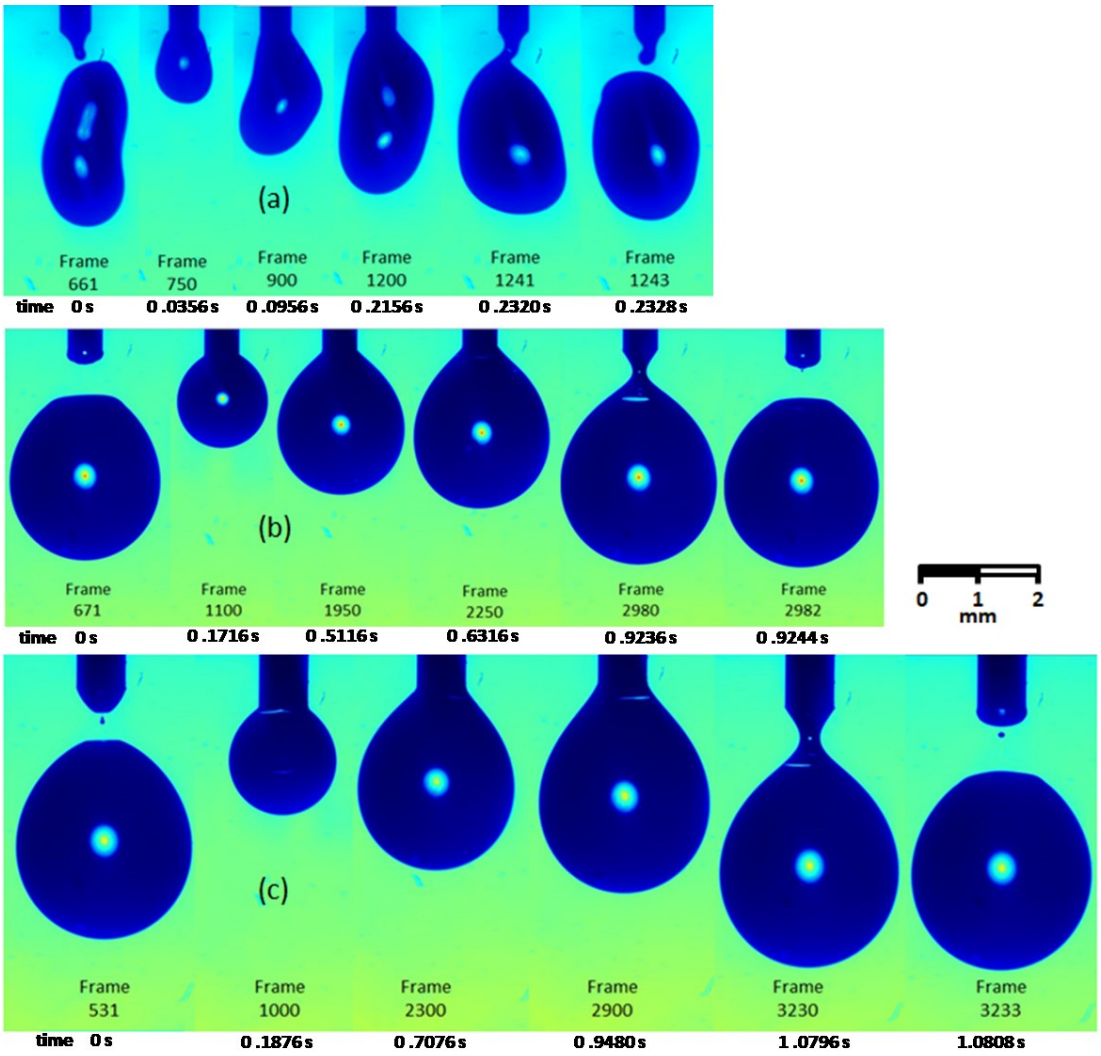

Figure 4-2 The stage of droplet formation at different needle outer diameter: (a) 0.5 mm, (b) 0.6 mm and (c) 0.8 mm. (Pictures are of the same scale).

For the example in Figure 4-2(b), the recording rate is 2500 Hz or 2500 fps (frames per second). Droplet formation appears in between frame numbers from 671 to 2982. The number of frames for one droplet to form is 2982 - 671 = 2311. Therefore, the time required to form a droplet is:

2311/2500 s^{-1} = 0.9244 s. The droplet formation rate is:

$$\varphi = \frac{1}{0.9244} s^{-1} = 1.082 \text{ s}^{-1}$$

The experimental formation time and formation rate for various outer diameters are presented in Table 4-1.

Table 4-1 Experimental data of formation time and formation rate (average)

Outer nozzle diameter [mm]	Formation time [s]	Formation rate [s^{-1}]
0.5	0.2328	4.295
0.6	0.9244	1.082
0.8	1.08	0.926

Note: number of Measurement: 5, std dev. 0.00067-0.00212 (formation time) and 0.00093-0.0123 (formation rate) see Appendix 4-2

4.1.3. The droplet diameter during falling d_{fl}

In this study, measurement of the diameter of droplet can be obtained by analyzing the video from the high-speed camera (manual calculation). For example, Figure 4-3 shows an experimental image to demonstrate how to calculate a droplet diameter manually for a droplet detached from a needle with outer diameter of 0.6 mm.

An estimate of a sphere-equivalent droplet diameter for a free falling non-spherical droplet can be calculated from its 2D shadowgraphic image by:

$$d_y = y_1 - y_2 \quad (4\text{-}1)$$

$$d_x = x_2 - x_1 \quad (4\text{-}2)$$

$$\bar{d} = \frac{d_y + d_x}{2} \quad (4\text{-}3)$$

= (-6.396 –(-9.127) + (1.662-(-0.9767))/2 = 2.684 mm

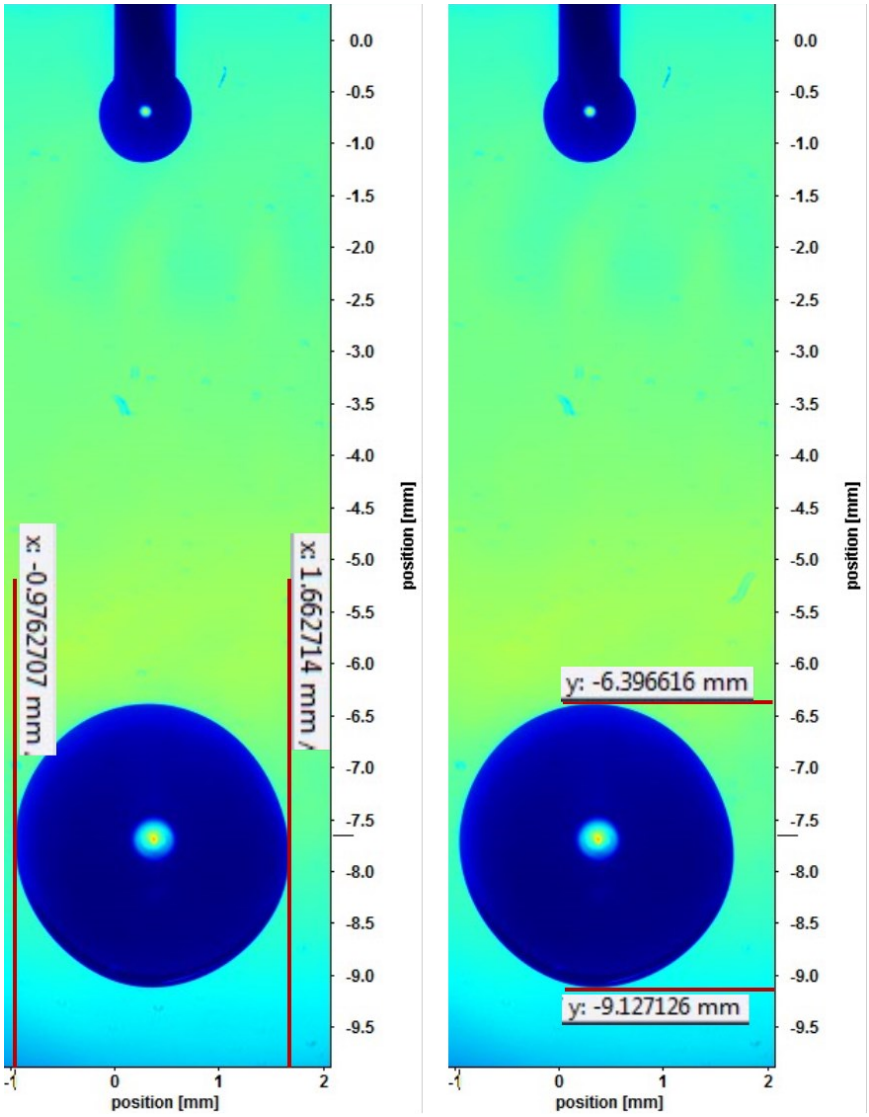

Figure 4-3 The calculation of droplet diameter of a falling droplet (outer needle diameter 0.6 mm, frame no.746)

The experimental findings for droplet diameters during falling at various nozzle diameters are presented in Table 4-2.

Alternatively to the manual calculation droplet diameters can be determined with the help of image processing software directly from the digital images, as shown in Figure 4-4.

Table 4-2 Experimental data of droplet diameters during falling

Outer nozzle dia. 0.5 mm		**Outer nozzle dia. 0.6 mm**		**Outer nozzle dia. 0.8 mm**	
Run	Droplet diameter[mm]	Run	Droplet diameter[mm]	Run	Droplet diamater[mm]
1	1.599	1	2.633	1	2.983
2	1.604	2	2.6815	2	3.005
3	1.598	3	2.691	3	3.058
4	1.607	4	2.651	4	2.935
5	1.6215	5	2.625	5	2.98
6	1.6305	6	2.699	6	2.999
		7	2.69	7	2.999
				8	3.066
Average	1.610		2.667		3.003
Std.Dev	0.012		0.028		0.040

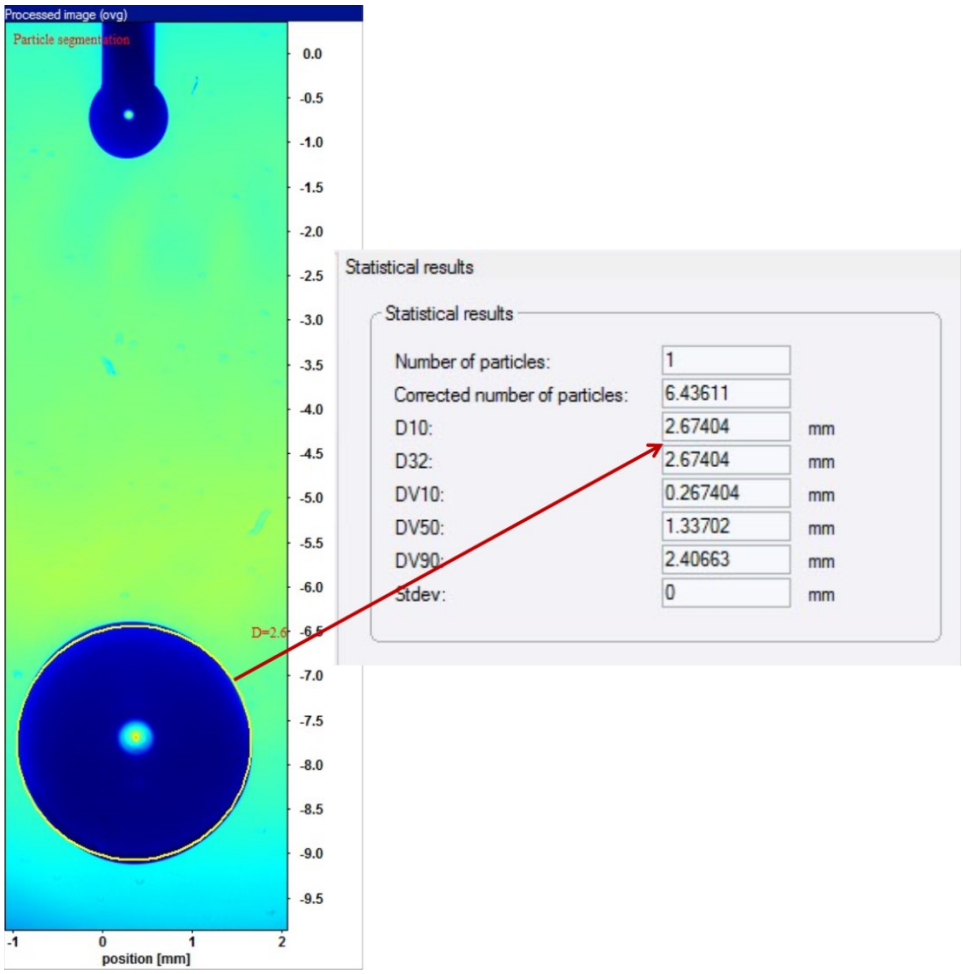

Figure 4-4 The determination of droplet diameter during falling by image processing software

Compared to the manually determined estimate of 2.684 mm the software supported measurement calculated 2.674 mm. There is a difference of approximately 0.70 percent which gives a fair agreement. Table 4-3 presents data of droplet diameters that were measured either manually or with software and percentage differences.

Table 4-3 The comparison of droplet diameter data by manual measurement and software

Outer nozzle diameter [mm]	Droplet diameter [mm]		Difference [%]
	Manual measurement	Software	
0.5	1.610	1.601	0.90
0.6	2.667	2.674	0.70
0.8	3.003	2.993	1.00

The droplet diameters during fall have varying diameters but the differences are not significant. This statement is in line with experimental results of other investigators [78, 79], with differences reported of 2.0 percent.

4.1.4. The droplet falling time t_{fl}

Due to the maximum image length of frames obtained with the Long Distance Microscope (10-12 mm) or alternatively obtained with the Nikon Lens (120 mm) taking a photograph of the whole droplet during falling was not possible. Therefore, droplet falling time over total fall-distance was calculated by Eq. 4-4.

$$t_{fl} = \frac{h}{V_{(t)}} \qquad 4\text{-}4$$

Where $V_{(t)}$denotes the velocity of droplet at certain time.

4.1.5. The droplet contact time t_d

The total droplet contact time as a summation of formation and fall can be calculated by:

$$t_d = t_{fr} + t_{fl} \quad 4\text{-}5$$

4.1.6. The droplet velocity $U_{(t)}$ and droplet terminal velocity U_t

The droplet velocity during falling can be calculated by observing the video from a high-speed camera with image processing software as shown in Figure 4-5, with Eq. 4-6.

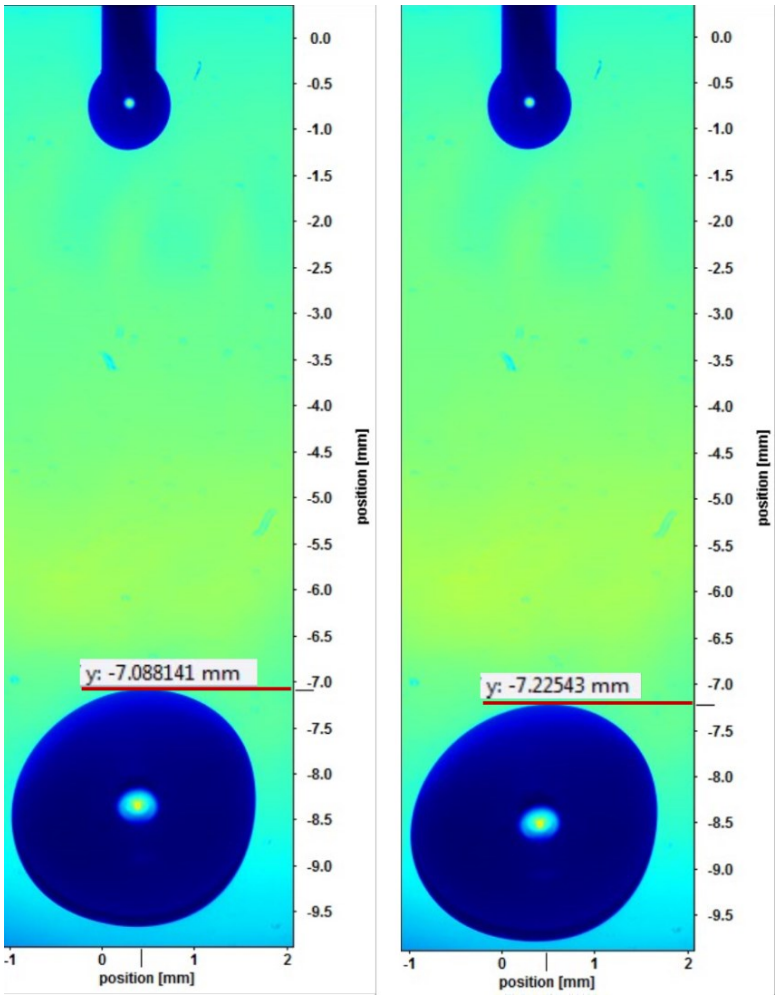

a) Frame No. 751 b) Frame No. 752

Figure 4-5 A way to calculate a droplet velocity for recording rate 2500 Hz

The recording rate is 2500 Hz or 2500 fps (frames per second). Then the droplet velocity for those positions from two subsequent frames is:

$$U_{1-2} = \frac{y_1 - y_2}{t_{1-2}} \quad 4\text{-}6$$

$$t_{1-2} = \frac{\Delta\, frame}{recording\ rate} \quad 4\text{-}7$$

$$t_{1-2} = \frac{1}{2500} = 0.0004 \text{ s}$$

$$U_{1-2} = \frac{-7.088 \text{ mm} - (-7.225 \text{ mm})}{4 \text{ x } 10^{-4} \text{s}} = 343.22 \text{ mm/s} = 0.343 \text{ m/s}$$

The measured droplet velocities in experiments with different droplet diameters and distances can be seen in Figure 4-6. Detailed data can be seen in Appendix 4-3.

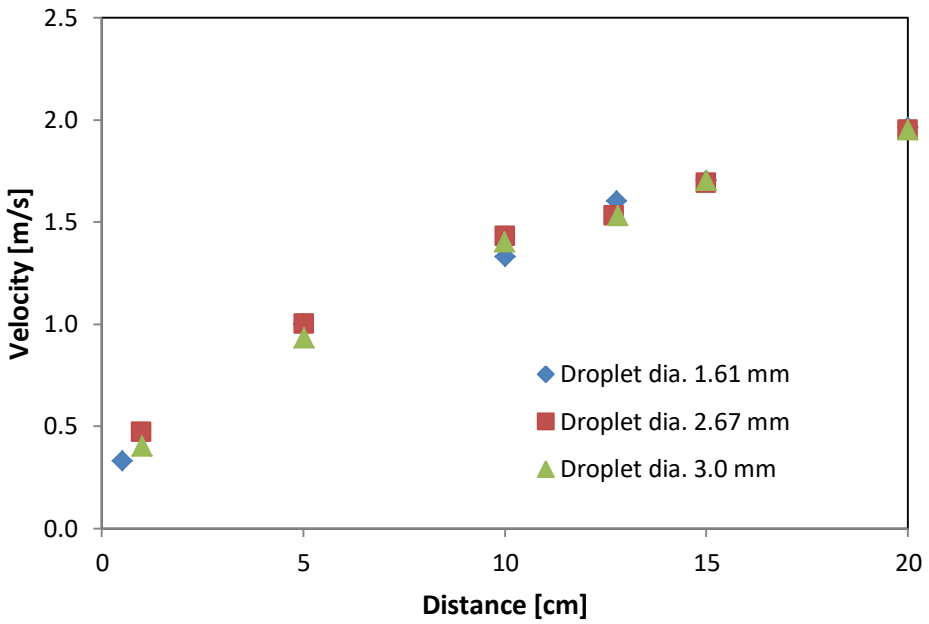

Figure 4-6 Experimentally determined droplet falling velocities at various droplet diameter and droplet positions (distance from needle tips).

4.2. Analysis of CO_2 concentration.

The measured droplet concentrations for CO_2 desorption experiments with different droplet diameters and distances can be seen in the Table 4-4.

Table 4-4 The experimental result of CO_2 concentration in solution before and after droplet detachment from needle for various droplet diameters and distances (c_1 = initial concentration and c_2 = end concentration)

h [cm]	d [mm]	t [s]	T [°C]	C_1 [mol/l]	C_2 [mol/l]
0	1.61	0.233	23.0	0.0273	0.0138
5	1.61	0.284	23.7	0.0288	0.0122
10	1.61	0.305	23.5	0.0282	0.0105
15	1.61	0.322	23.5	0.0286	0.0103
20	1.61	0.337	21.7	0.0335	0.0111
0	2.67	0.859	22.5	0.0298	0.0151
5	2.67	0.909	23.0	0.0302	0.0149
10	2.67	0.931	23.0	0.0293	0.0144
15	2.67	0.947	23.0	0.0272	0.0129
20	2.67	0.962	22.8	0.0298	0.0126
0	3.0	1.160	22.5	0.0295	0.0154
5	3.0	1.211	22.7	0.0289	0.0146
10	3.0	1.232	23.0	0.0290	0.0138
15	3.0	1.248	22.7	0.0308	0.0151
20	3.0	1.263	22.7	0.0291	0.0132

Note: droplet diameters from Table 4-3; average

4.3. Desorption rate during formation and falling

The desorption rate of CO_2 from water droplets during formation and falling at different distances and droplet diameters was found by experiments. Data are presented in Figure 4-7, Figure 4-8 and Figure 4-9, respectively.

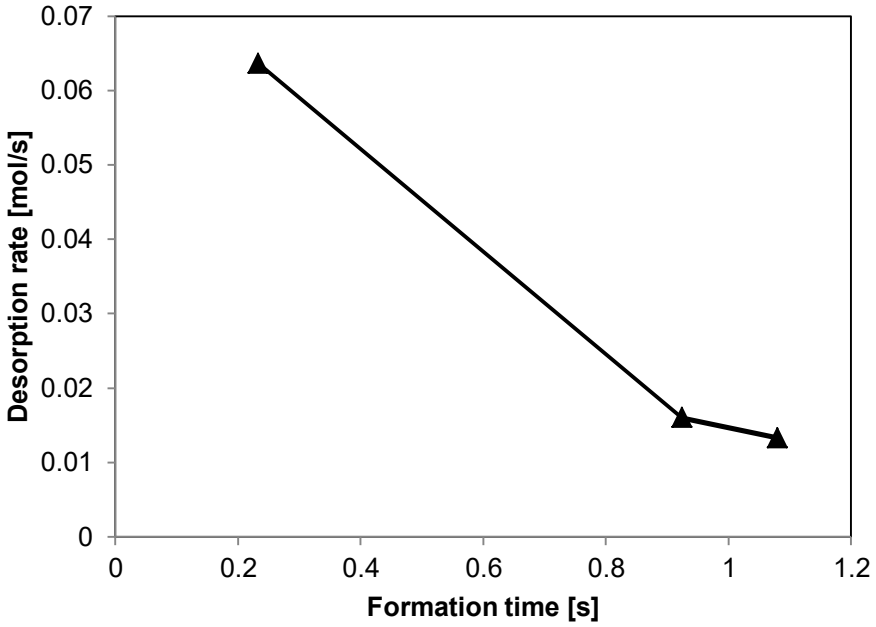

Figure 4-7 Desorption rate of CO_2 during different formation times

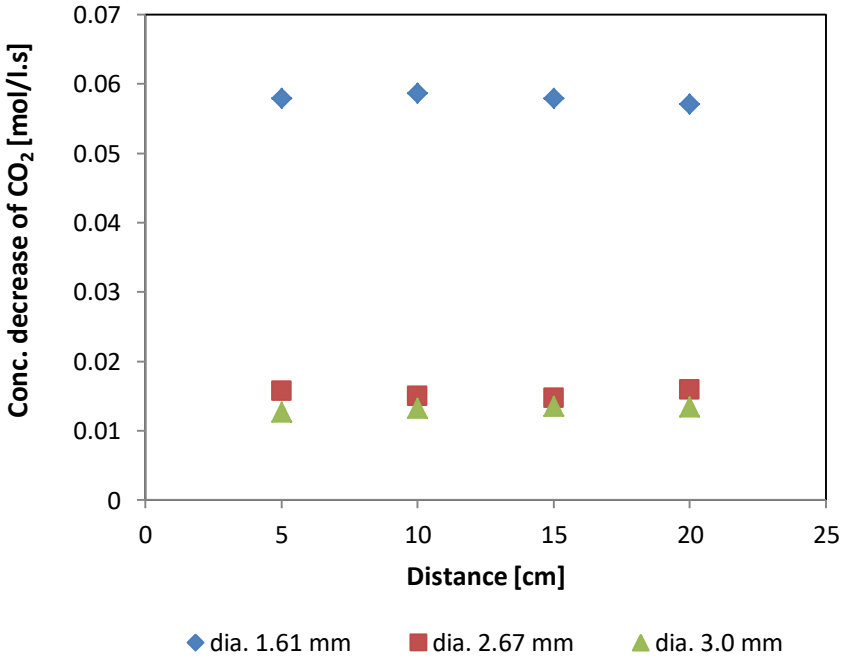

Figure 4-8 Concentration decrease of dissolved CO_2 for various falling distances and different droplet diameters

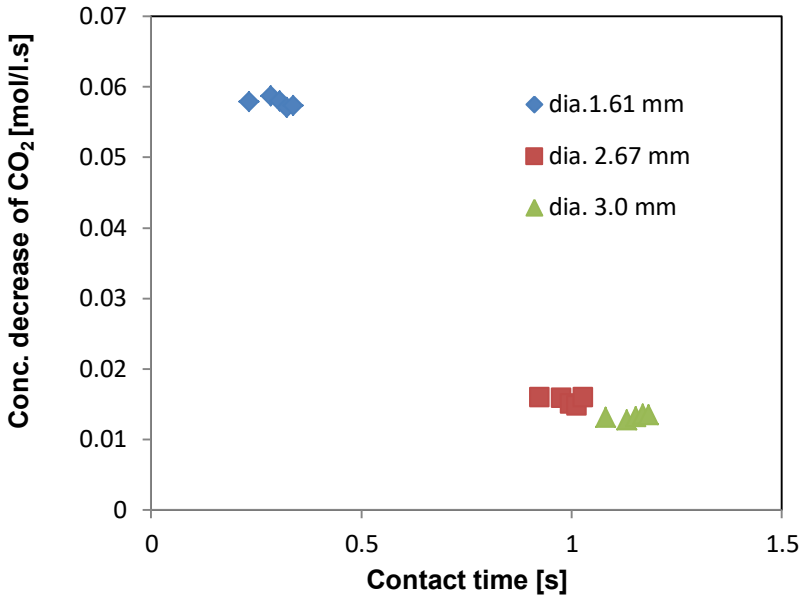

Figure 4-9 Concentration decrease of dissolved CO_2 for different droplet diameters

4.4. Mass transfer coefficients during formation and falling

The liquid phase mass transfer coefficient of CO_2 desorption from water droplets during formation and falling were obtained by experiment. Three needles with different diameters (0.5, 0.6 and 0.8 mm) were used. The physical-chemical parameters for different components that are used for the calculation are given inTable 4-5. Mass transfer coefficients are calculated based on the experimentally determined desorption rates according to Eq.2-39. The averages of experimental mass transfer coefficients are presented in Table 4-6.

Table 4-5 Physical-chemical parameters at 25°C for calculation of mass transfer coefficient

Parameter at 25°C	**Symbol**	**Units**	**Value**
Diffusivity CO_2 in water[32]	D_L	m^2/s	1.90E-09
Density of nitrogen[60]	ρ_G	kg/m^3	1.251
Density of water[91]	ρ_L	kg/m^3	997.0
Droplet diameter*	d	mm	1.61; 2.67; 3.0
Gravitational acceleration [60]	g	m/s^2	9.80
Dynamic viscosity (N_2)[60]	μ_G	$N.s/m^2$ (Pa.s)	1.76E-05
Drag coefficient**	C_D	-	0.5
Terminal velocity*	U_t	m/s	5.6; 7.49; 7.94
Surface tension of water[92]	σ	N/m	7.23E-02
Temperature*	T	°C	22-24

*Measured data from this study, ** calculated

Table 4-6 The measured mass transfer coefficient at various nozzle diameter and height; calculation according to Eq. 2-39

Experiment	**Outer nozzle diameter 0.5 mm**	**Outer nozzle diameter 0.6 mm**	**Outer nozzle diameter 0.8 mm**
Height [cm]	**k_L [m/s]**	**k_L [m/s]**	**k_L [m/s]**
0	7.85E-04	3.26E-04	3.01E-04
5	8.16E-04	3.24E-04	3.03E-04
10	8.70E-04	3.19E-04	3.23E-04
15	8.56E-04	3.25E-04	3.07E-04
20	8.52E-04	3.73E-04	3.35E-04

4.5. Comparison with model equations

4.5.1. Droplet diameter during formation

The droplet diameter during formation was determined based on the assumption that the droplet maintains its spherical shape during growth. The surface area of the droplet has an exponential correlation with time in the spherical droplet growth at constant volumetric rate [93]:

$$A_d = \pi d^2 = \pi d_{fr}^2 t_{fr}^{-2/3} t^{2/3} \quad \text{4-8}$$

Here A_d is the surface area of a droplet, d is the droplet diameter at time t, and t is the droplet growing time. The subscript fr denotes the final condition of formation phase. Thus, d_{fr} is the droplet diameter when the droplet is released from the needle and t_{fr} is the time that the droplet takes to accomplish growing.

Rearranging yields:

$$\frac{d^2}{d_{fr}^2} = \frac{t^{2/3}}{t_{fr}^{2/3}} \quad \text{4-9}$$

$$\frac{d}{d_{fr}} = \frac{t^{1/3}}{t_{fr}^{1/3}} \quad \text{4-10}$$

$d = d_{\overline{fr}}$, so

$$d_{\overline{fr}} = d_{fr}\left(\frac{t}{t_{fr}}\right)^{1/3} \quad \text{4-11}$$

The average of droplet diameter during formation $d_{\overline{fr}}$ can be computed by integrating Eq. 4-11 over time (from 0 to t_{fr}) which gives:

$$\int_{t=0}^{t=t_{fr}} \frac{d_{\overline{fr}}}{d_{fr}}.dt = t_{fr}^{-1/3} \int_{t=0}^{t=t_{fr}} t^{1/3}.dt \quad \text{4-12}$$

$$\frac{d_{fr}^{-}}{d_{fr}}\left(t\Big|_{\cdot t=0}^{t=t_{fr}}\right) = t_{fr}^{-1/3}\left(\frac{1}{4/3}t^{4/3}\Big|_{\cdot t=0}^{t=t_{fr}}\right) \quad 4\text{-}13$$

$$\frac{d_{fr}^{-}}{d_{fr}}\left(t_{fr}-0\right) = \frac{3}{4}t_{fr}^{-1/3}\left(t_{fr}^{4/3}-0\right) \quad 4\text{-}14$$

$$\frac{d_{fr}^{-}}{d_{fr}}\left(t_{fr}\right) = \frac{3}{4}\left(t_{fr}\right) \quad 4\text{-}15$$

$$d_{\overline{fr}} = \frac{3}{4}d_{fr} \quad 4\text{-}16$$

Where, d_{fr} is the droplet diameter when the droplet is released from the needle. It is assumed that the droplet diameter does not change during fall, so $d_{fr} = d_{fl}$.

Figure 4-10 illustrates the growth of the droplet diameter as a function of time during the droplet formation. The measured droplet diameters are assumed spherical during growth except for the small needle (0.5 mm). The experimental droplet diameters which are obtained from the high-speed camera are compared with the results as calculated from Eq. 4-11.

For nozzle diameter 0.6 mm and 0.8 mm, the experimental data are in good agreement with the model equation especially at the beginning period of droplet formation. This may be due to the fact that the droplets at the beginning of formation are spherical forms but at the end the droplets are elliptical, so they slightly differ from the equation. The differences of experimental droplet diameter and droplet diameter from equation are between 0.36 and 8 percent. However, for the droplets derived from the nozzle diameter of 0.5 mm, the differences are about 7 percent to 22 percent.

This phenomenon is caused by droplets not perfectly spherical and tends to be irregular (Figure 4-2) due to high pressure and rough nozzle tip. The detail information for differences of droplet diameter can be seen in Table 4-7.

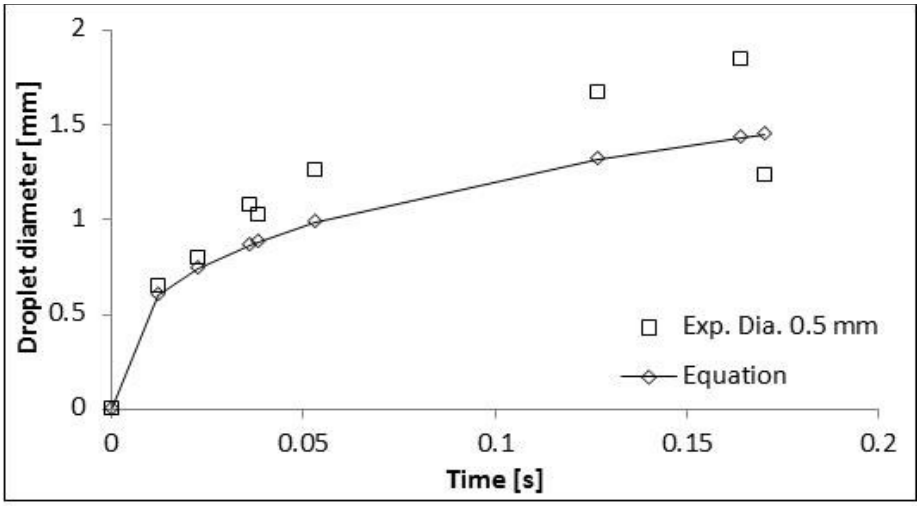

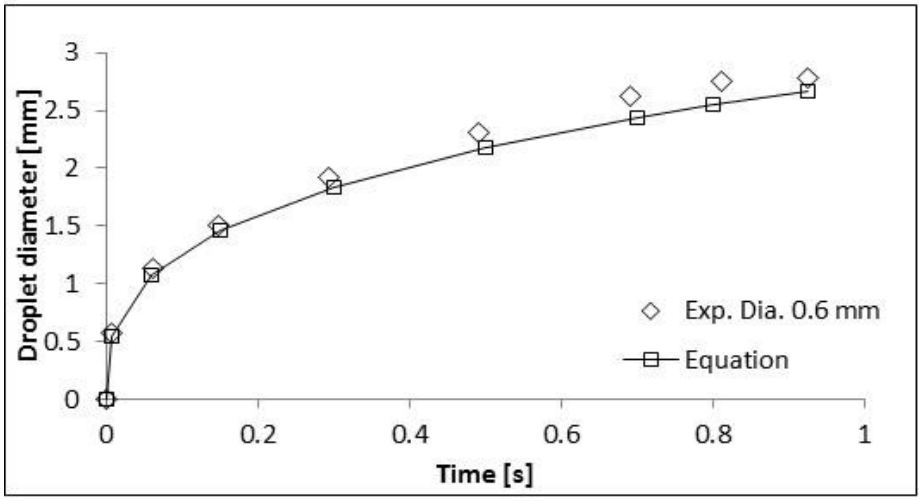

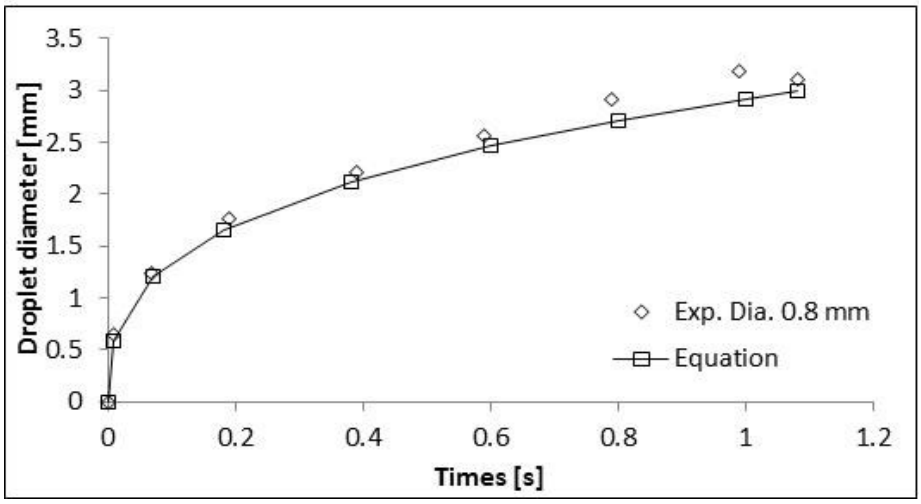

Figure 4-10 The droplet diameter as a function of time during formation; □, the calculated data from Eq. 4-11; ◊, the experimental data from high-speed video sequence.

Table 4-7 Data of droplet diameters during formation, comparing experiment with equation model

Outer nozzle dia. 0.5 mm		Diff.	Outer nozzle dia. 0.6 mm		Diff.	Outer nozzle dia. 0.8 mm		Diff.
Exp.	Model	[%]	Exp.	Model	[%]	Exp.	Model	[%]
0.65	0.60	7.57	0.57	0.55	3.57	0.65	0.60	7.95
0.79	0.74	6.84	1.13	1.07	4.78	1.24	1.23	0.36
1.07	0.86	19.43	1.51	1.46	3.24	1.76	1.69	4.03
1.02	0.88	13.52	1.91	1.84	3.98	2.22	2.17	2.34
1.26	0.98	21.62	2.31	2.18	5.51	2.57	2.52	1.85
1.67	1.31	21.19	2.62	2.44	7.10	2.91	2.78	4.72
1.85	1.43	22.39	2.74	2.55	7.15	3.20	2.99	6.38
1.23	1.45	17.68	2.78	2.67	3.92	3.11	3.07	1.29

4.5.2. Influence of droplet formation time in mass transfer.

Droplet formation stage plays an important role in the mass transfer if compared with other stages such as falling. It is related to a longer contact time of a drop in the gas phase. The cumulative time that is required by a droplet during formation until detachment from a needle can be seen in Figure 4-11. Increasing the water flowrate passing through the needle twice makes the droplets formation time becoming faster 2 times. For example, droplet formation time for droplet diameter of 3.0 mm at a flowrate of 1 ml/min is 0.615 seconds; while at a flowrate of 2 ml/min is 0.34 seconds.

A longer contact time generates a longer period of mass transfer for components that are absorbed by a droplet or released from a droplet into the gas phase. The importance of the long droplet formation time internal for the overall amount of mass transfer was judged differently by various authors. In their study, Dixon and Russell [31] concluded that the amount of CO_2 absorbed during droplet falling is less than that absorbed during droplet formation. However, this findings are in contrast to the conclusion argued by Whitman et al [30] and Han et al[36]. They argued otherwise that the amount

of CO_2 absorbed during droplet falling is higher than that absorbed during droplet formation.

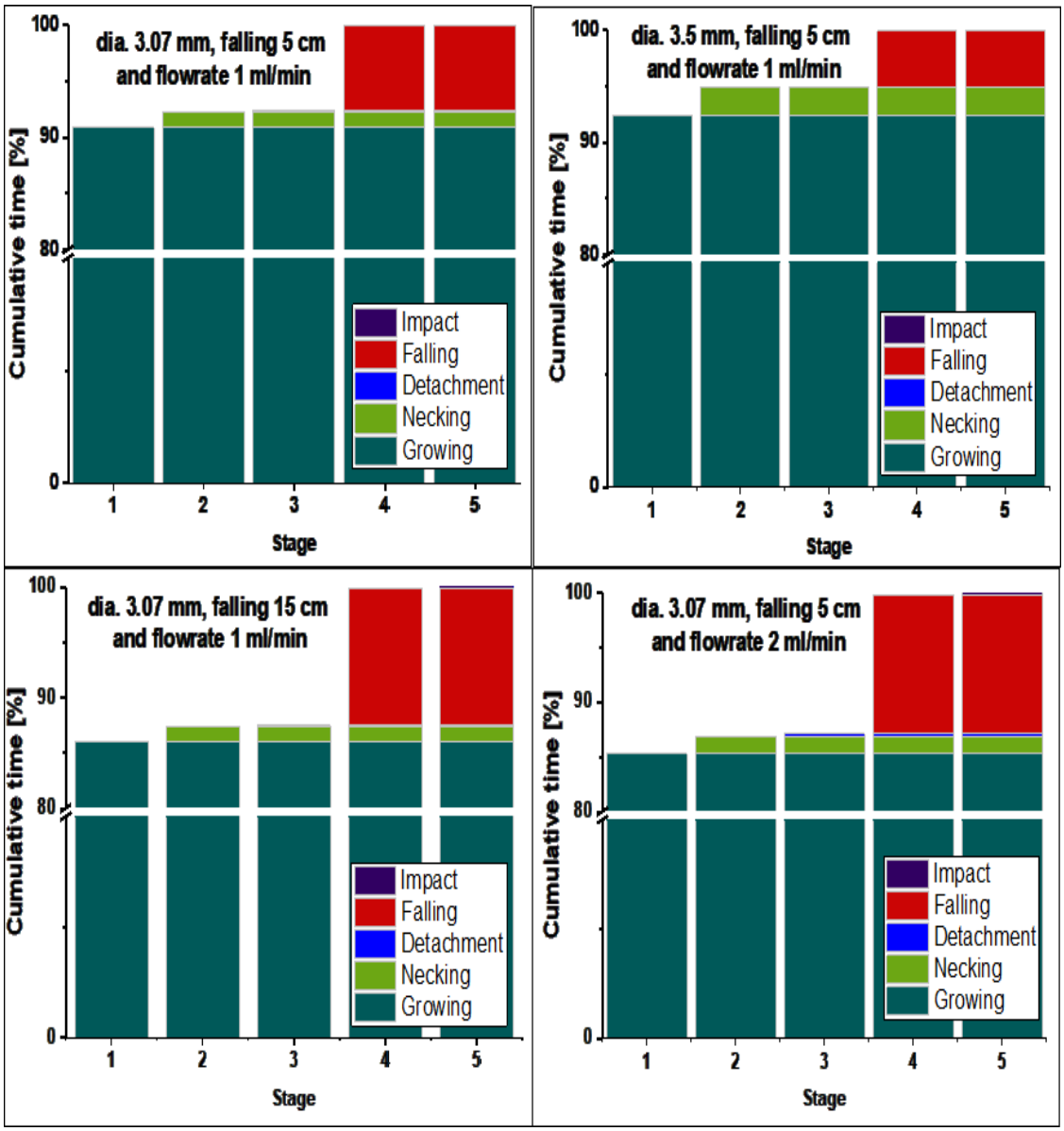

Figure 4-11 Time consumed by a droplet within subsequent stages of its lifetime, the volumetric flowrate and falling distance as parameters of each subplot.

4.5.3. Comparison of measured droplet velocity $U_{(t)}$ with model equation

The droplet velocity $U_{(t)}$ can be calculated by Eq. 4-17 which is derived for case of a free falling droplet with air resistance (drag) for the initial velocity $U_{(0)}$ = 0 m/s as a function of time and height of falling (h) [92]:

$$U(t) = U_t \left[1 - exp\left(\frac{-2gh}{{U_t}^2}\right)\right]^{1/2} \quad 4\text{-}17$$

The terminal velocity can be calculated using Eq.4-18, where *m* is mass of droplet, *g* is gravity constant, ρ is density of droplet, *A* is cross-sectional and C_D is drag coefficient. The coefficient of drag can be calculated for the droplet diameter d_d using Eq. 4-19 which is valid for Re number over 800 [94].

$$U_t = \sqrt{\frac{2mg}{\rho A C_D}} \quad 4\text{-}18$$

$$\log(C_D) = 0.15625(logd_d)^4 + 0.21924(logd_d)^3 + 0.70885(logd_d)^2 - 0.68973(logd_d) - 0.16055 \quad 4\text{-}19$$

The correlation between droplet velocity and distance of droplet is shown in Figure 4-12. For distance 0 cm to 15 cm, there exists no significant difference for the droplet velocity at different droplets diameter 1.61 mm, 2.67 mm and 3.0 mm, respectively. Generally, Figure 4-12 demonstrates a good conformity between the experimental results and the model equation (Eq.4-17).

Other experiment from Takagaki and Komori [94] almost find the same trend. Their experimental data of droplet velocity was coincident with numerical equation especially at below 50 cm after detachment from needle, as shown in Figure 4-13.

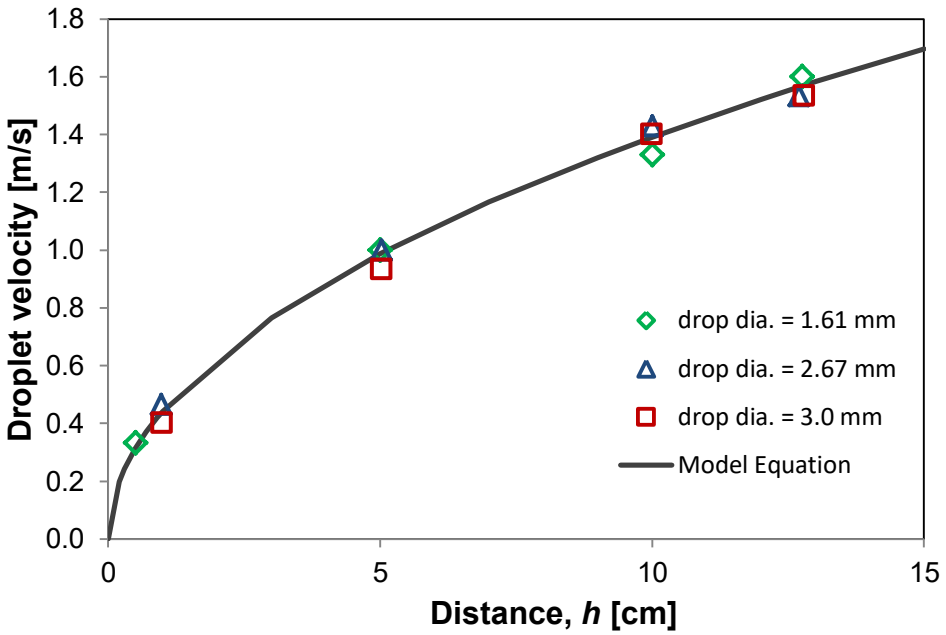

Figure 4-12. The correlation between measured droplet velocity $U_{(t)}$ and height of detachment for droplet diameter 1.61 mm, 2.67 mm and 3.0 mm. Solid line indicate the calculated droplet velocity according to Eq.4-17.

.

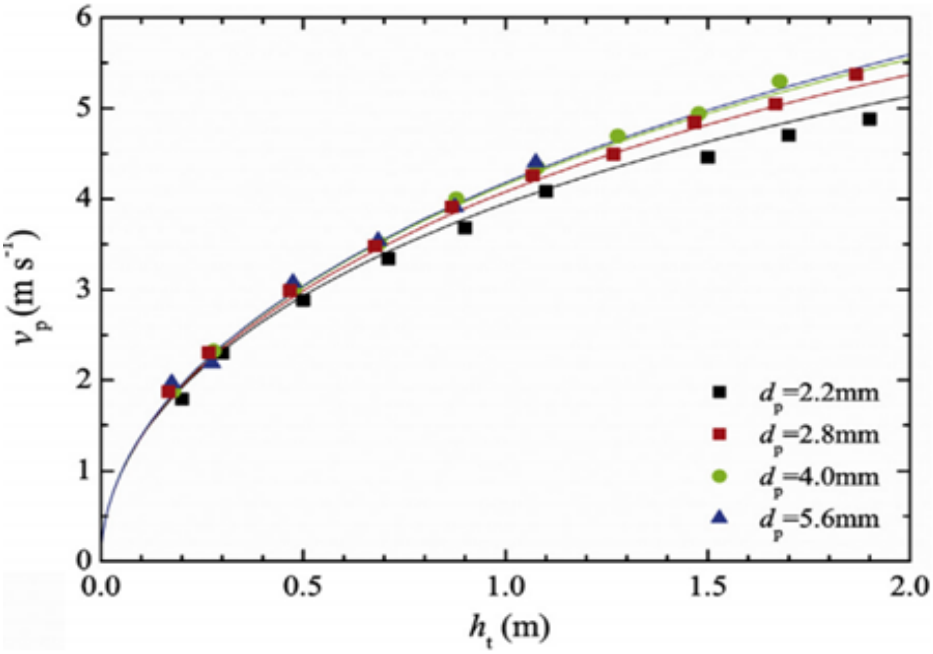

Figure 4-13. Relationship between needle elevation h_t and impinging velocity of drop v_p with the droplet diameter of 2.2 mm, 2.8 mm, 4.0 mm or 5.6 mm. Solid lines denote the numerical prediction. Measured data and equation from [94]

The experimental data for the terminal velocity of the droplets in the actual study as well as in [94] are also similar to a study conducted by Beard [95] at various atmospheric pressures especially at 1013 mbar and can be seen in the Figure. The large droplets have a higher droplet terminal velocity than the small ones due to droplet inertial force.

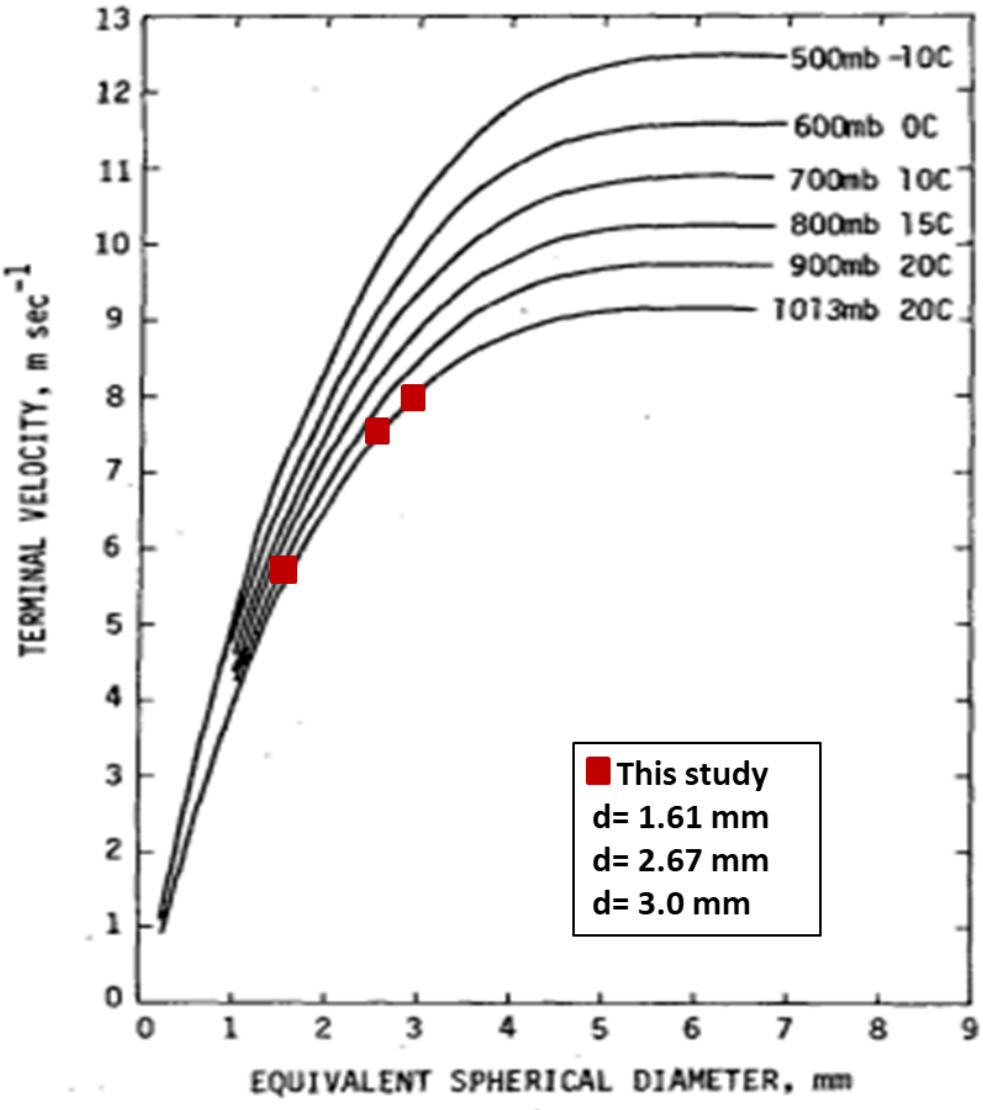

Figure 4-14. Terminal velocity of raindrops at five pressure levels in a summer atmosphere as function of the equivalent spherical diameter. Symbol denote the experimental data of the actual study for droplets diameter 1.61 mm, 2.67mm and 3.0 mm. Original figure from [95]; modified.

4.6. The effect of contact time on final CO_2 concentration during desorption

The concentration of CO_2during desorption from the droplets decreases according to the contact time between droplet and gas phase. The CO_2 concentrations decrease more significantly during the droplet formation compared to the droplet falling.

This decline was in line with a longer contact time during the droplet formation as described in the section 4.1.2 and Figure 4-11. The formation time plays an important role providing more than 85 percent of the overall contact time for a flowrate of 1 ml/minute.

Figure 4-15 to Figure 4-17 describe the CO_2 concentration changing drastically in the early stages of droplet formation. Besides the considerable duration of the formation time enhanced surface renewal during the droplet formation period is considered as the main reason for the strong concentration decline. It means there was CO_2 mass transfer from liquid to gas phase.

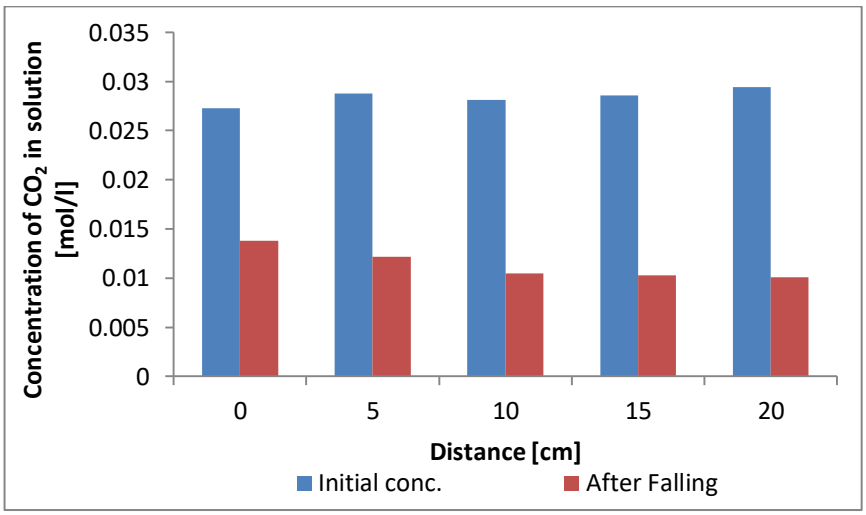

Figure 4-15. CO_2 concentrations in water droplet at initial solution and after falling at different distances for droplet diameter 1.61mm

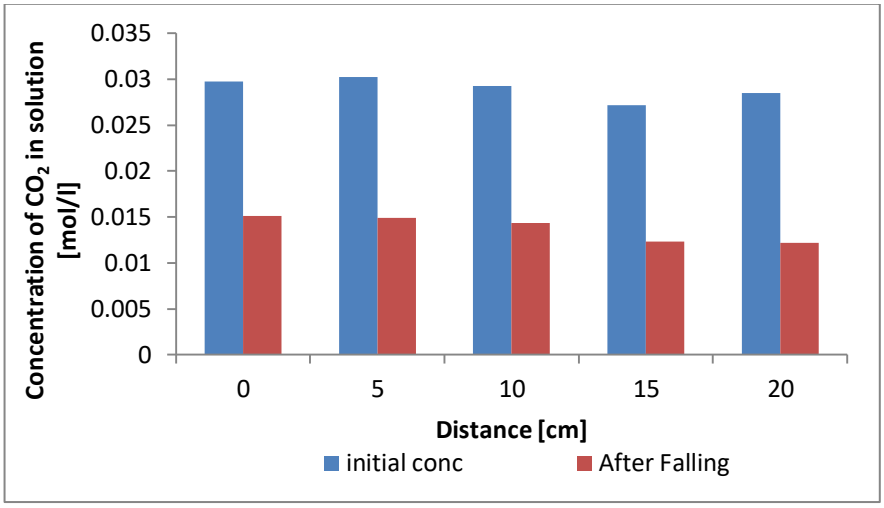

Figure 4-16. CO_2 concentrations in water droplet at initial solution and after falling at different distances for droplet diameter 2.67 mm

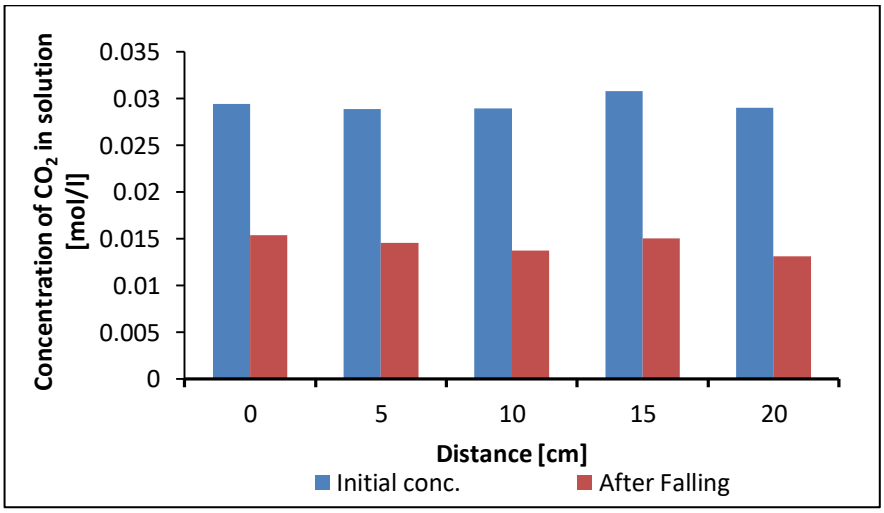

Figure 4-17. CO_2 concentrations in water droplet at initial solution and after falling at different distances for droplet diameter 3.0 mm

Trends like these were almost the same for the all droplet diameters, 1.61 mm, 2.67 mm and 3.0 mm respectively, and the rates of desorption in the period of falling droplets tend to decrease towards equilibrium. The raw data which are used for Figure 4-15, Figure 4-16 and Figure 4-17 can be seen in Appendix 4-4.

The concentrations of CO_2 desorbed during falling of fixed chamber length are less than that desorbed during formation as shown in Figure 4-18. The difference between the concentration of CO_2 in solution at the beginning (initial concentration) for different positions and the droplet formation time

and the falling showed an increasing trend in all diameters of droplets, as depicted in Figure 4-19. The graph tends to be constant especially for droplet diameters of 2.67 mm and 3.0, but for a droplet diameter of 1.61 mm the increase seems significant. The larger concentration changes occur in droplet formation. Experimental data and normalized data for CO_2 desorption are shown in Appendix 4-5 and Appendix 4-6.

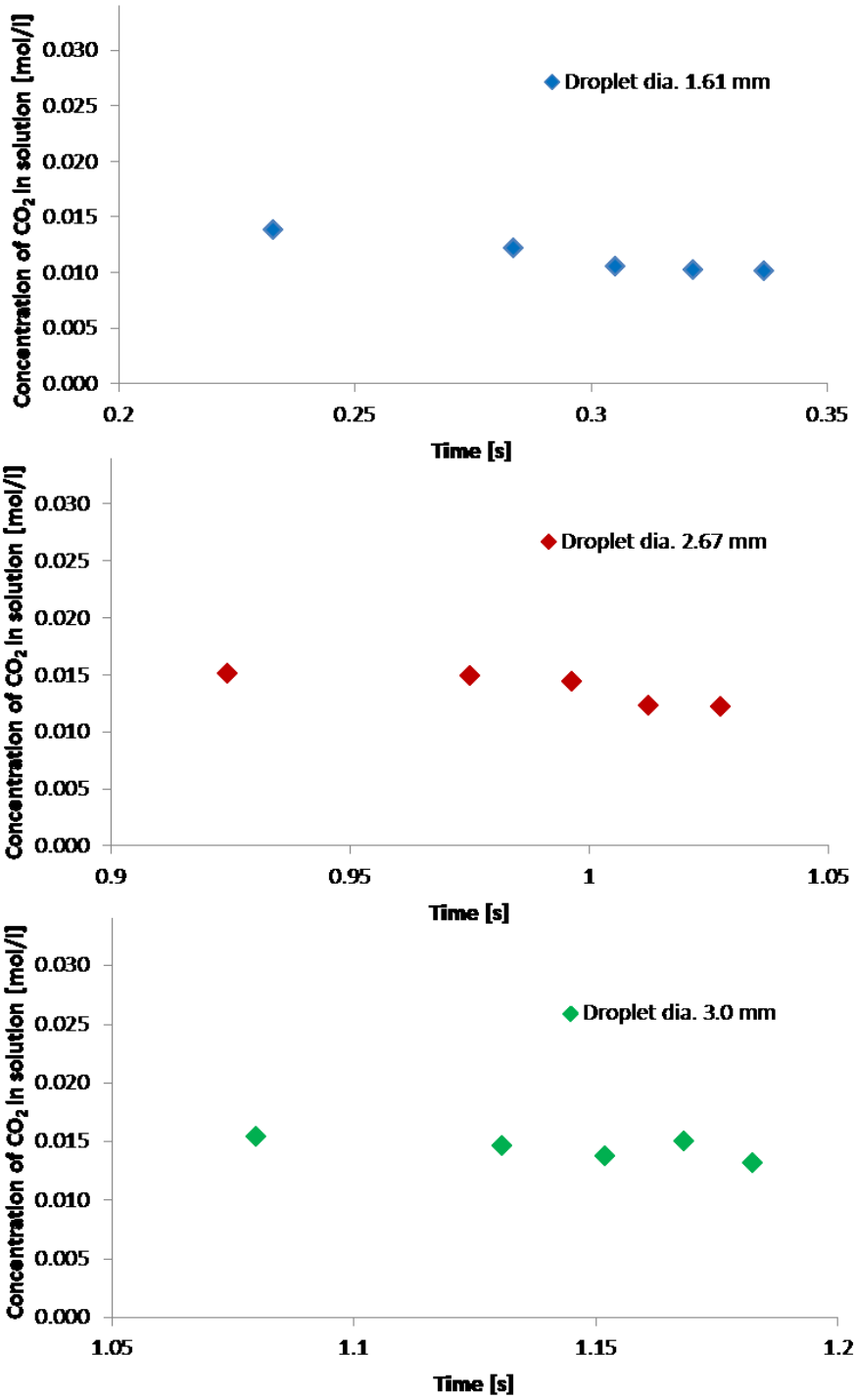

Figure 4-18 Concentration of CO_2 during formation and falling time

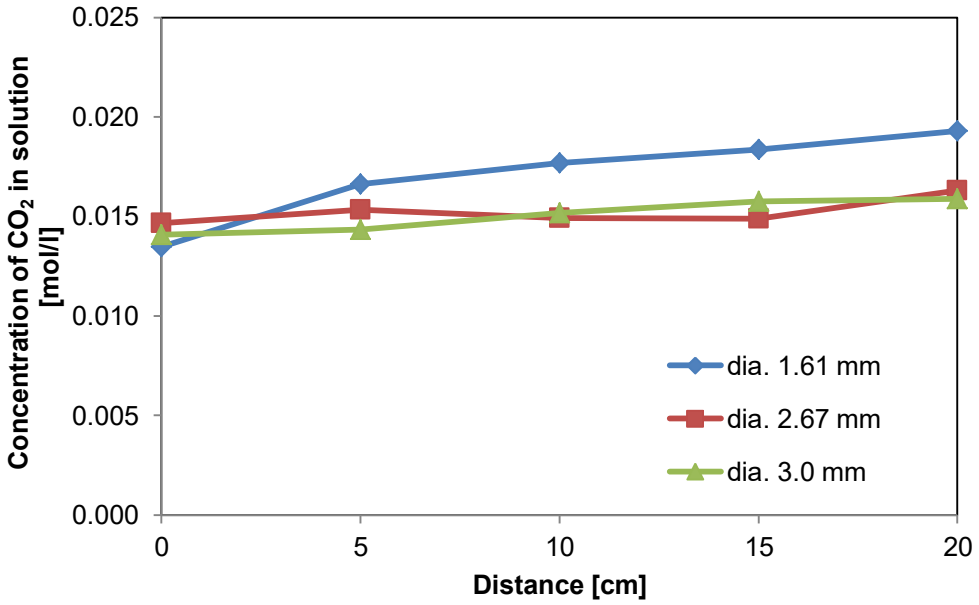

Figure 4-19 Concentration change of dissolved CO_2 after falling for various distances (0 cm = at droplet formation)

The data of the CO_2 concentrations in the solution in Figure 4-19 are obtained by using the precipitation-titration method (see section 3.7.2).

4.7. Comparison of desorption rate during formation and falling.

The desorption rate during formation increased as droplet diameter decreased and decreased as the contact time increased. Meanwhile during falling, the concentration decrease of droplet diameter 2.67 mm and 3.0mm showed only a slight difference. Contrary, in case of the droplet diameter of 1.61 mm, the concentration decreases during the fall showed three times higher values than the other droplets diameter as shown in Figure 4-8. This was due to the influence of desorption rate during droplet formation. During formation, pulsation or swing is observed sufficiently strong to enhance mass transfer from the liquid phase to the gas phase especially for a droplet diameter of 1.61 mm

As can been seen from Figure 4-7, the experimental desorption rate of CO_2 from water droplets during formation time decreases as the droplet formation time increases, especially in the first 0.8 s and then slow down afterwards. Han [36] has explained the rapid absorption decrease at the beginning of contact due to the influence of convection in the droplets as shown in Figure 4-20.

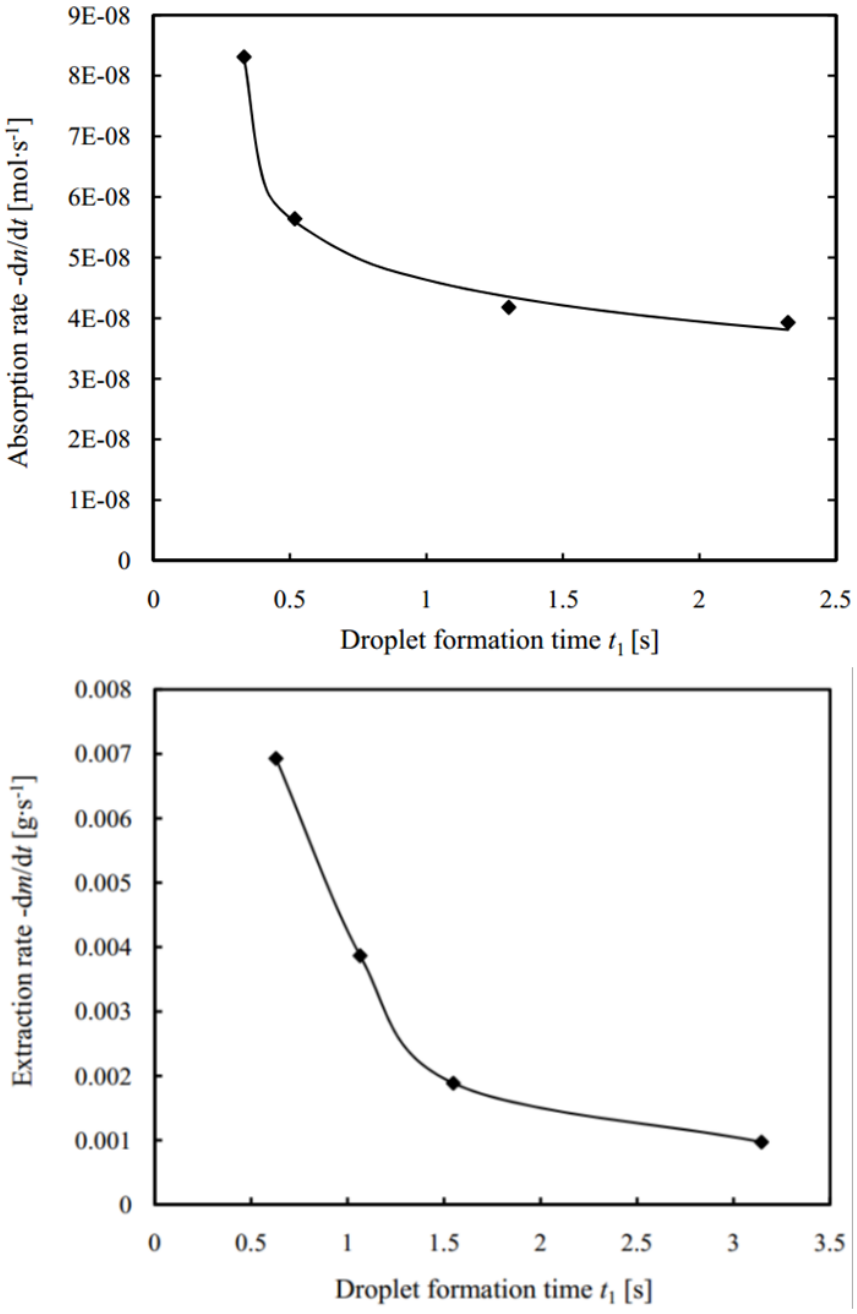

Figure 4-20 The experimental absorption rate of Rajan and Heideger [64] and Han et al. [36]; above graph is absorption rate of CO_2 in water and below graph is extraction rate of a slightly soluble organic drop and surrounding water with different droplet formation time.

4.8. Comparison of measured mass transfer coefficient and model calculations

The mass transfer coefficients of CO_2 desorption from water droplets during formation decreased as formation time increased. Han etal.[34] found the same trend on an absorption experiment for CO_2 into water droplet at 303.65K and 323.25K as shown in Figure 4-21. Rajan and Heideger [64] found a similar tendency in their study of liquid/liquid mass transfer system. They studied the mass transfer during formation time of a slightly soluble organic droplet in a surrounding aqueous phase with different needle diameters as shown in Figure 4-22. The overall trend of their graph is the same as in our experiment as shown in Figure 4-23.

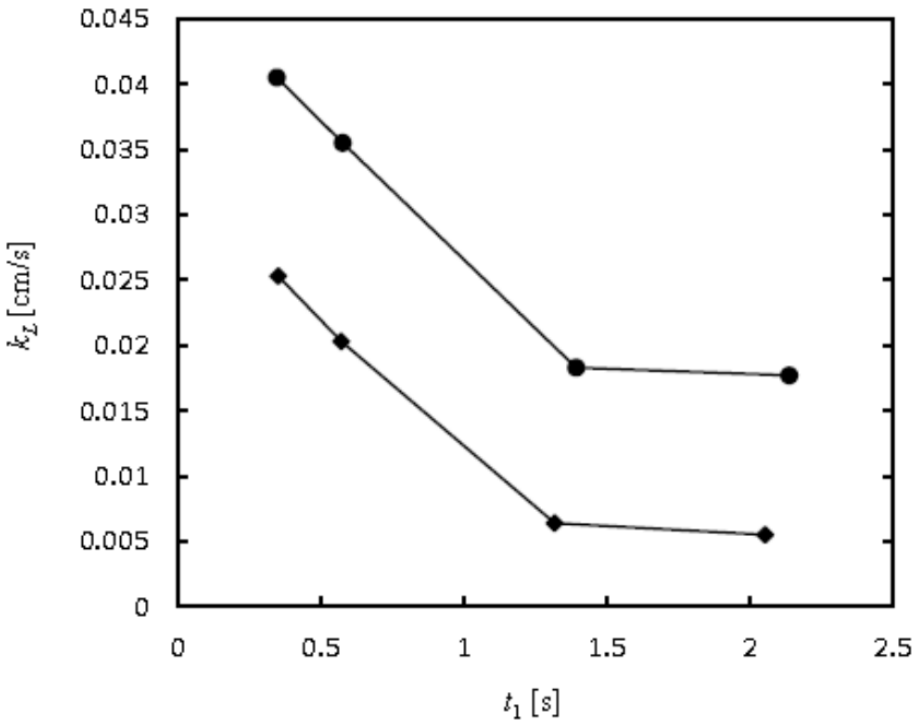

Figure 4-21 The variation of liquid phase mass transfer coefficient k_L of CO_2 into water droplets during formation and a fall over 0.59 m as a function of droplet formation time t_1 at different temperatures. ♦303.65K; ● 323.15 K. [34].

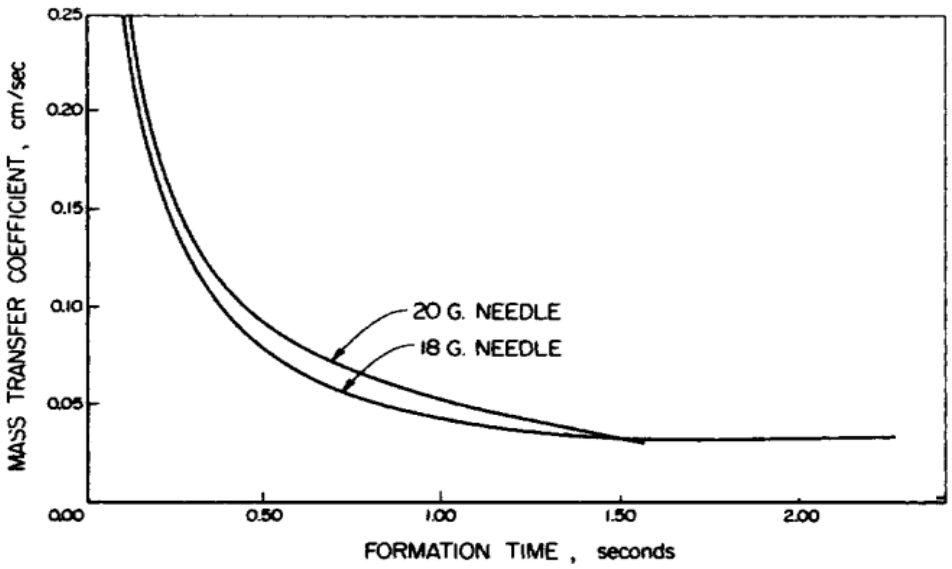

Figure 4-22. Effect of nozzle diameter on mass transfer coefficient during drop formation at flowrate 0.7953 ml/min [64].

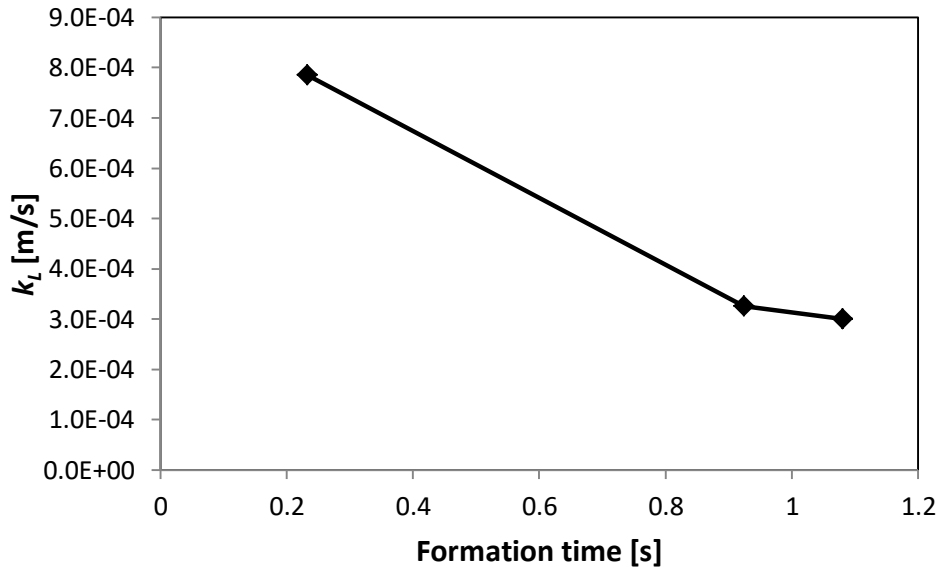

Figure 4-23. Mass transfer coefficients as a function of formation time; measured data from own experiments.

The mass transfer coefficient as a function of falling distance tends to be constant for all droplet diameters. The value of mass transfer coefficient for droplet diameter 2.67 mm and 3.0 mm tends to be the same. The effect of the droplet diameter is not clearly apparent on the mass transfer coefficient, except for droplet diameter 1.61 mm, where the value of mass transfer coefficient was twice as high compared to the other two droplet diameters as

shown in Figure 4-24. A small droplet has a larger surface area to volume ratio than a big droplet, providing better mass transfer under comparable hydraulic conditions. Due to its lower terminal velocity a smaller droplet will also experience an increased contact time, especially for longer contact distances. The later aspect was already mentioned by Oliver et.al [18].

Furthermore, since the velocity of the liquid issuing the needle drives the convection inside the droplet, mixing intensity during droplet formation might be more pronounced for smaller droplets, where the mixing effect is concentrated within a smaller volume. Increased convection within the droplet therefor enhances mass transfer within short droplet formation time.

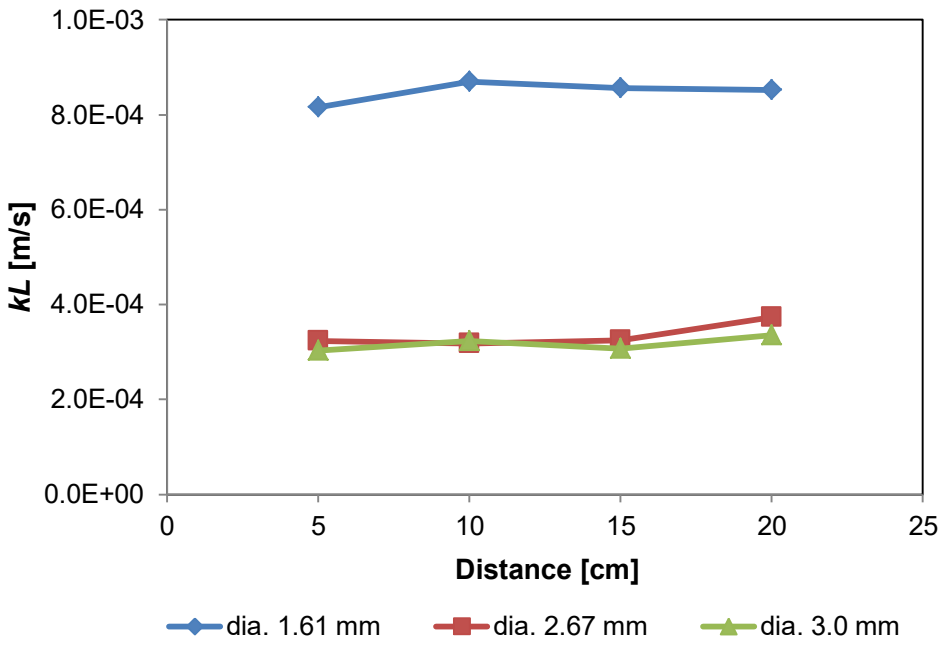

Figure 4-24. Mass transfer coefficients for various falling distances and droplet diameters; data from own experiments.

Convection inside droplets has a very significant effect on mass transfer if the droplet formation time is short. So for droplets having very short formation time, mass transfer rate decreases sharply along with increasing time of drip formation. On the other hand, convection becomes less important than the diffusion in total mass transfer for droplets having a large formation time. When the droplet formation is long enough, droplets will appear stagnant,

mass transfer between CO_2 and water droplets will be increasingly controlled by diffusion and the time of droplet formation will not affect the rate of mass transfer anymore. However, most of the literature sources present the results and discuss the descriptive model over a longer period of droplet formation.

Using the data obtained from the experiment, mass transfer coefficients were determined by the mass transfer equation model as documented in references such as Higbie and others. The calculated mass transfer coefficients based on model equations are presented in Table 4-8. Comparison of the mass transfer coefficients of some references to own experiment are shown in Table 4-9.

Table 4-8 Model based calculations of mass transfer coefficients

Model	**Droplet dia. 1.61 mm**	**Droplet dia. 2.67 mm**	**Droplet dia. 3.0 mm**
Higbie [57]	9.90E-05	5.00E-05	4.40E-05
Handlos and Baron [74]	4.35E-04	5.61E-04	5.94E-04
Ruckenstein [76]	1.50E-03	1.17E-03	2.53E-03
Angelo et al.[75]	9.80E-03	5.03E-04	4.61E-04
Hsu et al [77]	4.90E-04	3.40E-04	3.11E-04
Srinivasan and Aiken [33]	5.71E-04	7.24E-04	7.65E-04
Amokrane et al.[78]	2.78E-04	2.45E-04	2.40E-04
This study*	7.85E-04	3.26E-04	3.01E-04

* This value during formation

The predicted mass transfer coefficient for the internal circulation and the oscillation model as a function of droplet diameter is depicted on Figure 4-25. The experimental mass transfer coefficients (this study) were fit with the oscillation model by Hsu et al.[77] especially for droplet diameter of 2.67 mm (2670 μm) and 3.0 mm (3000 μm). For the droplet diameter of 1.61 mm the experiment closed to oscillation model by Angelo et al[75]. Figure 4-25 shows that the mass transfer of CO_2 desorption is mainly due to convective mass transfer by oscillation.

Table 4-9 The mass transfer coefficient of CO_2 absorbed by water; comparison with literature sources.

Author	t [s]	Droplet diameter [mm]	k_L [m/s]		Height [cm]	Temp [°C]
			during formation	during falling		
Whitman et al. [30]	0.5	5.46	1.20E-05	7.47E-04	52	24.5
	4.94		1.10E-05	9.39E-04	52	24.6
Dixon and Russell[31]	0.5	4.58	3.14E-04	2.94E-04	52	21
	5		5.70E-05	8.90E-05	52	21
Altwicker and Lindhjem [32]	0.1	0.6	0.00101 ± 0.00025		13	23
		1.2	0.00059 ± 0.00005		13	23
Srinivasan and Aiken[33]	0.002	0.0824	2.4E-03 - 6.4E-03		1	25
	0.352	2.533	2.53E-04		59	30
Han et al.[34]	2.053	2.586	5.50E-05		59	30
	0.413	2.54	1.73E-04		41	30
	0.643	2.434	1.16E-04		41	30

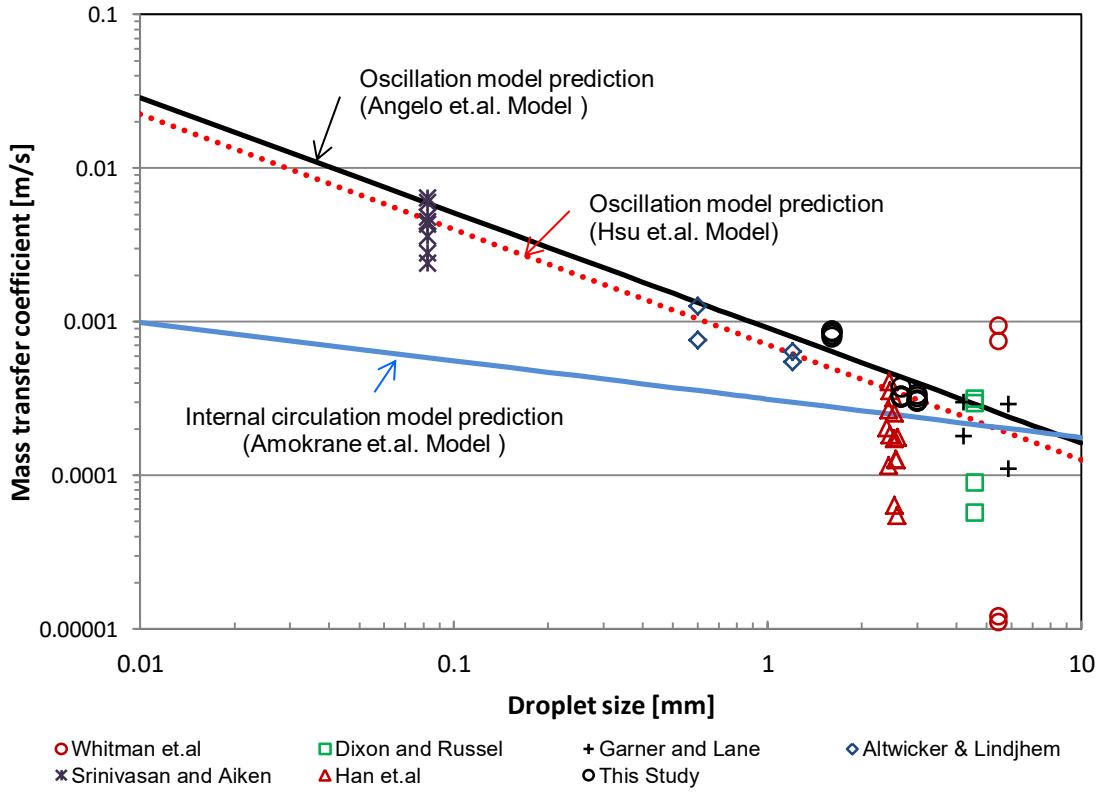

Figure 4-25 Mass transfer coefficients as a function of droplet diameter from literature sources and this study, together with predicted trend lines from models.

The ratio of CO_2 concentration after desorption (c_2) and initial CO_2 concentration (c_1) that has been obtained in the experiment is plotted as a function of time, and then compared with the existing models. The CO_2 concentration after desorption (c_2) from the model was obtained using Eq. 2-39. By assuming the initial CO_2 concentration for atmospheric condition, to be 0.0000135 mol/l, the mass transfer coefficients (k_L) are calculated on the basis of each model equation. For example, the comparison of data between experiments and the Hsu et al. model and the percentage difference of both can be seen in Table 4-10. The calculation of CO_2 concentration using the mass transfer model from various references is presented in Appendix 4-7.

Table 4-10 shows that the experimental data have little difference to the Hsu's model, especially for the droplet diameter of 2.67 mm and 3.0 mm except the nozzle diameter of 1.61 mm.

Table 4-10 A comparison on CO_2 desorption data between own experiment and model of Hsu et al.

Droplet diameter of 1.61 mm

time [s]	height [cm]	Own experiment			Model of Hsu			difference [%]
		c_1 [mol/l]	c_2 [mol/l]	c_2/c_1	c_1 [mol/l]	c_2 [mol/l]	c_2/c_1	
0.2328	0	0.027	0.014	0.506	0.03	0.020	0.650	14.39
0.2836	5	0.029	0.012	0.422	0.03	0.018	0.592	16.96
0.3052	10	0.028	0.010	0.372	0.03	0.017	0.569	19.66
0.3218	15	0.029	0.010	0.358	0.03	0.017	0.552	19.31
0.3368	20	0.029	0.010	0.343	0.03	0.016	0.536	19.30

Droplet diameter of 2.67 mm

time [s]	height [cm]	Own experiment			Model of Hsu			difference [%]
		c_1 [mol/l]	c_2 [mol/l]	c_2/c_1	c_1 [mol/l]	c_2 [mol/l]	c_2/c_1	
0.9244	0	0.030	0.015	0.508	0.03	0.015	0.494	1.40
0.9750	5	0.030	0.015	0.492	0.03	0.014	0.475	1.69
0.9963	10	0.029	0.014	0.490	0.03	0.014	0.468	2.27
1.0124	15	0.027	0.012	0.452	0.03	0.014	0.462	0.97
1.0274	20	0.029	0.012	0.428	0.03	0.014	0.457	2.85

Droplet diameter of 3.0 mm

time [s]	height [cm]	Own experiment			Model of Hsu			difference [%]
		c_1 [mol/l]	c_2 [mol/l]	c_2/c_1	c_1 [mol/l]	c_2 [mol/l]	c_2/c_1	
1.0800	0	0.029	0.015	0.522	0.03	0.015	0.511	1.18
1.1306	5	0.029	0.015	0.504	0.03	0.015	0.495	0.94
1.1519	10	0.029	0.014	0.476	0.03	0.015	0.488	1.27
1.1684	15	0.031	0.015	0.489	0.03	0.015	0.483	0.51
1.1825	20	0.029	0.013	0.453	0.03	0.014	0.479	2.63

Experimental and computation results are recapitulated in Figure 4-26 to Figure 4-28. In these figures, experimental results for droplet diameters of 1.61 mm, 2.67 mm and 3.07 mm were compared with some models of mass transfer coefficients. For droplet diameters of 2.67 mm and 3.0 mm, the experimental results are in good agreement with the model from Hsu et al. [77]. This model is a semi empirical equation that predicts the mass transfer coefficient based on the surface stretch model, and is valid for droplet diameters in the range of 0.6 to 6.0 mm. For droplet diameter of 1.61 mm, the experimental results do not fit with Hsu's model, however a good agreement with Angelo's model [75] is found. It should be mentioned that the video recordings as illustrated in Figure 4-2 for the droplet diameter of 1.61 mm also confirmed good mixing due to pulsation or oscillation during the droplet formation.

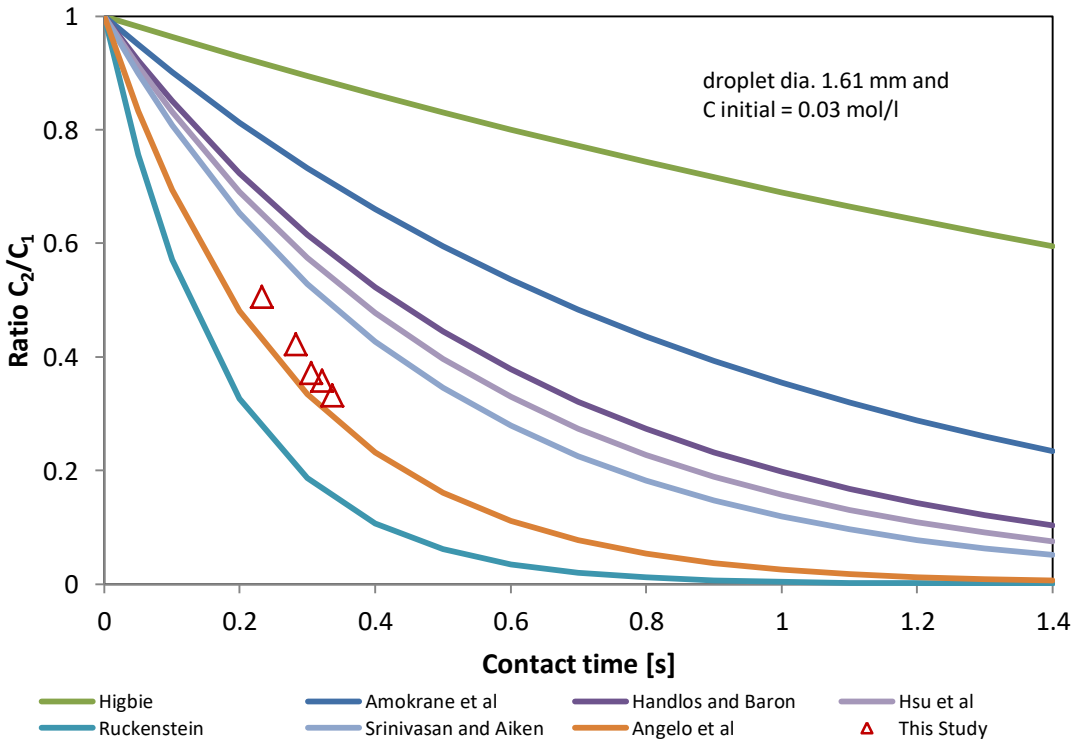

Figure 4-26 Ratio of concentration of CO_2 desorption at different contact times for droplet diameter 1.61 mm and for different models (average)

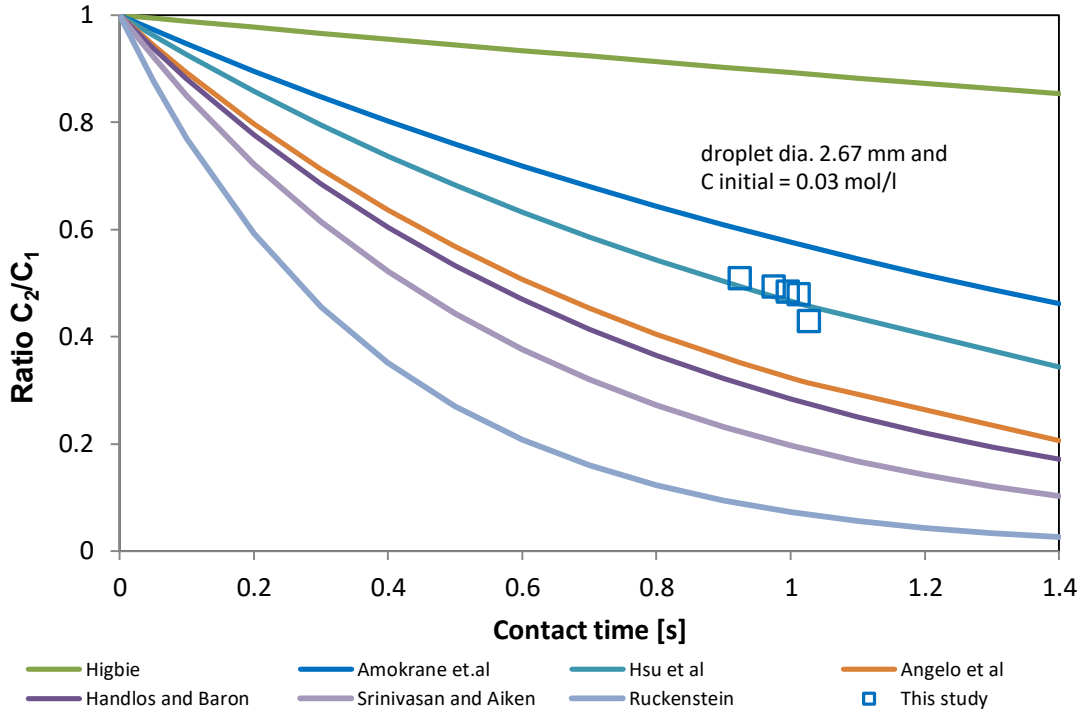

Figure 4-27 Ratio of concentration of CO_2 desorption at different contact times for droplet diameter 2.67 mm and for different models (average)

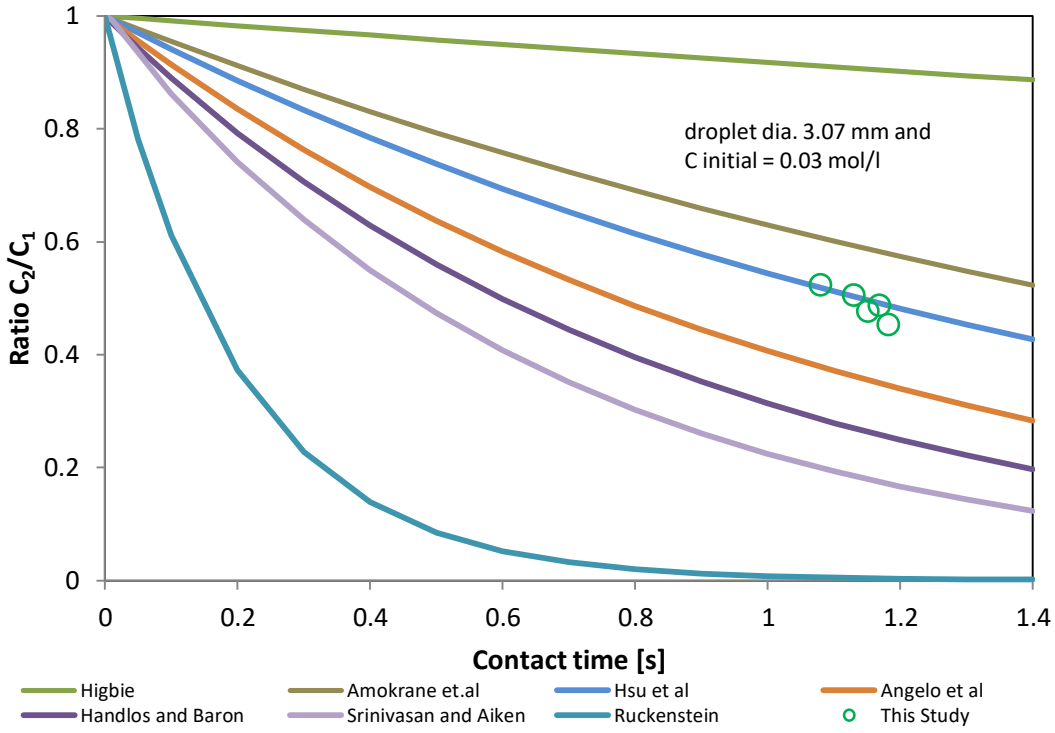

Figure 4-28 Ratio of concentration of CO_2 desorption at different contact times for droplet diameter 3.0 mm and for different models (average).

Trends in Figure 4-26 to Figure 4-28 are the same as those shown by some other investigators. Walcek and Pruppacher [96] conducted a study to predict the theoretical absorption of SO_2 with water droplets in the air that have been verified satisfactorily by their experimental results for less than 500 drops of radii as shown in Figure 4-29.

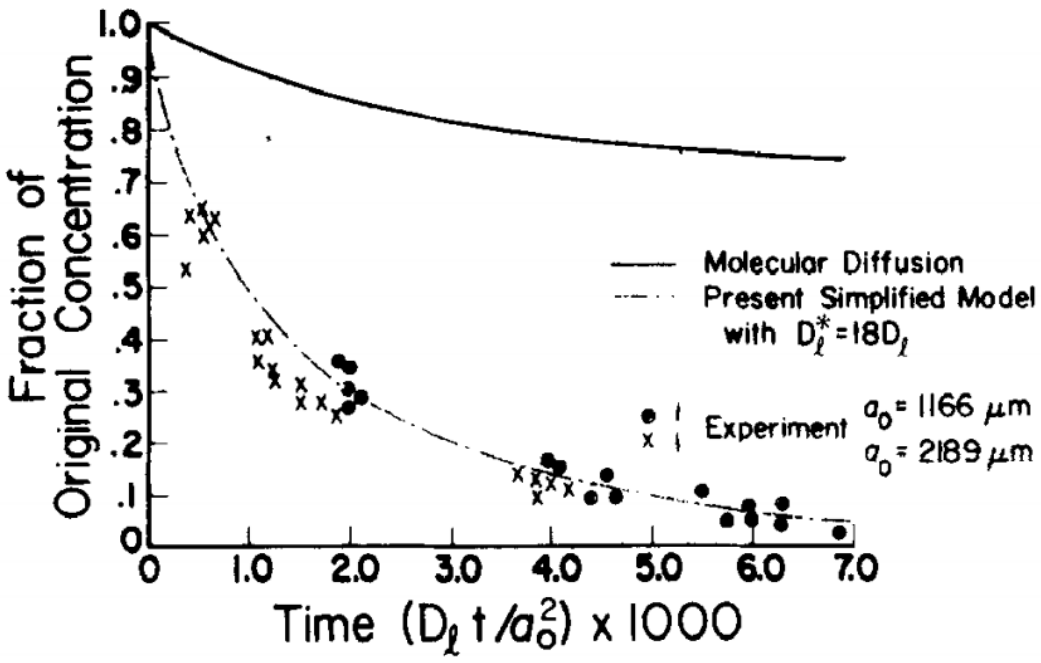

Figure 4-29 A comparison of theory and experiment for the desorption from drops of a = 1166 μm and 2189 μm. Concentration expressed as a fraction of the initial concentration is plotted against a non-dimensionalized time. [96]

A similar study was also done by Mitra and Hannemann [97]. They have conducted experimental and theoretical research to investigate the SO_2 desorption rate from water droplets falling at the terminal velocity in air. The experiments were conducted in the Mainz vertical wind tunnel where water droplets of various diameters containing S (IV) in various free concentrations were suspended in the tunnel's vertical airflow. The results of this experiment were compared with the predictions of the three theoretical models and with experiments derived from Walcek et al. [96] studied on a 1.17 mm droplet radius [S (IV)] initial = 0.1 mole/liter and at 15 ° C. The obtained results by the investigator as mentioned above can be seen in Figure 4-30.

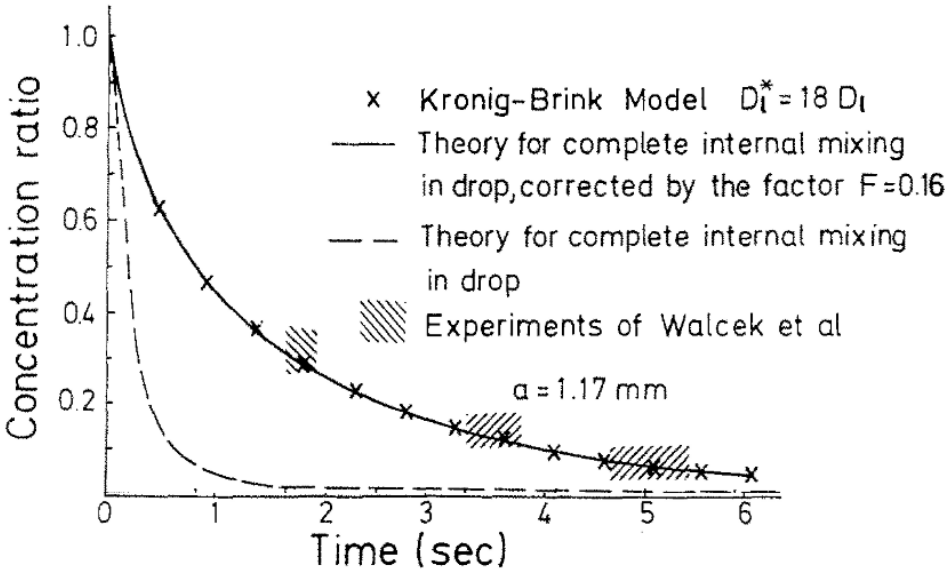

Figure 4-30 Comparison of the rate of desorption of SO_2 from a water drop as observed by the experiments of Walcek et al [96], the predictions of the Kronig-Brink model, the uncorrected theory for complete internal mixing, and the theory for complete internal mixing corrected by a factor F; a 1.17 mm droplet radius [S (IV)] initial = 0.1 mole/ liter and at 15 ° C. [97]

4.9. Analysis of dimensionless numbers based on experimental data and comparison with models

Droplet diameters did not significantly affect the Reynolds numbers at the same height level due to differences in droplet velocities for different diameters tend to be the same (see Figure 4-6). The drag coefficient of all investigated droplets is therefore clearly in the transition regime (Figure 4-31).

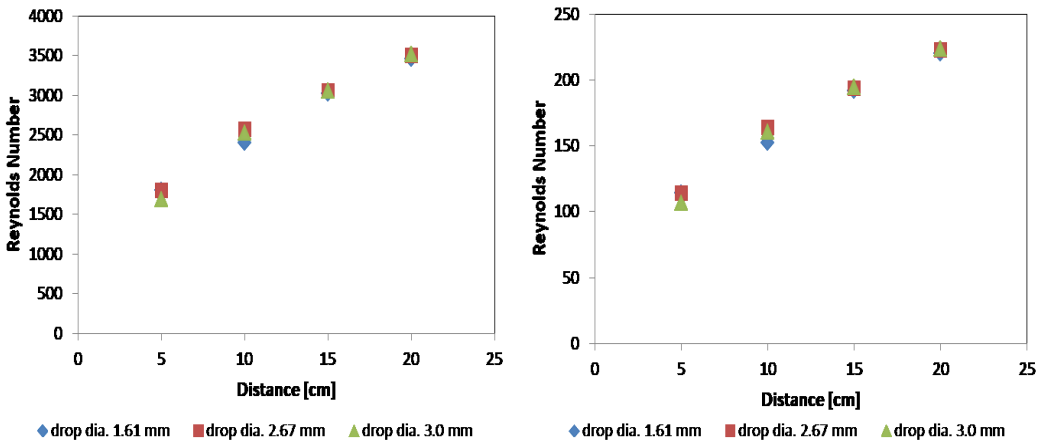

Figure 4-31 Reynolds number of falling droplet with various droplet diameter and falling distances (left in liquid-side; right in gas-side).

The Weber number in this study is seem in Figure 4-32. The Weber numbers are generated from the experimental condition of falling droplets and turn out to always be small than 1. That implies only small deformation of spherical droplet shape to be induced by the rather small relative velocities involved in our experiments. Note, that Weber numbers at least would have to exceed We = 6 to induce relevant droplet deformation by air flow. The deviation of ideal droplet shape as monitored by the video pictures therefore are mainly caused by the droplet formation at the nozzle tip.

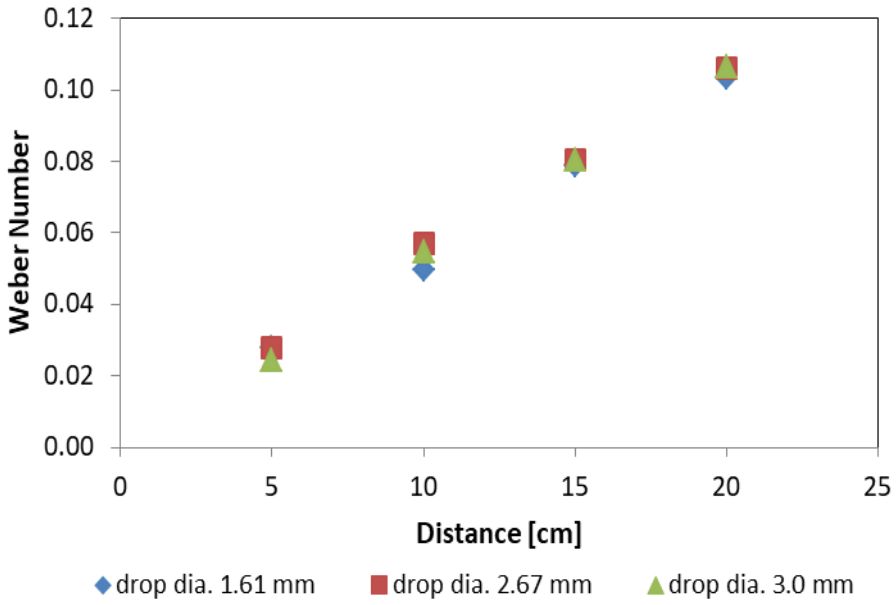

Figure 4-32 Weber number for various droplet diameters and distances within the droplet falling experiments.

Additional information considering droplet deformation during impact on the kerosene layer are presented in the Appendix 4-8.

Figure 4-33 provides a comparison of the Sherwood numbers calculated according to the dimensionless number correlation in Table 2-2 with Sherwood numbers quatifying the experimental findings. Generally experimetal Sherwood numbers are located within the parameter range spanned by the correlation. Although the models cover the experimental order of magnitute of the mass transfer intensity in dimensionless form the

general trends of the experimental data series against falling distances are clearly different compare to one of the models. Therefrom we conclude that currently available mass transfer models are not fully capable of covering the droplet mass transfer dynamics at least for the condition studied in our experiment. Detail data of dimensionless numbers can been seen in Appendix 4-9.

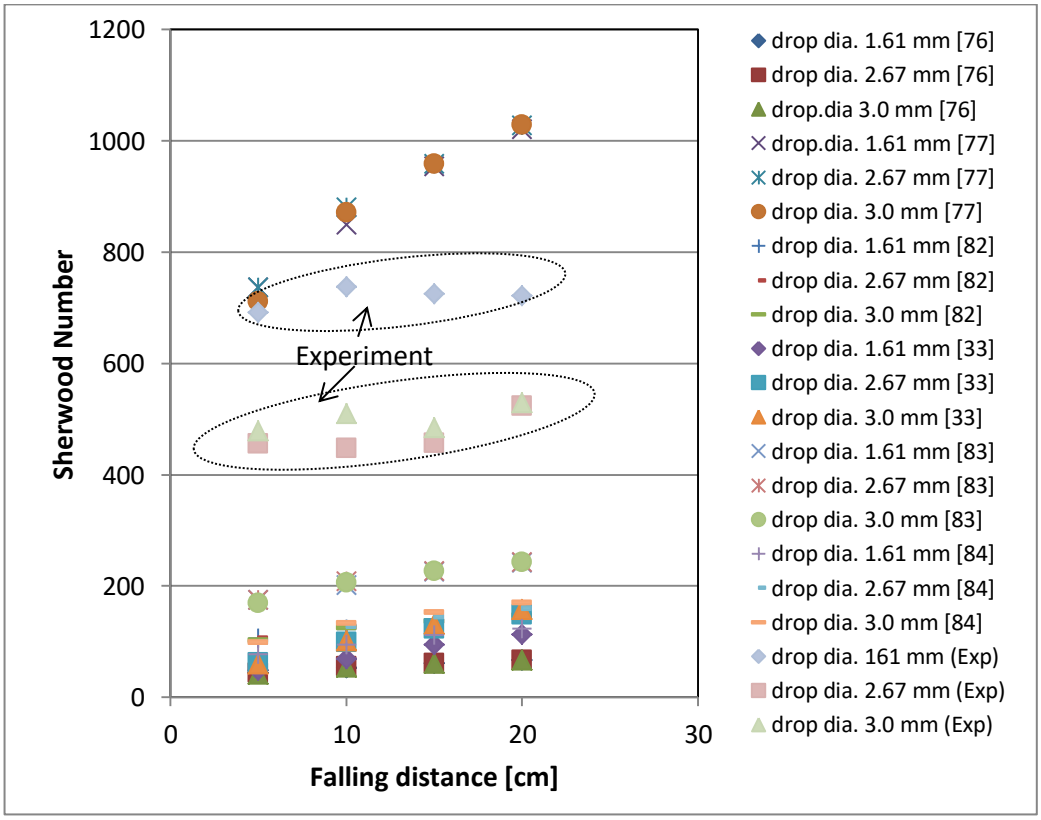

Figure 4-33 Sherwood number of models compared with experiment.

5. CONCLUSIONS AND SUGGESTIONS

5.1. Conclusions

In this study, an experimental apparatus was manufactured to investigate desorption of CO_2 from water droplets. The water droplets were produced by pumping the liquid through different needles with outer diameters of 0.5 mm, 0.6 mm and 0.8 mm and at constant flowrate 1 ml/minute. The water droplet fell through a rectangular gas chamber one by one continuously over different distances 5, 10, 15 and 20 cm before being deposited under kerosene. The droplet diameters that are generated from the different needles were 1.61, 2.67 and 3.0 mm. The shape of the droplets generally was spherical during falling.

The observation of droplet diameters was performed by means of a combination of high-speed camera and an imaging processing (shadowgraphy method). Measurement of droplet diameter was done using software and manual calculation. The difference between the two calculations is approx. 0.37 percent and that means that manual calculations show precise results.

The determination of droplet velocity also used an observation video from the high-speed camera with image processing software. There were no significant differences of droplet velocity for all droplets diameter 1.61 mm, 2.67 mm and 3.0 mm within the investigated falling distance of 15 cm, respectively when compared with the model equation.

The molar amount of CO_2 desorption from the water droplets decreases as the contact time increases. The CO_2 concentration decreased more significantly during formation, mainly because contact times during the formation were dominant compared to falling.

The desorption rate during falling for a droplet diameter of 1.61 mm showed three times higher values than the other droplets diameters (2.67 mm and 3.0 mm) due to the influence of pulsation during droplet formation as mentioned in the section 4.8 and Figure 4-2.

The mass transfer coefficients of CO_2 desorption from water droplets increase as the droplet diameter increases both during formation and falling. The mass transfer coefficients during falling increase with increasing height of falling but not significantly.

Comparison of experimental results with the model equations of Hsu et al. showed good agreement for droplet diameter 2.67 mm and 3.0 mm. Meanwhile for droplet diameter 1.61 mm a good fit is received with the mass transfer model of Angelo et al. This influence was attributed to strong pulsation during droplet formation particularly on a small nozzle (see Figure 4-2).

Reynolds numbers at the same height were not affected by the droplet diameter differences. The regimes of the drag coefficient were transition. Weber numbers of this study at experimental conditions were smaller than 1 which implies the droplet still spherical shapes although being little deformation during falling. Existing Sherwood numbers models have not been suitable with our experiment.

5.2. Suggestions for future work

Some suggestions need to be considered for future work as follows:

a. Measurement of droplet diameter and droplet velocity requires re-arrangement, because with the current camera setup it was not possible to capture images more than 15 mm in length, as previously mentioned. Eventually, a mechanical electrical traversing system can be applied to facilitate capturing of pictures without changing the gas chamber.

b. A rectangular droplet chamber was built for determination mass transfer coefficient of CO_2 desorption from water droplets. In addition, the current device might be useful to measure mass transfer coefficients of CO_2 absorption by water droplet and studying a selection of other absorbents (NaOH, MEA, Sulfite or Ammonia etc.) for spray column applications.

c. It is difficult to obtain a small droplet smaller than 1 mm by pumping through the needle even with a small needle. Therefore the use of a piezoelectric generator serves as alternative for generating a small droplet in micro diameter range.

d. In this work, the concentration of CO_2 after desorption was investigated only by titration analysis within the aqueous phase. Currently no attempts were undertaken to measure the CO_2 concentration development in gas field, e.g. based on an IR analyzer [98–100].

Nomenclature

A_d droplet surface area, [m^2 or cm^2]

A_{max} maximum surface area during droplet oscillation, [m^2 or cm^2]

a acceleration [m/s^2]

c concentration of CO_2 in liquid, [mol/m^3ormol/l]

c_{Ab} concentration of component A in liquid bulk, [mol/m^3ormol/l]

c_{Ai} concentration of component A in liquid interface, [mol/m^3ormol/l]

C_D drag coefficient

C_{g^*} concentration of gas in equilibrium, [mol/m^3ormol/l]

C_{gb} solute concentration in gas bulk, [mol/m^3ormol/l]

C_{gi} solute concentration in gas interface, [mol/m^3ormol/l]

$C_{g,tot}$ total concentration in gas phase, [mol/m^3ormol/l]

C_{HCl} concentration of HCl solution, [mol/m^3ormol/l]

C_{NaOH} concentration of NaOH solution, [mol/m^3ormol/l]

C_{l^*} concentration of liquid in equilibrium, [mol/m^3ormol/l]

c_{l^*} equilibrium concentration of CO_2 in liquid, [mol/m^3ormol/l]

C_{lb} solute concentration in liquid bulk, [mol/m^3ormol/l]

C_{li} solute concentration in liquid interface, [mol/m^3ormol/l]

$C_{l,tot}$ total concentration in liquid phase, [mol/m^3or mol/l]

D diffusion coefficient, [m^2/s or cm^2/s]

D_{AB} diffusion coefficient or diffusivity for component A in B, [m^2/s or cm^2/s]

D_L diffusion coefficient of liquid side, [m^2/s or cm^2/s]

d diameter, [mm or μm]

d_d droplet diameter, [mm or μm]

d_{fl} droplet diameter during falling, [mm or μm]

d_{fr} droplet diameter during formation, [mm or μm]

d_j jet diameter, [mm or μm]

d_n nozzle diameter, [mm or μm]

d_{10} average diameter of droplet, [mm or μm]

d_{32} Sauter mean diameter of droplet, [mm or μm]

F_b buoyant forceF_D drag force

f oscillation frequency of droplet [1/s]

g acceleration of gravity [m/s^2 or cm/s^2]

H	Henry's coefficient, [dimensionless]
H'	Henry's coefficient, [atm m^3/mol]
h	droplet falling height, [cm or mm]
K_G	overall gas phase mass transfer coefficient, [m/s or cm/s]
K_L	overall liquid phase mass transfer coefficient, [m/s or cm/s]
k_g, k_G	gas-side mass transfer coefficient, [m/s or cm/s]
k_l, k_L	liquid-side mass transfer coefficient, [m/s or cm/s]
K	equilibrium constants for reaction
lj	jet length [cm or mm]
N	molar flux, [mol/m^2.s]
N_A	molar flux of component A, [mol/m^2.s]
n	amount of mol of substance, [mol]
n_{CO2}	amount of CO_2 dissolved, [mol]
m	mass of droplet, [g or mg]
Oh	Ohnesorge number, $We^{1/2}/Re$
p_{Ab}	partial pressure of component A in the bulk, [atm]
p_{Ai}	partial pressure of component A in the interface, [atm]
Re	Reynolds number, ρUd/μ
s	fraction of surface renewal
Sc	Schmidt number, μ/(ρ D)
Sh	Sherwood number, k_Ld/D
T	temperature, [°C]
t	time, [s]
t_d	droplet contact time, [s]
t_e	exposure time, [s]
t_{fl}	droplet falling time, [s]
t_{fr}	droplet formation time, [s]
U	velocity, [m/s or cm/s]
U_d	droplet velocity, [m/s or cm/s]
U_t	terminal velocity, [m/s or cm/s]
U_j	jet velocity, [m/s or cm/s]
u_*	interfacial droplet velocity, [m/s]
V_d	droplet volume, [m^3 or mm^3]
V_{HCl}	volume of HCl solution, [ml]
V_{NaOH}	volume of NaOH solution, [ml]

W	weight force
We	Weber number, $U^2\rho d/\sigma$
x	distance to x direction, [mm]
y	distance to y direction, [mm]
[ ]	concentration, mol/l
α	constants in Eq. 2-14
β	value between 0.5 – 1 in Eq. 2-14
Δ	differences
δ	film thickness [mm or μm]
δ_G	gas-side film thickness [mm or μm]
δ_L	liquid-side film thickness [mm or μm]
μ	dynamic viscosity, [Pa.s or N.s/m^2 or kg/(m·s)]
μ_G	dynamic viscosity of gas phase, [Pa.s or N.s/m^2 or kg/(m·s)]
μ_L	dynamic viscosity of liquid phase, [Pa.s or N.s/m^2 or kg/(m·s)]
ρ	density [kg/m^3 or gr/cm^3]
ρ_G	density of gas phase [kg/m^3 or gr/cm^3]
ρ_L	density of liquid phase [kg/m^3 or gr/cm^3]
λ	wavelength [cm or mm]
σ	surface tension [N/m]
ω	constant, here $\omega = 0.8$
φ	droplet formation rate, s-1
ε	distortion parameter, (A_{max}/A_d)-1, here $\varepsilon = 0$ and $\varepsilon = 0.3$

Subscripts

x	x direction
y	y direction
*	interfacial
1	initial
2	end

Superscripts

*	equilibrium
-	mean

References

[1] T. Boden, G. Marland, and Andres R. J., *Global fossil-fuel CO_2 emissions.* [Online] Available: http://cdiac.ornl.gov/trends/emis/tre_glob.html.

[2] J. Albo, P. Luis, and A. Irabien, “Carbon dioxide capture from flue gases using a cross-flow membrane contactor and the Ionic liquid 1-Ethyl-3-methylimidazolium Ethylsulfate,” *Industrial & Engineering Chemistry Research*, vol. 49, no. 21, pp. 11045–11051, 2010.

[3] Cheng-Hsiu Yu and Chih-Hung Huang and Chung-Sung Tan, “A Review of CO_2 capture by absorption and adsorption,” *Aerosol and Air Quality Research*, vol. 12, pp. 745–769, 2012.

[4] European Environment Agency, *Greenhouse gas emission trends and projections in Europe 2012: Tracking progress towards Kyoto and 2020 targets*.

[5] T. Stocker, C. B. Field, and O. Edenhofer, *Evidence from the 2013 Intergovernmental Panel on Climate Change (IPCC): Report for geography teachers / National Centre for Atmospheric Science, Natural Environment Research Council, Royal Society Community*.

[6] Daniel Vallero, *Fundamental of air pollution*: Academic Press Publications, 2014.

[7] B. Shimekit and H. Mukhtar, “Natural gas purification technologies - major advances for CO_2 separation and future directions,” in *Advances in Natural Gas Technology 2012*, pp. 235–270.

[8] T. L. Tarbuck and G. L. Richmond, “Adsorption and Reaction of CO_2 and SO_2 at a Water Surface,” (ENG), *Journal of the American Chemical Society*, vol. 128, no. 10, pp. 3256–3267, 2006.

[9] T. N. G. Borhani, A. Azarpour, V. Akbari, S. R. Wan Alwi, and Z. A. Manan, “CO_2 capture with potassium carbonate solutions: A state-of-the-art review,” *International Journal of Greenhouse Gas Control*, vol. 41, pp. 142–162, 2015.

[10] R. Thiruvenkatachari, S. Su, H. An, and X. X. Yu, “Post combustion CO_2 capture by carbon fibre monolithic adsorbents,” *Progress in Energy and Combustion Science*, vol. 35, no. 5, pp. 438–455, 2009.

[11] Y. Tamhankar *et al.,* “Aqueous Amine Spray Absorption and Droplet Distribution Data for CO_2 Capture Applications,” *Energy Procedia*, vol. 63, pp. 293–300, 2014.

[12] G. V. Lowry, J. K. Stolaroff, and D. W. Keith, “CO_2 extraction from ambient air using alkali-metal hydroxide solutions: niche markets to industrial scale implementation,” *Preprints of Papers- American Chemical Society, Division of Fuel Chemistry*, vol. 49, no. 1, pp. 362–363, 2004.

[13] Z. Qing, G. Yincheng, and N. Zhenqi, “Experimental studies on removal capacity of carbon dioxide by a packed reactor and a spray column using aqueous ammonia,” *Energy Procedia*, vol. 4, pp. 519–524, 2011.
[14] Z. Niu, Y. Guo, and W. Lin, “Experimental studies on removal of carbon dioxide by aqueous ammonia fine spray,” *Science in China Series E: Technological Sciences*, vol. 53, no. 1, pp. 117–122, 2010.
[15] J. K. Stolaroff, D. W. Keith, and G. V. Lowry, “Carbon dioxide capture from atmospheric air using sodium hydroxide spray,” *Environmental Science & Technology*, vol. 42, no. 8, pp. 2728–2735, 2008.
[16] I. Taniguchi, Y. Takamura, and K. Asano, “Experimental study of gas absorption with a spray column,” *Journal of Chemical Engineering of Japan*, vol. 30, no. 3, pp. 427–433, 1997.
[17] Y. Lim, M. Choi, K. Han, M. Yi, and J. Lee, “Performance characteristics of CO_2 capture using aqueous ammonia in a single-nozzle spray tower,” *Industrial & Engineering Chemistry Research*, vol. 52, no. 43, pp. 15131–15137, 2013.
[18] Oliver Seyboth, Barna Heidel, and Guenther Scheffknecht, Eds., *Absorption of CO_2 by spray droplets in a post combustion capture spray scrubbing process with amine based solvents*, 2013.
[19] M. Songolzadeh, M. Soleimani, M. T. Ravanchi, and R. Songolzadeh, “Carbon dioxide separation from flue gases: a technological review emphasizing reduction in greenhouse gas emissions,” (ENG), *The Scientific World Journal*, pp. 1–34, 2014.
[20] M. Wang, A. Lawal, P. Stephenson, J. Sidders, and C. Ramshaw, “Post-combustion CO_2 capture with chemical absorption: A state-of-the-art review,” *Chemical Engineering Research and Design*, vol. 89, no. 9, pp. 1609–1624, 2011.
[21] B. Sreenivasulu, D. V. Gayatri, I. Sreedhar, and K. V. Raghavan, “A journey into the process and engineering aspects of carbon capture technologies,” *Renewable and Sustainable Energy Reviews*, vol. 41, pp. 1324–1350, 2015.
[22] A. A. Olajire, “CO2 capture and separation technologies for end-of-pipe applications – A review,” *Energy*, vol. 35, no. 6, pp. 2610–2628, 2010.
[23] Z. Niu, Y. Guo, Q. Zeng, and W. Lin, “A novel process for capturing carbon dioxide using aqueous ammonia,” *Fuel Processing Technology*, vol. 108, pp. 154–162, 2013.
[24] E. Henley and Seader, J.D and and Roper, D.K., *Separation Process Principles*: John Wiley & Son Inc., 2011.
[25] W.-H. Chen, S.-M. Chen, and C.-I. Hung, “A theoretical approach of absorption processes of air pollutants in sprays under droplet-droplet interaction,” (eng), *The Science of the total environment*, vol. 444, pp. 336–346, 2013.
[26] J. Kuntz and A. Aroonwilas, “Mass transfer in a spray column for CO_2 removal,” in *IEEE EIC Climate Change, 2016*, 1–6, 2006.

[27] A. Turpin, A. Couvert, A. Laplanche, and A. Paillier, “Experimental study of mass transfer and H_2S removal efficiency in a spray tower,” *Chemical Engineering and Processing: Process Intensification*, vol. 47, no. 5, pp. 886–892, 2008.
[28] J. Kuntz and A. Aroonwilas, “Performance of spray column for CO_2 capture application,” *Industrial & Engineering Chemistry Research*, vol. 47, no. 1, pp. 145–153, 2008.
[29] J. Kuntz and A. Aroonwilas, “Mass-transfer efficiency of a spray column for CO_2 capture by MEA,” *Energy Procedia*, vol. 1, no. 1, pp. 205–209, 2009.
[30] W. G. Whitman, L. Long, and H. Y. Wang, “Absorption of gases by a liquid drop,” *Industrial and Engineering Chemistry*, vol. 18, no. 4, pp. 363–367, 1926.
[31] B. E. Dixon and A. A. W. Russell, “The absorption of carbon dioxide by liquid drops,” *Journal of the Society of Chemical Industry*, vol. 69, no. 9, pp. 284–288, 1950.
[32] E. R. Altwicker and C. E. Lindhjem, “Absorption of gases into drops,” *AIChe Journal*, vol. 34, no. 2, pp. 329–332, 1988.
[33] V. Srinivasan and R. Aiken, “Mass transfer to droplets formed by the controlled jet-physical breakup of a cylindrical absorption,” *Chemical Engineering Science*, vol. 43, no. 12, pp. 3141–3150, 1988.
[34] J. Han, D. A. Eimer, and M. C. Melaaen, “Liquid phase mass transfer coefficient of carbon dioxide absorption by water droplet,” *Energy Procedia*, vol. 37, pp. 1728–1735, 2013.
[35] J. Elhajj, M. Al-Hindi, and F. Azizi, “A Review of the absorption and desorption processes of carbon dioxide in water systems,” *Ind. Eng. Chem. Res.*, vol. 53, no. 1, pp. 2–22, 2014.
[36] J. Han, “Mass transfer characteristics of CO_2 absorption into liquid droplets,” Dissertation, Telemark University College, Porsgrunn, Norway, 2014.
[37] A. Aboudheir, P. Tontiwachwuthikul, A. Chakma, and R. Idem, “Kinetics of the reactive absorption of carbon dioxide in high CO2-loaded, concentrated aqueous monoethanolamine solutions,” *Chemical Engineering Science*, vol. 58, no. 23-24, pp. 5195–5210, 2003.
[38] Edwin van Elk, “Gas Liquid Reactions: Influence of liquid bulk and mass transfer on process performance,” Thesis, Twente University, 2001.
[39] A. L. Kohl and Nielsen, Richard B., *Gas Purification,* 5th ed. Houston, Texas: Gulf Publishing Company, 1997.
[40] E. A. Pinilla, J. M. DÍaz, and J. Coca, “Mass transfer and axial dispersion in a spray tower for gas-liquid contacting,” *The Canadian Journal of Chemical Engineering*, vol. 62, no. 5, pp. 617–622, 1984.
[41] The Cooperative Research Centre for Greenhouse Gas Technologies (CO2CRC), “Pre-Combustion capture of carbon dioxide,” The Cooperative Research Centre for Greenhouse Gas Technologies

(CO2CRC). [Online] Available: http://old.co2crc.com.au/dls/factsheets/Pre-comb_Solvent.pdf.
[42] Rayleigh, “On the instability of jets,” *Proceedings of the London Mathematical society*, vol. 10, pp. 4–13, 1878.
[43] H. Liu, Ed., *Science and ngineering of droplets*. New Jersey: Elsevier, 1999.
[44] Clift R., Grace J.R., and and Weber M.E., *Bubbles, Drops, and Particles*. New York: Academic Press, 1978.
[45] S. P. Lin and R. D. Reitz, “Drop and pray ormation from a iquid jet,” *Annual Review of Fluid Mechanics*, vol. 30, no. 1, pp. 85–105, 1998.
[46] S. Ellermeyer, “Falling Objects,” 2003.
[47] J.R. Welty, C.E. Wicks, R.E.Wilson, and G.L.Rorrer, *Fundamentals of Momentum, Heat and Mass Transfer*: John Wiley & Son Inc., 2008.
[48] Baehr, H.D and Stephan, K, *Heat and Mass Transfer*. Verlag Berlin: Springer, 1998.
[49] Krunal Shah, *Difference between absorption and adsorption.* [Online] Available: http://www.chemalone.com/difference-between-absorption-and-adsorption/.
[50] G. Versteeg and W. Swaalj, “Solubility and diffusivity of acid gases (CO_2,N_2O) in aqueous alkanolamine solutions,” *Journal of Chemical and Engineering Data*, vol. 33, no. 1, pp. 29–34, 1988.
[51] Coulson, J.M and Richardson, J.F, *Fluid Flow Heat and Mass Transfer*: Butterworth, 1999.
[52] C. J. Geankoplis, *Transport processes and separation process principles: (includes unit operations),* 4th ed. Upper Saddle River, NJ: Prentice Hall Professional Technical Reference, 2003.
[53] A. M. Kutepov, A. S. Latkin, and V. V. Potapov, “Motion of and mass transfer into a liquid droplet in the swirling flow of the geothermal medium,” *Theoretical Foundations of Chemical Engineering*, vol. 34, no. 2, pp. 134–140, 2000.
[54] W. G. Whitman and D. S. Davis, “Comparative absorption rates for various gases,” *Industrial and Engineering Chemistry*, vol. 16, no. 12, pp. 1233–1237, 1924.
[55] W. K. Lewis and W. G. Whitman, “Principles of gas absorption,” *Industrial and Engineering Chemistry*, vol. 16, no. 12, pp. 1215–1220, 1924.
[56] W. G. Whitman, “The two film theory of gas absorption,” *International Journal of Heat and Mass Transfer*, vol. 5, no. 5, pp. 429–433, 1962.
[57] E. L. Cussler, *Diffusion: Mass transfer in fluid systems,* 3rd ed. Cambridge: Cambridge University Press, 2009.
[58] P. Danckwert, “Significance of liquid-film coefficients in gas absorption,,” *Industrial and Engineering Chemistry*, vol. 43, no. 6, pp. 1460–1467, 1951.

[59] Robert E Treyball, *Mass-Transfer Operation*: McGraw-Hill Book Company, 1981.
[60] R. H. Perry and D. W. Green, *Perry's chemical engineers' handbook,* 8th ed. New York: McGraw-Hill Professional; London : McGraw-Hill [distributor], 2008.
[61] Toor, H.L and Marchello, J.M, "Film-penetration model for mass and heat transfer," *AIChe Journal*, vol. 4, no. 1, pp. 97–101, 1958.
[62] Yinghui Liu, Dunyu Liu and Terry Wall, "Reporting of well stirred scrubber result : scrubbing of SO_2 and CO_2 by caustic solutions at atmospheric pressure," The University of Newcastle Australia.
[63] A. H. P. Skelland and R. M. Wellek, "Resistance to mass transfer inside droplets," *AIChE J.*, vol. 10, no. 4, pp. 491–496, 1964.
[64] S. M. Rajan and W. J. Heideger, "Drop formation mass transfer," *AIChe Journal*, vol. 17, no. 1, pp. 202–206, 1971.
[65] Williamson, R.V and Mathews, J.H, "Rate of absorption and equilibrium of carbon dioxide in alkaline solutions," *Industrial and Engineering Chemistry*, pp. 1157–1161, 1924.
[66] M. Kordač and V. Linek, "Dynamic measurement of carbon dioxide volumetric mass transfer coefficient in a well-mixed reactor using a pH probe: Analysis of the salt and supersaturation effects," *Industrial & Engineering Chemistry Research*, vol. 47, no. 4, pp. 1310–1317, 2008.
[67] G. A. Hill, "Measurement of overall volumetric mass transfer coefficients for Carbon Dioxide in a well-mixed reactor using a pH probe," *Industrial & Engineering Chemistry Research*, vol. 45, no. 16, pp. 5796–5800, 2006.
[68] Y. Adewuyi and Carmichael, "A theoretical investigation of gaseous absorption by water droplet from SO_2-HNO_3-NH_3-CO_2-HCl Mixtures," *Atmospheric Environment*, vol. 16, no. 4, pp. 719–729, 1981.
[69] Anonymous, "Behaviour of carbonic acid as a Brønsted acid," [Online] Available: http://www.derangedphysiology.com/main/core-topics-intensive-care/acid-base-disturbances/Chapter%202.0.3/buffering-acute-respiratory-acid-base-disturbances.
[70] S. S. Sadhal, P. S. Ayyaswamy, and J. N. Chung, *Transport phenomena with drops and bubbles*. New York, London: Springer, 1997.
[71] A. H. Lefebvre, *Atomization and Sprays*. New York: Hemisphere Publishing Corporation, 1989.
[72] N. K. Yeh, "Liquid phase mass transfer in spray contactors," University of Texas, Austin, USA, 2002.
[73] J. T. Davies and E. K. Rideal, *Interfacial phenomena*. New York: Academic Press, 1961.
[74] A. E. Handlos and T. Baron, "Mass and heat transfer from drops in liquid-liquid extraction," *AIChE J.*, vol. 3, no. 1, pp. 127–136, 1957.

[75] J. B. Angelo, E. N. Lightfoot, and D. W. Howard, “Generalization of the penetration theory for surface stretch: Application to forming and oscillating drops,” *AIChe Journal*, vol. 12, no. 4, pp. 751–760, 1966.
[76] E. Ruckenstein, “Mass transfer between a single drop and a continuous phase,” *International Journal of Heat and Mass Transfer*, vol. 10, no. 12, pp. 1785–1792, 1967.
[77] C.-T. Hsu and S.-M. Shih, “Semiempirical equation for liquid-phase mass-transfer coefficient for drops,” *AIChe Journal*, vol. 39, no. 6, pp. 1090–1092, 1993.
[78] H. Amokrane, A. Saboni, and B. Caussade, “Experimental study and parameterization of gas absorption by water drops,” *AIChe Journal*, vol. 40, no. 12, pp. 1950–1960, 1994.
[79] H. Amokrane and B. Caussade, “Gas absorption into a moving spheroidal water drop,” *Journal of the Atmospheric Sciences*, vol. 56, no. 12, pp. 1808–1829, 1999.
[80] A. Saboni and S. Alexandrova, “Sulfur dioxide absorption and desorption by water drops,” *Chemical Engineering Journal*, vol. 84, no. 3, pp. 577–580, 2001.
[81] J. T. Davies and S. T. Ting, “Mass transfer into turbulent jets,” *Chemical Engineering Science*, vol. 22, no. 12, pp. 1539–1548, 1967.
[82] S. Alexandrova, M. Marion, E. Lepinasse, and A. Saboni, “Mass transfer modeling of SO_2 into large water drops,” *Chemical Engineering & Technology*, vol. 27, no. 6, pp. 676–680, 2004.
[83] M. Marion, E. Lépinasse, and A. Saboni, “SO_2 absorption and desorption by an accelerating water droplet undergoing vaporization,” *International Journal of Heat and Fluid Flow*, vol. 27, no. 2, pp. 290–297, 2006.
[84] M. Kulmala, P. Korhonen, A. Laaksonen, and T. Vesala, “Changes in cloud properties due to NO x emissions,” *Geophysical Research Letters*, vol. 22, no. 3, pp. 239–242, 1995.
[85] J. B. Wedding, Y. J. Kim, and R. S. Dennison, “Mass transfer from water droplets under simulated free-fall conditions,” *Atmospheric Environment (1967)*, vol. 20, no. 5, pp. 1039–1045, 1986.
[86] S. T. Hoh, M. M. Farid, and J. Chen, “Mass transfer to droplets formed by the controlled breakup of a cylindrical jet – physical absorption,” *Chemical Engineering Science*, vol. 73, pp. 329–333, 2012.
[87] P. Wang and H. Pruppacher, “Acceleration to terminal velocity of cloud and rain drops,” *Journal of Applied Meteorology*, vol. 16, 275–280, 1977.
[88] N. K. Yeh and G. T. Rochelle, “Liquid-phase mass transfer in spray contactors,” *AIChe Journal*, vol. 49, no. 9, pp. 2363–2373, 2003.
[89] L. Scriven and R. Pigford, “On phase equilibrium at the gas-liquid interface during absorption,” *AIChE J.*, vol. 4, no. 4, pp. 439–444, 1958.
[90] J. Schwarz and J. Smolík, “Mass transfer from a drop—I. Experimental study and comparison with existing correlations,” *International Journal of Heat and Mass Transfer*, vol. 37, no. 14, pp. 2139–2143, 1994.

[91] W.-H. Chen, “Dynamics of sulfur dioxide absorption in a raindrop falling at terminal velocity,” *Atmospheric Environment*, vol. 35, no. 28, pp. 4777–4790, 2001.

[92] Anonymous, *Vertical Trajectory.* [Online] Available: http://hyperphysics.phy-astr.gsu.edu/hbase/Mechanics/quadrag.html#c1.

[93] A. T. Popovich, R. E. Jervis, and O. Trass, “Mass transfer during single drop formation,” *Chemical Engineering Science*, vol. 19, no. 5, pp. 357–365, 1964.

[94] N. Takagaki and S. Komori, “Air–water mass transfer mechanism due to the impingement of a single liquid drop on the air–water interface,” *International Journal of Multiphase Flow*, vol. 60, pp. 30–39, 2014.

[95] K. Beard, “Terminal velocity and shape of cloud and precipitation drops aloft,” *Journal of the Atmospheric Sciences*, vol. 33, p. 851, 1976.

[96] C. Walcek, H. R. Pruppacher, J. Topalian, and S. Mitra, “On the scavenging of SO_2 by cloud and raindrops:: II. An experimental study of SO_2 absorption and desorption for water drops in air,” *Journal of the Atmospheric Science*, vol. 1, pp. 291–306, 1984.

[97] S. Mitra and A. Hannemann, “On the scavenging of SO_2 by large and small rain drops:: V. A wind tunnel and theoretical study of the desorption of SO_2 from water drops containing S(IV),” *Journal of Atmospheric Chemistry*, vol. 16, pp. 201–218, 1993.

[98] J. Zosel, W. Oelßner, M. Decker, G. Gerlach, and U. Guth, “The measurement of dissolved and gaseous carbon dioxide concentration,” *Meas. Sci. Technol.*, vol. 22, no. 7, p. 72001, 2011.

[99] S. Schaden, M. Haberkorn, J. Frank, J. R. Baena, and B. Lendl, “Direct determination of carbon dioxide in aqueous solution using mid-infrared quantum cascade lasers,” (eng), *Applied spectroscopy*, vol. 58, no. 6, pp. 667–670, 2004.

[100] Schumacher, T.E and Smucker, J.M, “Measurement of CO_2, dissolved in aqueous solutions using a modified infrared gas analyzer system,” *Plant Physiol.*, vol. 72, pp. 212–214, 1983.

Appendix

Appendix 3-1 The procedure of desorption experiments for liquid droplets and gas.

1. Close valves V01, V02, V05, V06 and V07. Open valves V03 and V04.
2. Blow the chamber for 30 minutes until the chamber is totally filled with N_2 and CO_2 in the chamber is vented through valve V04.
3. Close valve V04. Open valves V02 and V05. Fill kerosene into the chamber through drain valve V06 until desired level. Close valve V06
4. Turn on the peristaltic pump to generate droplets by dripping.
5. Take the video by the high-speed camera to obtain the droplet diameter, the droplet formation rate and the droplet velocity.
6. Wait until the sample was enough to be taken. Stop the pump.
7. Open V07 to let the sample drain to the sample bottle.
8. Drain the kerosene from the chamber through valve V05 .
9. Clean and dry the chamber with laboratory paper tissue.
10. Blow nitrogen through the chamber until the inner wall is dry.
11. Repeat step 2 for next level.

Appendix 3-2. Procedure for Image Processing

1. Turn on PC, until the desktop screen appears.
2. Turn on Camera, until “beep” sound, it signed that the camera is already to use.
3. Click icon “DaVis High-speed” for starting.
4. If there is command “702 camera error: Initialization of camera 2 (imager pro HS) failed. Camera 2 not found” click OK, because only one camera is used.
5. Appear Login Menu, and click “Login” and then appear menu screen.
6. If start new file, press “New” icon and create new project name and then click OK.
   If start with previous or last file, click name’s file.
7. Before operating the software, ensure the scale with pressing “Scaling” icon
   Or if have been calibration or scaling, press “Recording” icon

For scaling with Vernier callipers

1. Place the Vernier callipers where it is seen in camera. Use maximum area of interest (2100x2100)
2. Press “Live Mode” icon. Adjust the sharping of picture by adjusting the button rod at LDM (right and left direction)
3. Press “Recording” icon for recording the experiment. And the press “start recording” button
4. Press “Exit” button and press or click “scaling” icon
5. Open file of recording scaler.
6. Press “scale” icon on action menu and place or adjust “+” cursor to the place that will scale. For Vernier, put “+” cursor on the above and bottom side of Vernier callipers or scaler.

7. On distance point, put an exact number for example: 5 mm, and then click OK and then press or click “finish” icon.
8. On the screen appears dialog menu “Calibration and camera scale have changed”, and click at point 3 “overwrite active project” and then click OK.

Recording menu

1. Click “recording” icon
2. Set the parameter like: high speed recording, timing, light source and camera by click “setup” icon.
3. On “Device Setting” and high speed recording menu, choose Laser at “ON” position.
4. Put a number at “Set exposure” (for example 1 us). Higher number will brighten the light or lamp.
5. At Timing : select/put a number for recording rate (for example: 100 Hz) Recording rate is time for one image, in this case: 0.01 second/image. Timing depends on maximum rate at camera menu and is also depends on area of interest. The smaller area of interest is the higher maximum rate.
6. On recording sequence, click image acquisition. On parameter menu; put some value/number of images (from 1 to 3136).
7. On recording sequence: check list “store immediately after recording”.
8. After setting all items, press “Live Mode” to show the real picture and to quit live mode press “stop”.
9. Press “recording” to record the picture and press “start recording”.
10. Press “play” button for showing the previous recording or last recording.
11. Press “exit” to exit recording menu.

Appendix 3-3 The graph and calibration data of pH probe.

Run	Volume of HCl	Volume of NaOH	Delta Volume
	ml	ml	ml
1	20	19.956	0.044
2	20	20.116	0.116
3	20	20.152	0.152
4	20	20.046	0.046
5	20	20.086	0.086
6	20	20.052	0.052
7	20	19.902	0.098
8	20	20.078	0.078
9	20	19.992	0.008
10	20	19.994	0.006
11	20	20.148	0.148
12	20	19.986	0.014
	average	**20.042**	0.094
	stddev	**0.078**	
	stderror	**0.021**	

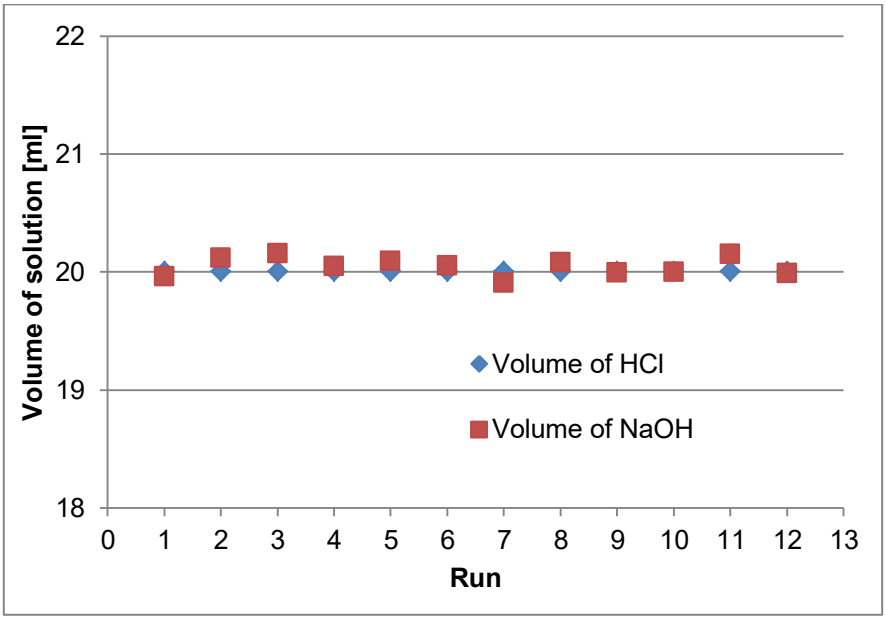

Appendix 3-4 Analyse CO_2 in sample solution by titration method.

Equipment

1. Titration unit, Titrino GP 736 Metrohm
2. Titrating burette 50 ml and bottle 1000 ml, Rotilabo
3. Volumetric pipette 50 ml, class A
4. Micropipette 5 ml, Rotilabo
5. Funnel glass
6. Erlenmeyer flask 250 ml
7. Silicon/rubber plug with capillary tube
8. Heating plate plus magnetic stirrer, IKA RET Basic
9. Vacuum pump
10. Filter equipment, Nalgene

Chemical and Material

1. Sodium bicarbonate, $NaHCO_3$ 0.1 M Carl Roth
2. Barium chloride dehydrate, $BaCl_2$ $2H_2O$ 0.1 M Carl Roth
3. Sodium hydroxide solution, 0.1 M Carl Roth
4. Distilled water
5. Membrane filter paper, 0.45 μm or less

Procedure

1. Make two parallels or more of sample and one blank sample by following procedure.
2. Take a 1-5 ml sample liquid (depend on prediction of concentration CO_2 in sample) added with 25 ml 0.1 M $BaCl_2$ solution and 50 ml 0.1 M NaOH solution in a 250 ml Erlenmeyer flask.

3. Put the plug with the capillary tube in order to avoid CO_2 absorption from surrounding air.
4. This mixture is boiled for 3 to 5 minutes, cooled to ambient temperature in a bath.
5. Filter the solution with filtration equipment through membrane filter paper.
6. Wash the Erlenmeyer flask with distilled water to make sure all the precipitation have been in filter.
7. The residue or cake is rinsed with 100-150 ml distilled water.
8. The cake and the filter are dried in an oven for minimum 30 minutes at 60°C.
9. Transfer the cake and the filter to a 150 ml beaker glass and then add distilled water up to 50 ml.
10. The solution is titrated with 0.1 M HCl solution to pH 2 until all solid is dissolved and finally the excess (unreacted) HCl is back titrated with 0.1 M NaOH solution to pH 7.
11. Record the amount of HCl and NaOH that have been used.

Appendix 3-5 The spreadsheet of a calculation of CO_2 concentration by titration method

Code	V_{sample} [ml]	V_{HCl} [ml]	V_{NaOH} [ml]	n_{CO2} [mol]	n_{CO2}/V_{sample} [mol/l]
Blank	0	9.832	9.534	0.0000149	
B1	1	9.462	8.876	0.0000293	0.01440
B2	1	9.268	8.668	0.0000300	0.01510

c_{HCl} and c_{NaOH} = 0.1 mol/l

Average of CO_2 concentration = (0.0144 + 0.01510): 2 = 0.01475 mol/ l

Appendix 3-6 The data of verification method

Date	31/01/2017
HCl concentration	0.1 M
NaOH concentration	0.1 M

Code	V_{sample} [ml]	V_{HCL} [ml]	V_{NaOH} [ml]	n_{CO2} [mol] sample	n_{CO2} [mol] real	n_{CO2} [mol/l]
Blank	0	7.898	7.536	0.0000181		
M.1.1	1	8.858	8.252	0.0000303	0.0000122	0.01220
M.2.1	2	9.15	8.44	0.0000355	0.0000174	0.00870
						0.01045
Blank	0	7.434	7.096	0.0000169		
H.1.2	1	8.058	7.344	0.0000357	0.0000188	0.01880
M.1.2	1	7.49	6.756	0.0000367	0.0000198	0.01980
						0.01930
Blank	0	7.446	7.108	0.0000169		
M.1.05	5	8.334	7.466	0.0000434	0.0000265	0.00530
M.1.05	10	9.218	8.004	0.0000607	0.0000438	0.00438
						0.00484
Blank	0	7.236	7.014	0.0000111		
M.2.3	1	8.414	7.616	0.0000399	0.0000288	0.02880
M.3.3	1	8.54	7.686	0.0000427	0.0000316	0.03160
						0.03020

Appendix 4-1 Temporal evolution of pending droplets diameters formed at different nozzle tips (formation period).

Outer nozzle dia. 0.5 mm		**Outer nozzle dia. 0.6 mm**		**Outer nozzle dia. 0.8 mm**	
time [s]	Droplet dia. [mm]	time [s]	Droplet dia. [mm]	time [s]	Droplet dia. [mm]
0.012	0.65	0.008	0.57	0.008	0.70
0.022	0.79	0.063	1.13	0.068	1.24
0.036	1.07	0.148	1.51	0.188	1.76
0.038	1.02	0.294	1.91	0.388	2.22
0.053	1.26	0.492	2.31	0.588	2.57
0.127	1.67	0.692	2.62	0.788	2.91
0.164	1.85	0.812	2.74	0.988	3.20
0.170	1.23	0.924	2.78	1.081	3.11

Appendix 4-2 Experimental data of forrmation time and formation rate.

Outer nozzle diameter [mm]	Formation time [s]	Formation rate [s^{-1}]
0.5	0.2328	4.2955
	0.234	4.2735
	0.232	4.3103
	0.2328	4.2955
	0.2324	4.3029
Average	0.2328	4.2956
Std. dev.	0.000611	0.011249
0.6	0.9244	1.0818
	0.9256	1.0804
	0.9232	1.0832
	0.924	1.0823
	0.9248	1.0813
Average	0.9244	1.0818
Std. dev.	0.00080	0.00094
0.8	1.0768	0.9287
	1.0828	0.9235
	1.0804	0.9256
	1.0808	0.9252
	1.078	0.9276
Average	1.07976	0.9261
Std. dev.	0.00213	0.00182

Appendix 4-3 Experimentally determined droplet falling velocities at various droplet size and droplet positions (distance from needle tips).

Droplet diameter 1.61 mm		**Droplet diameter 2.67 mm**		**Droplet diameter 3.07 mm**	
distance [cm]	velocity [m/s]	distance [cm]	velocity [m/s]	distance [cm]	velocity [m/s]
0.50	0.33	0.98	0.47	0.99	0.40
5.00	1.00	5.02	1.00	5.02	0.93
10.00	1.33	10.00	1.43	9.99	1.40
12.76	1.60	12.70	1.53	12.80	1.53
15.00	1.70	15.00	1.69	15.00	1.70
20.00	1.96	20.00	1.95	20.00	1.95

Appendix 4-4 Experimental data for CO_2 desorption

h [cm]	d [mm]	t [s]	T [°C]	Original		
				C_1 [mol/l]	C_2 [mol/l]	k_L [m/s]
0	1.61	0.2328	23.0	0.0273	0.0138	1.27E-03
5	1.61	0.2836	23.7	0.0288	0.0122	1.36E-03
10	1.61	0.3052	23.5	0.0282	0.0105	1.22E-03
15	1.61	0.3218	23.5	0.0286	0.0103	1.24E-03
20	1.61	0.3368	21.7	0.0294	0.0111	3.05E-03
0	2.67	0.8590	22.5	0.0298	0.0151	7.75E-04
5	2.67	0.9096	23.0	0.0302	0.0149	7.94E-04
10	2.67	0.9309	23.0	0.0293	0.0144	6.80E-04
15	2.67	0.9470	23.0	0.0272	0.0129	5.33E-04
20	2.67	0.9620	22.8	0.0285	0.0126	7.53E-04
0	3.0	1.1600	22.5	0.0295	0.0154	6.24E-04
5	3.0	1.2106	22.7	0.0289	0.0146	5.67E-04
10	3.0	1.2319	23.0	0.0290	0.0138	5.76E-04
15	3.0	1.2484	22.7	0.0308	0.0151	7.29E-04
20	3.0	1.2625	22.7	0.0291	0.0132	5.83E-04

Appendix 4-5 Normalized CO_2 desorption data

h [cm]	d [mm]	t [s]	T [°C]	Normalized		
				C_1 [mol/l]	C_2 [mol/l]	k_L [m/s]
0	1.61	0.2328	23.0	0.03	0.0151	1.79E-03
5	1.61	0.2836	23.7	0.03	0.0127	1.58E-03
10	1.61	0.3052	23.5	0.03	0.0112	1.53E-03
15	1.61	0.3218	23.5	0.03	0.0108	1.47E-03
20	1.61	0.3368	21.7	0.03	0.0100	1.43E-03
0	2.67	0.8590	22.5	0.03	0.0152	8.01E-04
5	2.67	0.9096	23.0	0.03	0.0148	7.68E-04
10	2.67	0.9309	23.0	0.03	0.0147	7.52E-04
15	2.67	0.9470	23.0	0.03	0.0143	7.48E-04
20	2.67	0.9620	22.8	0.03	0.0127	7.74E-04
0	3.0	1.1600	22.5	0.03	0.0157	6.71E-04
5	3.0	1.2106	22.7	0.03	0.0151	6.56E-04
10	3.0	1.2319	23.0	0.03	0.0143	6.63E-04
15	3.0	1.2484	22.7	0.03	0.0147	6.46E-04
20	3.0	1.2625	22.7	0.03	0.0136	6.61E-04

Appendix 4-6 Data experimental for concentration of CO_2 in liquid solution for droplet diameter 1.61 mm, 2.67 mm and 3.0 mm

Droplet diameter: 1.61 mm

Distance [cm]	c1 [mol/l]	c2 [mol/l]
0	0.0239	0.0114
0	0.0307	0.0163
0	0.0273	0.0137
average	0.02731	0.013783
std.dev	0.00278	0.001981
5	0.0283	0.0126
5	0.0293	0.0118
5	0.0289	0.0122
average	0.028833	0.012175
std.dev	0.000411	0.000337
10	0.0286	0.0108
10	0.0277	0.01018
10	0.0282	0.01046
average	0.028167	0.01047
std.dev	0.000368	0.000245
15	0.0286	0.01025
15	0.0294	0.0102
15	0.0278	0.01029
average	0.0286	0.010247
std.dev	0.000653	3.68E-05
20	0.0335	0.01113
20	0.0253	0.00907
20	0.0293	0.01011
average	0.029367	0.010102
std.dev	0.003348	0.00084

Droplet diameter 2.67 mm

Distance [cm]	c1 [mol/l]	c2 [mol/l]
0	0.0301	0.01570
0	0.02945	0.01455
0	0.02976	0.01514
average	0.02977	0.01513
std.dev	0.000265456	0.000469539
5	0.02815	0.01405
5	0.0323	0.0157
5	0.03023	0.01488
average	0.030226667	0.014876667
std.dev	0.001694232	0.000673614
10	0.0292	0.01475
10	0.0273	0.01310
10	0.0313	0.01520
average	0.029266667	0.01435
std.dev	0.001633673	0.000902774
15	0.0272	0.0128
15	0.0264	0.0123
15	0.028	0.0119
average	0.0272	0.012303333
std.dev	0.000653197	0.000363349
20	0.0284	0.01219
20	0.0298	0.01261
20	0.0272	0.01180
average	0.028466667	0.012198333
std.dev	0.001062492	0.000328693

Droplet diameter 3.0 mm

Distance [cm]	c1 [mol/l]	c2 [mol/l]
0	0.0265	0.014
0	0.0295	0.0145
0	0.0294	0.01465
0	0.0325	0.01845
average	0.029475	0.0154
std.dev	0.00212176	0.001777287
5	0.0272	0.01405
5	0.0274	0.013
5	0.0314	0.0164
5	0.0297	0.0149
average	0.028925	0.0145875
std.dev	0.00173403	0.001244174
10	0.0267	0.01375
10	0.0324	0.014925
10	0.0293	0.01375
10	0.0274	0.01265
average	0.02895	0.01376875
std.dev	0.00220737	0.000804552
15	0.03075	0.01595
15	0.02996	0.01505
15	0.03165	0.01415
average	0.03078667	0.01505
std.dev	0.00069043	0.000734847
20	0.0279	0.0114
20	0.0312	0.0149
20	0.02954	0.01316
average	0.02954667	0.013153333
std.dev	0.00134723	0.001428877

Appendix 4-7. Calculation of CO_2 concentration using mass transfer coefficient equations from various literature sources

Table 1. The CO_2 desorption data and ratio C_2/C_1 for droplet diameter 1.61 mm

Droplet diameter 1.61 mm			k_L, mass transfer coefficient (model)													
			Amokrane		Higbie		Handlos		Ruckenstein		Angelo		Srinivasan		Hsu	
t [s]	Cli [mol/l]	C_1 [mol/l]	C_2 [mol/l]	C_2/C_1	C_2 [mol/l]	C_2/C_1	C_2 [mol/l]	C_2/C_1	C_2 [mol/l]	C_2/C_1	C_2 [mol/l]	C_2/C_1	C_2 [mol/l]	C_2/C_1	C_2 [mol/l]	C_2/C_1
0	0.0000135	0.03	0.030	1.000	0.030	1.000	0.030	1.000	0.030	1.000	0.0300	1.000	0.030	1.000	0.030	1.000
0.05	0.0000135	0.03	0.028	0.949	0.029	0.982	0.028	0.922	0.02268	0.756	0.0250	0.833	0.027	0.899	0.027	0.912
0.1	0.0000135	0.03	0.027	0.901	0.029	0.964	0.026	0.850	0.01715	0.572	0.0208	0.694	0.024	0.808	0.025	0.831
0.2	0.0000135	0.03	0.024	0.813	0.028	0.928	0.022	0.723	0.00980	0.327	0.0128	0.427	0.020	0.654	0.021	0.691
0.3	0.0000135	0.03	0.022	0.733	0.027	0.895	0.018	0.615	0.00561	0.187	0.0106	0.355	0.016	0.528	0.017	0.574
0.4	0.0000135	0.03	0.020	0.660	0.026	0.862	0.016	0.523	0.00321	0.107	0.0098	0.328	0.013	0.427	0.014	0.477
0.5	0.0000135	0.03	0.018	0.595	0.025	0.831	0.013	0.445	0.00184	0.061	0.0093	0.309	0.010	0.345	0.012	0.397
0.6	0.0000135	0.03	0.016	0.537	0.024	0.800	0.011	0.378	0.00106	0.035	0.0088	0.292	0.008	0.279	0.010	0.330
0.7	0.0000135	0.03	0.015	0.484	0.023	0.771	0.010	0.322	0.00061	0.020	0.0023	0.078	0.007	0.226	0.008	0.274
0.8	0.0000135	0.03	0.013	0.436	0.022	0.743	0.008	0.273	0.00035	0.012	0.0016	0.054	0.005	0.183	0.007	0.228
0.9	0.0000135	0.03	0.012	0.393	0.021	0.716	0.007	0.233	0.00021	0.007	0.0011	0.038	0.004	0.148	0.006	0.190
1.0	0.0000135	0.03	0.011	0.355	0.021	0.690	0.006	0.198	0.00012	0.004	0.0008	0.026	0.004	0.119	0.005	0.158
1.1	0.0000135	0.03	0.010	0.320	0.020	0.665	0.005	0.168	0.00008	0.003	0.0006	0.018	0.003	0.097	0.004	0.131
1.2	0.0000135	0.03	0.009	0.288	0.019	0.641	0.004	0.143	0.00005	0.002	0.0004	0.013	0.002	0.078	0.003	0.109
1.3	0.0000135	0.03	0.008	0.260	0.019	0.617	0.004	0.122	0.00003	0.001	0.0003	0.009	0.002	0.063	0.003	0.091
1.4	0.0000135	0.03	0.007	0.234	0.018	0.595	0.003	0.104	0.00003	0.001	0.0002	0.006	0.002	0.051	0.002	0.075

Table 2. The CO_2 desorption data and ratio C_2/C_1 for droplet diameter 2.67 mm

Droplet diameter 2.67 mm			k_L, mass transfer coefficient (model)													
			Amokrane		Higbie		Handlos		Ruckenstein		Angelo		Srinivasan		Hsu	
t [s]	Cli [mol/l]	C_1 [mol/l]	C_2 [mol/l]	C_2/C_1	C_2 [mol/l]	C_2/C_1	C_2 [mol/l]	C_2/C_1	C_2 [mol/l]	C_2/C_1	C_2 [mol/l]	C_2/C_1	C_2 [mol/l]	C_2/C_1	C_2 [mol/l]	C_2/C_1
0	0.0000135	0.030	0.030	1.000	0.0300	1.000	0.030	1.000	0.0300	1.000	0.030	1.000	0.0300	1.000	0.0300	1.000
0.05	0.0000135	0.030	0.029	0.973	0.0298	0.994	0.028	0.939	0.0263	0.877	0.028	0.945	0.0277	0.922	0.0289	0.963
0.1	0.0000135	0.030	0.028	0.946	0.0297	0.989	0.026	0.882	0.0231	0.770	0.027	0.893	0.0255	0.850	0.0278	0.927
0.2	0.0000135	0.030	0.027	0.896	0.0293	0.978	0.023	0.777	0.0178	0.592	0.024	0.798	0.0217	0.722	0.0258	0.858
0.3	0.0000135	0.030	0.025	0.848	0.0290	0.967	0.021	0.685	0.0137	0.456	0.021	0.712	0.0184	0.614	0.0239	0.795
0.4	0.0000135	0.030	0.024	0.802	0.0287	0.956	0.018	0.604	0.0105	0.351	0.019	0.636	0.0157	0.522	0.0221	0.737
0.5	0.0000135	0.030	0.023	0.759	0.0283	0.945	0.016	0.533	0.0081	0.270	0.017	0.568	0.0133	0.443	0.0205	0.683
0.6	0.0000135	0.030	0.022	0.718	0.0280	0.934	0.014	0.470	0.0062	0.208	0.015	0.508	0.0113	0.377	0.0190	0.633
0.7	0.0000135	0.030	0.020	0.680	0.0277	0.924	0.012	0.414	0.0048	0.160	0.014	0.453	0.0096	0.320	0.0176	0.586
0.8	0.0000135	0.030	0.019	0.643	0.0274	0.913	0.011	0.365	0.0037	0.123	0.012	0.405	0.0082	0.272	0.0163	0.543
0.9	0.0000135	0.030	0.018	0.609	0.0271	0.903	0.010	0.322	0.0028	0.095	0.011	0.352	0.0069	0.232	0.0148	0.494
1.0	0.0000135	0.030	0.017	0.576	0.0268	0.893	0.009	0.284	0.0022	0.073	0.010	0.332	0.0059	0.197	0.0143	0.475
1.1	0.0000135	0.030	0.016	0.545	0.0265	0.883	0.008	0.251	0.0017	0.056	0.010	0.324	0.0050	0.167	0.0140	0.468
1.2	0.0000135	0.030	0.015	0.516	0.0262	0.873	0.007	0.221	0.0013	0.044	0.010	0.319	0.0043	0.142	0.0139	0.462
1.3	0.0000135	0.030	0.015	0.489	0.0259	0.863	0.006	0.195	0.0010	0.034	0.009	0.313	0.0036	0.121	0.0137	0.457
1.4	0.0000135	0.030	0.014	0.462	0.0256	0.853	0.005	0.172	0.0008	0.026	0.006	0.206	0.0031	0.103	0.0103	0.344

Table 3. The CO_2 desorption data and ratio C_2/C_1 for droplet diameter 3.0 mm

Droplet diameter 3.0 mm			k_L, mass transfer coefficient (model)													
			Amokrane		Higbie		Handlos		Ruckenstein		Angelo		Srinivasan		Hsu	
t [s]	Cli [mol/l]	C_1 [mol/l]	C_2 [mol/l]	C_2/C_1	C_2 [mol/l]	C_2/C_1	C_2 [mol/l]	C_2/C_1	C_2 [mol/l]	C_2/C_1	C_2 [mol/l]	C_2/C_1	C_2 [mol/l]	C_2/C_1	C_2 [mol/l]	C_2/C_1
0	0.0000135	0.030	0.030	1.000	0.030	1.000	0.030	1.000	0.030	1.000	0.030	1.000	0.030	1.000	0.030	1.000
0.05	0.0000135	0.030	0.029	0.976	0.030	0.996	0.028	0.942	0.023	0.777	0.029	0.955	0.030	0.993	0.029	0.965
0.1	0.0000135	0.030	0.029	0.953	0.030	0.991	0.027	0.888	0.018	0.603	0.027	0.912	0.026	0.858	0.028	0.932
0.2	0.0000135	0.030	0.027	0.909	0.029	0.983	0.024	0.789	0.011	0.364	0.025	0.832	0.022	0.737	0.026	0.868
0.3	0.0000135	0.030	0.026	0.867	0.029	0.974	0.021	0.700	0.007	0.220	0.023	0.758	0.019	0.632	0.024	0.809
0.4	0.0000135	0.030	0.025	0.826	0.029	0.965	0.019	0.622	0.004	0.133	0.021	0.692	0.016	0.543	0.023	0.754
0.5	0.0000135	0.030	0.024	0.788	0.029	0.957	0.017	0.552	0.002	0.080	0.019	0.631	0.014	0.466	0.021	0.703
0.6	0.0000135	0.030	0.023	0.751	0.028	0.949	0.015	0.490	0.001	0.049	0.017	0.575	0.012	0.400	0.020	0.655
0.7	0.0000135	0.030	0.021	0.716	0.028	0.940	0.013	0.436	0.001	0.030	0.016	0.525	0.010	0.343	0.018	0.610
0.8	0.0000135	0.030	0.020	0.683	0.028	0.932	0.012	0.387	0.001	0.018	0.014	0.478	0.009	0.294	0.017	0.569
0.9	0.0000135	0.030	0.020	0.651	0.028	0.924	0.010	0.343	0.000	0.011	0.013	0.436	0.008	0.253	0.016	0.530
1.0	0.0000135	0.030	0.019	0.621	0.027	0.916	0.009	0.305	0.000	0.007	0.012	0.398	0.007	0.217	0.015	0.494
1.1	0.0000135	0.030	0.018	0.592	0.027	0.908	0.008	0.271	0.000	0.004	0.011	0.363	0.006	0.186	0.014	0.460
1.2	0.0000135	0.030	0.017	0.565	0.027	0.900	0.007	0.241	0.000	0.003	0.010	0.331	0.005	0.160	0.013	0.429
1.3	0.0000135	0.030	0.016	0.538	0.027	0.892	0.006	0.214	0.000	0.002	0.009	0.302	0.004	0.137	0.012	0.400
1.4	0.0000135	0.030	0.015	0.513	0.027	0.884	0.006	0.190	0.000	0.001	0.008	0.275	0.004	0.118	0.011	0.372

Appendix 4-8 Information when water droplets collision a layer of kerosene

Distance [cm]	Droplet diameter		
	1.61 mm	**2.67 mm**	**3.0 mm**
After detached 0 cm	no splash, sometimes float	no splash, sometimes float	no splash, sometimes float
5	No splash, coalescence	No splash, coalescence	No splash, coalescence
10	splash (+), secondary jet and secondary droplet	splash (+), secondary jet and secondary droplet	splash (+), secondary jet and secondary droplet
15	splash (++), secondary jet and secondary droplet	splash (++), secondary jet and secondary droplet	splash (++), secondary jet and secondary droplet
20	splash (+++), secondary jet and secondary droplet	splash (+++), secondary jet and secondary droplet	splash (+++), secondary jet and secondary droplet

Appendix 4-9 Dimensionless number in this study

Distance [cm]	**Re Number**			**We number**		
	dia. 1.61 mm	dia. 2.67 mm	dia. 3.0 mm	dia. 1.61 mm	dia. 2.67 mm	dia. 3.0 mm
5	1802	1802	1681	0.03	0.03	0.02
10	2396	2576	2522	0.05	0.06	0.05
15	3021	3052	3056	0.08	0.08	0.08
20	3461	3509	3516	0.10	0.11	0.11
Distance [cm]	**Oh Number**			**Schmidt number**		
	dia. 1.61 mm	dia. 2.67 mm	dia. 3.0 mm	dia. 1.61 mm	dia. 2.67 mm	dia. 3.0 mm
5	0.0001	0.0001	0.0001	470	470	470
10	0.0001	0.0001	0.0001	470	470	470
15	0.0001	0.0001	0.0001	470	470	470
20	0.0001	0.0001	0.0001	470	470	470

Appendix 4-10 Ratio of C_2/C_1 at different contact times and different Sh number models (droplet diameter 1.61 mm 2.67 and 3.0 mm)).

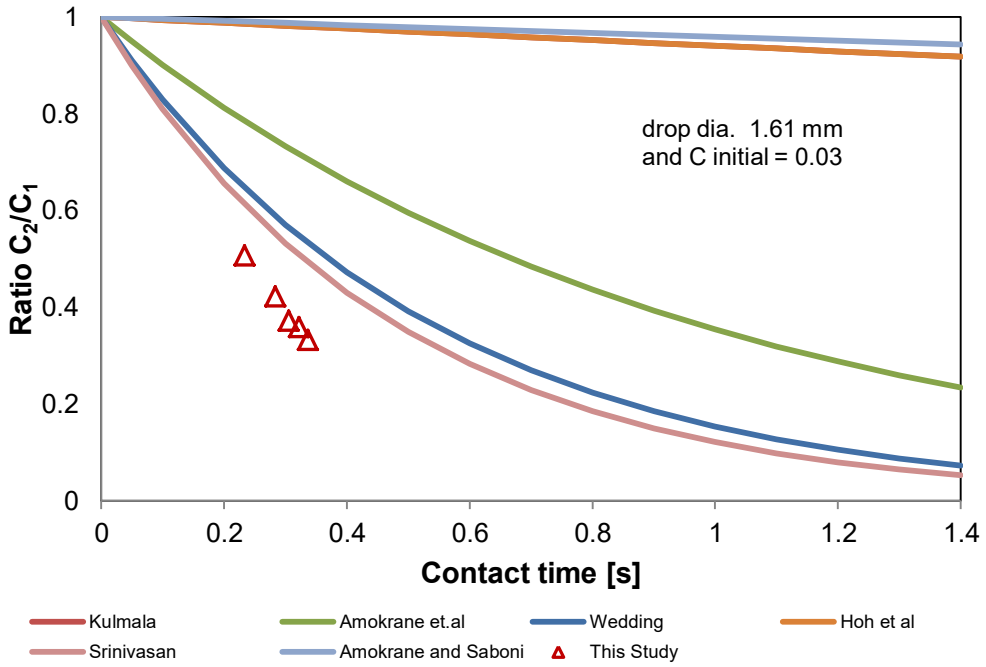

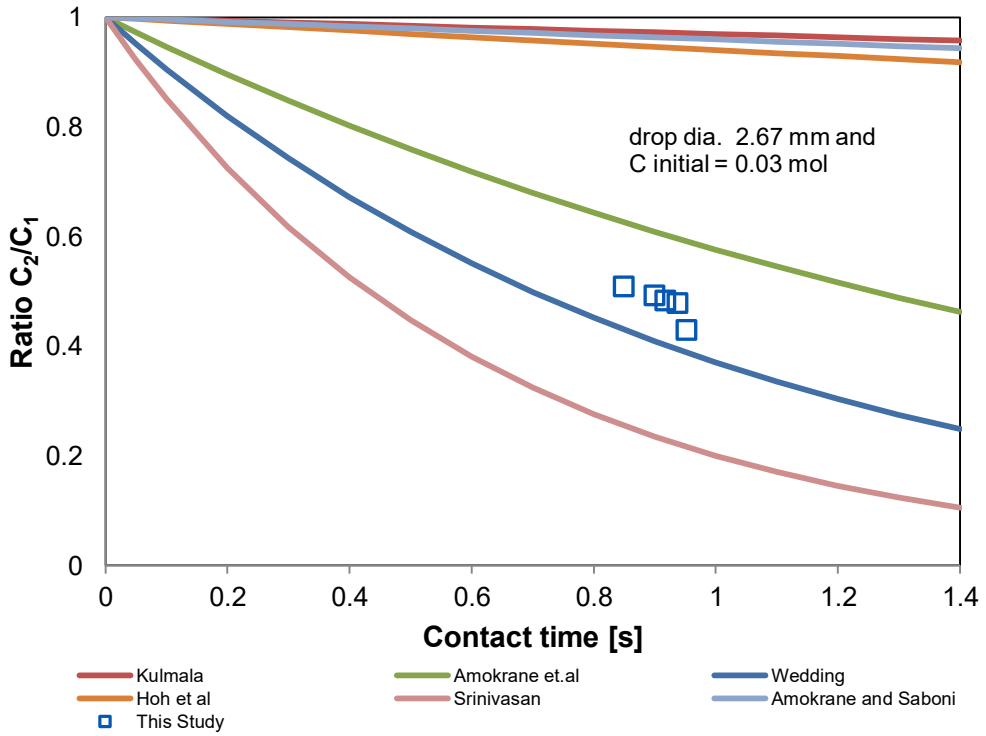

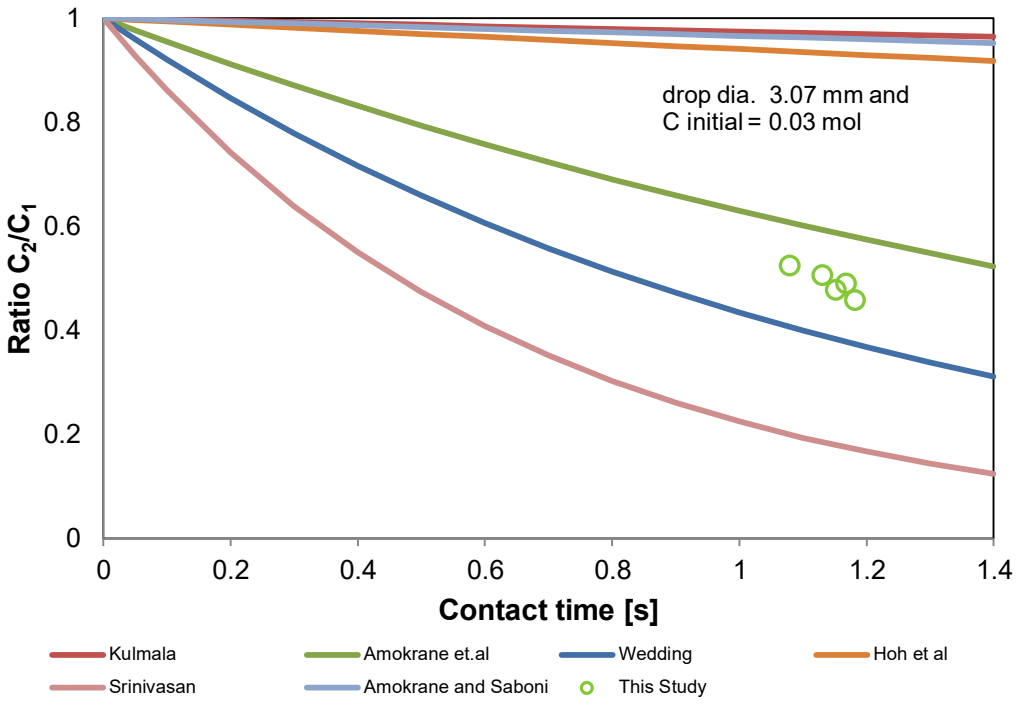
drop dia. 3.07 mm and
C initial = 0.03 mol
Ratio C_2/C_1
Contact time [s]
0
0.2
0.4
0.6
0.8
1
1.2
1.4
Kulmala
Amokrane et.al
Wedding
Hoh et al
Srinivasan
Amokrane and Saboni
This Study